universität wien

MASTERARBEIT / MASTER'S THESIS

Titel der Masterarbeit / Title of the Master's Thesis

„Manipulating the mechanosensory apparatus of melanoma cells: an integrated morphometric and proteomic approach“

verfasst von / submitted by

Jakob Schwarz BSc

angestrebter akademischer Grad / in partial fulfilment of the requirements for the degree of

Master of Science (MSc)

Wien, 2023 / Vienna 2023

Studienkennzahl lt. Studienblatt / degree programme code as it appears on the student record sheet:	A 066 659
Studienrichtung lt. Studienblatt / degree programme as it appears on the student record sheet:	Masterstudium Lebensmittelchemie UG2002
Betreut von / Supervisor:	Ass.-Prof. Giorgia Del Favero, Privatdoz.

Acknowledgments/Danksagung

Zunächst möchte ich meinen Dank gegenüber meiner Betreuerin Giorgia Del Favero aussprechen, die mich mit ihrer Begeisterung und Freude jeden Tag inspiriert und motiviert hat, mir bei wissenschaftlichen Problemstellungen stets mit offenem Ohr zur Seite stand und mich auch meine eigenen Ideen einbringen lies. Auch Professor Gerner möchte ich für seine Unterstützung und Motivation danken.

Es war mir eine Ehre in Kooperation mit der Arbeitsgruppe der Universität in Tel Aviv, unter der Leitung von Professor Isaac Witz am Melanom-Projekt mitarbeiten zu können.

Zusätzlicher Dank gebührt außerdem den Mitgliedern der Arbeitsgruppen von Prof. Del Favero, Prof. Gerner und Prof. Marko, wobei besonders Endre Kiss, Eva Attakpah und Georg Aichinger hervorzuheben sind.

Ich möchte mich bei meiner Familie, meinen Freunden und Wegbegleitern, die mich während dieser Zeit wissentlich, aber manchmal auch unwissentlich tatkräftig unterstützt haben, bedanken. Für andere sind es oftmals nur unbewusste Kleinigkeiten gewesen, welche mich in schwierigen Zeiten wieder auf den richtigen Weg zurückgeführt und wachgerüttelt haben - Besonders Lucia, Antonia, Jutta, Christof und Alex.

Ganz besonderer Dank gebührt meiner Mama sowie meiner Lebensgefährtin Lisa, ohne eure Unterstützung wäre vieles nicht möglich gewesen.

Eidesstattliche Erklärung

Hiermit versichere ich, dass ich diese Arbeit eigenständig und ohne unerlaubte Hilfe verfasst habe.

Jegliche Übernahme von inhaltlichen oder wörtlichen Zitaten wurde in unmittelbarer Nähe zu diesem erkenntlich gemacht.

Diese Arbeit wurde bis zum jetzigen Zeitpunkt, nicht in dieser, und auch keiner anderen Form bei einer Prüfung vorgelegt.

Ort, Datum Unterschrift

Abstract

Melanoma arises from the malignant transformation of melanocytes. It only represents 5-10 % of skin cancer, but accounts for 90 % of the deadly outcomes - the overall deadliest form of all skin cancers and has a high capacity for metastasis. Morphological changes during epithelial-to-mesenchymal transition (EMT), e.g. cells become more spindle shaped, contribute to metastasis, and metastasis is always accompanied by a loss of adhesion. The focus of this thesis is on the two last mentioned items. Two corresponding xenograft derived cell lines of cutaneous (YDFR-C) and brain metastatic (YDFR-CB) cells from the same patient were examined. The adhesion behavior of the mentioned tumor cells (YDFR-C and YDFR-CB) were examined with the aid of a de-adhesion assay, morphological changes were determined by Imaging, and the impact of the three chosen drugs (Celecoxib, Lovastatin, and Yoda-1) on them was investigated. Moreover, a total protein profiling of both cell lines in every condition (untreated control, Celecoxib, Lovastatin, and Yoda-1) was performed.

It could be proven that adhesion in the metastatic YDFR-CB cell line is more pronounced than in the cutaneous YDFR-C cell line. Against other scientific observations, Lovastatin strengthened adhesion in brain metastatic YDFR-CB cells and had furthermore no impact on the adhesion behavior of cutaneous YDFR-C cells. Nevertheless, it had a strong impact on the cell morphology as cells became more spindle-like. Yoda-1 treatment seemed to be contrary concerning the adhesion behavior and the morphologic changes: Cells which had not experienced shear stress before (YDFR-C) showed a strong response concerning de-adhesion behavior, whereas cells already having experienced shear stress (YDFR-CB) once before, showed a strong morphological response. It seems that nicotinamide N-methyltransferase (NNMT) could function as a molecular biomarker for melanoma. To date, this thesis is the first to compare and put in relation the de-adhesion behavior of human melanoma cells originated from a primary and secondary tumor of the same patient.

Zusammenfassung

Das Melanom entsteht aus der malignen Transformation von Melanozyten. Obwohl es nur 5-10 % aller Hautkrebsarten einnimmt, ist es für 90 % der Todesfälle verantwortlich und bildet somit die tödlichste Hautkrebsart. Ein Grund dafür ist seine hohe Bereitwilligkeit zur Metastasierung. Morphologische Veränderung (z.B. die Zellen werden spindelförmiger) während der epithelial-zu-mesenchymal Transition (EMT) trägt zur Metastasenbildung bei, und Metastasierung ist auch immer mit einem Verlust von Adhäsion verbunden. Auf den beiden letztgenannten Punkten liegt der Fokus dieser Arbeit. Zwei korrespondierende, von Patientenmaterial abgeleitete Xenograft-Zelllinien von kutanen Zellen (YDFR-C) und Gehirnmetastasen (YDFR-CB) desselben Patienten wurden untersucht. Es wurde das Adhäsionsverhalten beider Zelllinien (YDFR-C und YDFR-CB) mithilfe eines De-Adhäsions-Assays bestimmt, morphologische Veränderungen anhand von Imaging erfasst und deren Beeinflussung durch die drei ausgewählten Drugs Celecoxib, Lovastatin und Yoda-1 untersucht. Zusätzlich wurde ein gesamtes proteomisches Profil beider Zelllinien (YDFR-C und YDFR-CB) und jedes Zustandes (unbehandelte Kontrolle, Celecoxib, Lovastatin, Yoda-1) erstellt.

Die Ergebnisse zeigten, dass Sekundärtumore (YDFR-CB Zelllinie) ein stärkeres Adhäsionsverhalten als Primärtumore (YDFR-C Zelllinie) aufwiesen. Entgegen anderen wissenschaftlichen Beobachtungen zeigte Lovastatin in dieser Untersuchung eine Verstärkung des Adhäsionsverhaltens in der metastatischen YDFR-CB Zelllinie und beeinflusste das Adhäsionsverhalten in der YDFR-C Zelllinie nicht. Jedoch veränderte sich die Morphologie beider Zelllinien signifikant in Richtung einer spindelartigen Form. Die Behandlung mit Yoda-1 zeigte ein konträres Bild von Adhäsionseigenschaften und morphometrischen Veränderungen auf: Das Adhäsionsverhalten von Zellen, welche bisher noch keiner Scher-Beanspruchung ausgesetzt waren (YDFR-C) wurde bei Behandlung mit Yoda-1 stark beeinflusst, wohingegen Zellen, welche bereits einmal einer Scher-Beanspruchung ausgesetzt waren (YDFR-CB), starke morphologische Veränderung aufwiesen. Des Weiteren scheint N-Methyltransferase (NNMT) als ein molekularer Biomarker für das Melanom zu fungieren. Zurzeit ist diese Arbeit die erste, welche das Adhäsionsverhalten von menschlichen Melanom Zellen untersucht, die aus einem primären, sowie sekundären Tumor desselben Patienten stammen.

Table of contents

2 List of abbreviations

A	Adenine base
ACTH	Adrenocorticotropic hormone
AJ	Adherens junctions
ALM	Acral lentiginous melanoma
AR	Aspect Ratio
BC	Before Christ
BER	Base excision repair
BMI	Body mass index
C	Cytosine base
cAMP	Cyclic adenosine monophosphate
CPD	Cyclobutane pyrimidine dimers
CSD	Cumulative solar damage
CXB	Celecoxib
DRA	Dose response analysis
EC	Extracellular cadherin
ET-value	Effective time value
ECM	Extracellular matrix
EMT	Epithelial-to-mesenchymal transition
EPG	Epidemial growth factor
FAK	Focal adhesion kinase
G	Guanine base
IARC	International Agency for Research on Cancer
KC	Keratinocyte
LINC	Linker of nucleoskeleton and cytoskeleton
LMM	Lentigo maligna melanoma
MC	Melanocyte
MC1R	Melanocortin 1 receptor
MITF	Microphthalmia-associated transcription factor
mMN	Metastatic melanoma
MMP	Metalloproteinase
MN	Melanoma
MTD	Mechanotransduction
NER	Nucleotide excision repair
NM	Nodular melanoma
PM	Plasma membrane
POMC	Pro-opiomelanocortin
RGP	Radial growth phase

ROS	Reactive oxygen species
SES	Socioeconomic status
SKF	Src family kinases
SOTP	Solid organ transplant patients
SSM	Superficial spreading melanoma
T	Thymine base
TYR	Tyrosinase
TYRP-1	Tyrosine-related protein-1
TYRP-2	Tyrosine-related protein-2
UV	Ultra violet
UVR	Ultraviolet radiation
VGP	Vertical growth phase
WHO	World Health Organization
α-MSH	Melanocyte-stimulating hormone

3 Introduction

Skin cancer, which is generally classified into the two subtypes melanoma and non-melanoma [1, 2], is increasing during the last years [3–6] and is one of the most common group of cancers worldwide [5–7]. The most widespread among the non-melanoma subtypes are the basal cell carcinoma accounting for 80 – 85 %, and the squamous cell carcinoma accounting for 15 – 20 % of all cases [2].

The melanoma subtype on the other hand divides into three categories (based on their point of origin): cutaneous melanoma, mucosal melanoma and ocular 4 [8], with cutaneous melanoma being the far most common category with more than 90 % of melanoma cases [9], which arise from the malignant transformation of melanocytes [10, 11]. In this thesis we focus on cutaneous melanoma which can be in situ (limited to the epidermis) and invasive (where melanocytes invade the dermis). There are four major forms of invasive cutaneous melanoma and their percentual range of occurrence [11]:

Table 1: Major forms of cutaneous melanoma [11], adapted by author

major forms of cutaneous melanoma	abbreviation	percentual range of occurrence
Superficial spreading melanoma	SSM	41 %
Nodular melanoma	NM	16 %
Lentigo maligna melanoma	LMM	2.7-14 %
Acral lentiginous melanoma	ALM	1-5 %*

*higher percentage in African American or Asian population

For the sake of completeness it should be mentioned that in the 4th edition of the “WHO classification of skin tumors” of the year 2018 [12], an updated melanoma classification (based on pathways) [13] was presented, in which the melanoma subtypes were divided into two groups based on their etiology, namely in those arising from sun exposure (further divided depending on the degree of cumulative solar damage [CSD]) and those arising independently from sun exposure (named as “non-solar” category) [11, 14]. Thus 9 types of melanoma development could be distinguished (based on their clinical and histologic morphology, epidemiology, and genomic characteristics) [14], 7 of them being cutaneous melanoma [15] (and including the 4 major forms of cutaneous melanoma mentioned above). The development of each melanoma subtype was assigned to a pathway from the underlying precursor lesion onwards [14].

The term “malignant melanoma”, especially used from the 1950-ies onwards, implies that there might be “benign melanoma” as well, which can lead to confusion and misunderstanding. In recent years the term “melanoma” has become more current as a

melanoma is always malignant [16]. The term “cutaneous melanoma” is often used synonymously with “melanoma” as well in many articles [1, 4, 6, 8, 11, 17–19]. Therefore, in this thesis, “malignant melanoma” as well as “cutaneous melanoma” will be termed “melanoma” (MN).

3.1 Melanoma in our society – a short overview

The expression “melanoma” is derived from the two Greek words *melas* meaning “dark” and *oma* meaning “tumor”. Its earliest historical evidence was found in Peruvian mummies radiocarbon dated about 400 BC [20]. Today, MN only represents 5 – 10 % of skin cancer [7] but accounts for 90 % of the deadly outcomes [11] – the overall deadliest form of skin cancers [3, 5, 11, 17, 18], which accounts for 1.7 % of all new cancer cases diagnosed worldwide [21]. For the year 2020, 325,000 new cases (53.5 % male I 46.5 % female) of MN were expected worldwide and 57,000 deaths (56.1 % male I 43.9 % female) correlated with MN. For 2040 the worldwide prediction is even worse: 510,000 new cases (a 56.9 % increase) are estimated annually and 96,000 correlated deaths (a 68.4 % increase) [6]. The current MN data for the US (estimated for 2022) [22], the EU-27 and Austria (estimated for 2020) [23] listed in Figure 1 show that men are more affected than women.

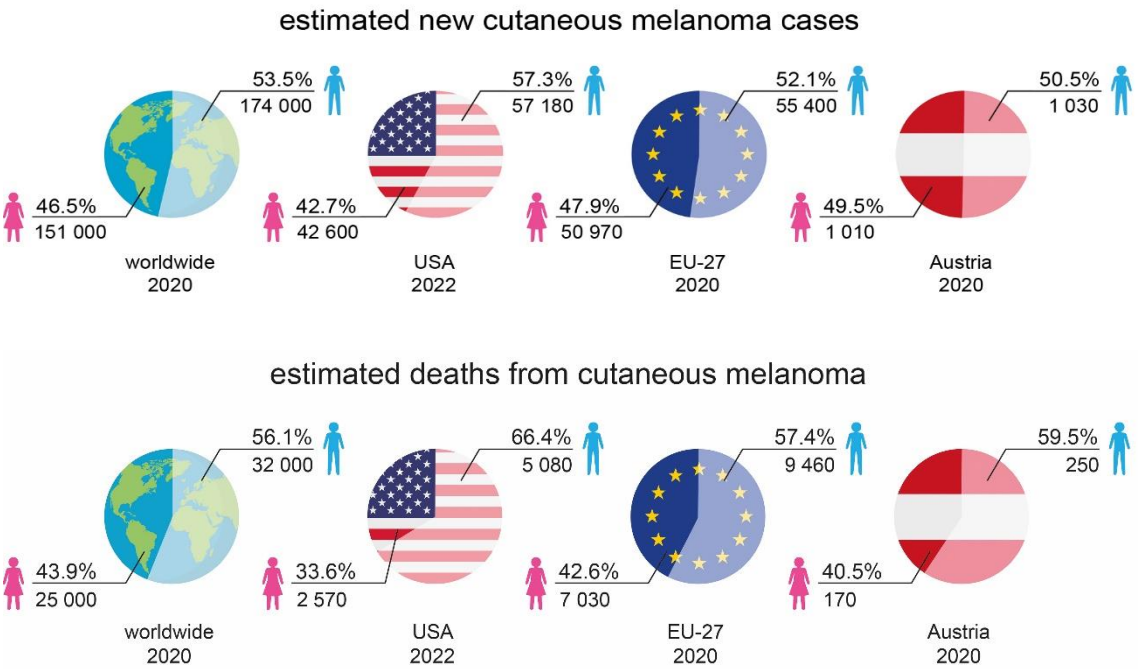

Figure 1: estimated new melanoma cases and deaths based on data published in [6, 22, 23], designed by author

The MN incidence-rates vary strongly between countries because of different racial skin phenotypes (the risk to develop MN in the American white population is on average approximately 30 times higher compared to the African American population - calculated from [24], see also 4.4) and variations in sun exposure [25]. In regions of the world where most people with light complexion have intermittent intense sun exposure – during short holidays for example – 80% of MNs develop [26]. The most vulnerable and affected phenotypes are elderly people with fair skin, blue eyes and red hair [7].

The incidence also differs according to age (see also 4.3). Younger and middle-aged people are more affected (with a linearly rise between 25 to 50 years [25], with a peak at 65 [27] and a median age of 57 years when diagnosed). Differences between sexes also occur. Women predominate until the age of 40, whereas at the age of 75 men´s incidence is 3 times higher. According to parts of the body, MN in women prevails at arms and legs, in men at the back [25]. UV-exposure also plays an important role (see also 4.1). More than 5 incidents of severe sunburn double the risk to develop MN [4], sunburns in childhood and adolescence are even responsible for the highest risk at all [4, 26]. UV radiation from artificial sources like sunbeds is also associated with an increased risk to develop MN, so that sunbeds are formally classified to be carcinogenic in humans [4].

3.1.1 Metastasis

MN arises from the malignant transformation of melanocytes [10, 11], which stem from greatly migratory neural crest cells [28]. The differentiating step from a pre-cancerous neoplasm to malignant cancer is its invasion through the basement membrane [29]. When tumor cells detach from the original primary tumor and spread through the vascular or lymphatic systems to form new (secondary) tumors at distant locations (e.g organs), this is called metastasis [30–33]. Metastasis is the major reason for treatment failure [30, 33] and the high mortality rate of cancer [31, 32, 34] - up to 90 % of all cancer deaths result from metastasis [32, 35].

There are 5 different stages for MN lesions to be classified (0, I, II, III, IV) – see Figure 2. The lower the stage, the better the prognosis. Stage 0 means melanoma in situ [36], without spreading into deeper parts of the skin – e.g. dermis [3]. Stage IV denotes distant metastatic MN [36], where metastasis has occurred from the primary tumor to remote parts of the body like (but not limited to) liver, lungs or brain [3, 5], for more details see [37].

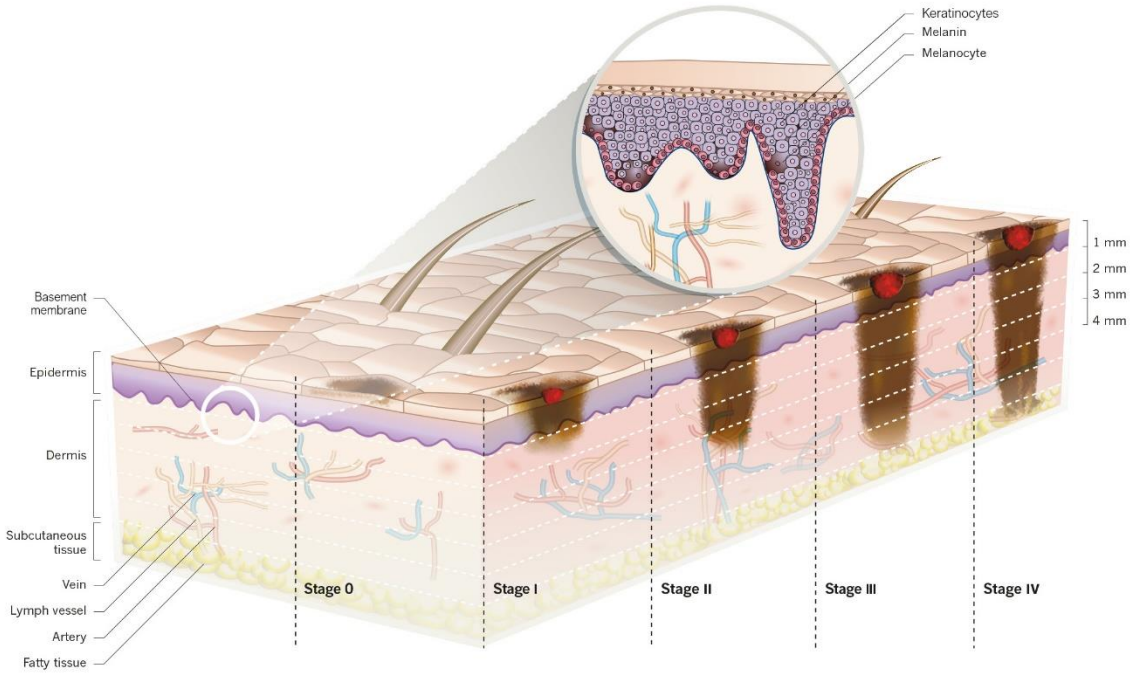

Figure 2: Architecture of the skin and overview over the different diagnostic stages of melanoma [37], adapted by author

At the time of diagnosis, about 90 % of MN are primary tumors with no signs of metastasis at all (stage 0) [11]. These primary MN patients are successfully treated by surgery [3, 5] and show an approximated 5-year survival rate of 99 % [5] and a 10-year survival rate of 75 – 95 %. Nevertheless, although even thin tumors can disseminate, more than 85 % of MN will not metastasize [11].

Prognosis becomes significantly worse with patients at a late-stage disease (stage IV) [18]. The 5-year survival rate for metastatic MN is about 27 % [5], the10-year survival rate is only about 10 % [3].

Brain metastasis is diagnosed in 60 % of metastatic MN patients and found in 80 % at autopsy of affected people. The 5-years survival rate amounts to 23 % [8], but the 1-year overall survival rate could be extended from 20 – 25 % to 80 – 85 % because of the great advances of systemic therapy [38]. Generally, mortality rate has decreased significantly since the first immune checkpoint inhibitors (like ipilimumab) and BRAF kinase inhibitors (like vemurafenib) were approved [39]. During pregnancy, MN is the most common malignancy (31 % of all cancers), but only 0.9 % of women will get this diagnosis while being pregnant. Still, current data suggest that pregnancy neither affects the melanoma risk nor melanoma survival. This is also the case with contraceptive pill and hormone replacement therapy [11].

3.2 Architecture of the skin and the role of melanocytes

As an aggressive cancer, MN appears on the skin and starts in melanocytes [40] – cells helping to protect the skin from UVR damage [41].

The skin is the largest organ of the human body and accounts for about 15 – 17 % of the total body weight – adults have between 1.5 to 2 m^2 of skin [7]. Its primary function is to protect against and repair environment-based physiological and molecular damage [42]. It is structured into three layers, the epidermis, dermis, and hypodermis. The epidermis (avascular and enervated) is made of different types of stratified cells, of which the keratinocytes (80 %) and the melanocytes (5 – 10 %) are the most common [1]. The epidermis is 0.03 – 0.13 mm thick [7]. The basement membrane (0.5 – 1 µm thick) separates the epidermis from the dermis, which consists of collagen, elastin fibers, fibroblasts and the amorph extracellular matrix (ECM). It includes blood and lymphatic vessels [1] and is 1.1 mm thick [7]. The hypodermis is the deepest layer of the skin and is not clearly separated from the dermis. It connects the skin with the underlying muscles and contains adipocytes [1] – see Figure 2.

Melanocytes (MCs) take part in the defense system against ultraviolet radiation (UVR)-mediated DNA damage (further details in 4) providing melanin, a complex macromolecule that absorbs and scatters UVR, to the adjacent keratinocytes (KCs). In the skin of an average individual there are nearly 3 billion cutaneous MCs, corresponding to about 1,500 MCs per mm^2. They divide less than twice a year [41], and their proliferation and melanin production is induced by UVR mediated DNA damage of KCs in a p53 dependent manner (see Figure 3). The tumor-suppressor protein p53 stimulates transcription from POMC (pro-opiomelanocortin) gene promoter. POMC is a multicomponent precursor polypeptide and is then processed into α-MSH (melanocyte-stimulating hormone), ACTH (adrenocorticotropic hormone) and β-endorphin [43]. The secreted α-MSH binds to its receptor MC1R (melanocortin 1 receptor) on the surface of the MCs in the basal epidermis [44]. MC1R transduces this extracellular signal to the downstream effector MITF (microphthalmia-associated transcription factor) in a cAMP (cyclic adenosine monophosphate) dependent way [45], thus stimulating melanin production in specialized lysosomal-related organelles named melanosomes [46]. MITF regulates the expression of the main enzymes in melanogenesis, tyrosinase (TYR), tyrosine-related protein-1 (TYRP-1) and tyrosine-related protein-2 (TYRP-2) [46]. These enzymes are mainly involved in the transformation of the amino acid tyrosine into melanin [47]. Melanin is then transferred via melanosomes from MCs to KCs where it protects their nucleus from UVR mediated DNA damage [41]. Each MC can provide about 40 KCs with melanin [48]. Besides providing a shield against UVR, melanin may

also have negative effects and can attenuate the efficiency of radiotherapy, chemotherapy and phototherapy, what can promote tumor growth and progression [49]. COX-2 is linked to pigmentation – in MC, silencing COX-2 suppresses melanogenesis and reduces pigmentation [50].

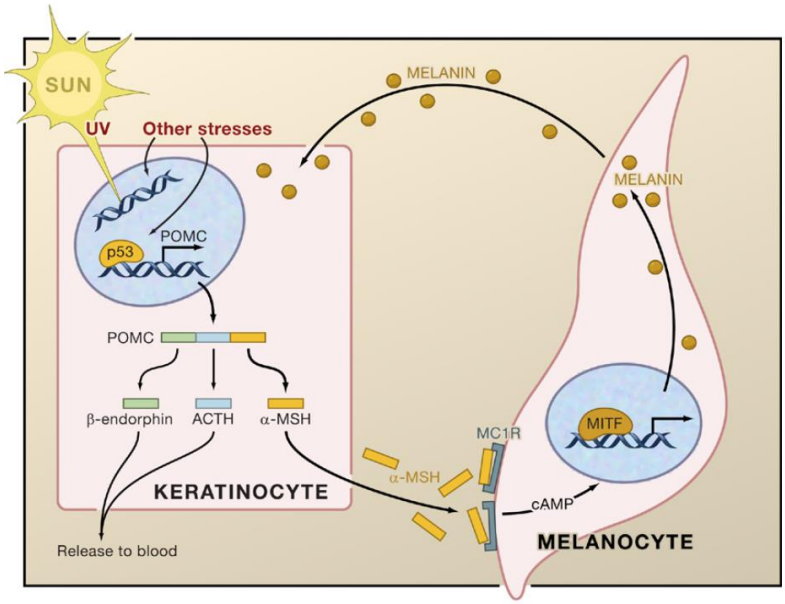

Figure 3: melanin production induced by UVR [51]

There are two major kinds of melanin, eumelanin and pheomelanin [45]. Eumelanin is an insoluble [46], inert, dark brown/black pigment [52] which is prevalent in people with brown and black hair [53]. The more eumelanin is present in the epidermis, the darker the skin complexion appears and the better the UVR shielding properties are [52]. Pheomelanin is a soluble [46], sulfur containing [53], reddish/yellow pigment which prevails in individuals with red hair, pale skin and freckles. Pheomelanin has a poor UV protection capacity compared to eumelanin and amplifies UVA mediated ROS [54].

4 Melanoma risk factors

There are environmental and host risk factors that lead to the development of MN [4, 13, 25, 39], but it is important to note that MN is not a single tumor entity and therefore does not follow a homogeneous profile of risk factors and prognosis [55].

4.1 Ultraviolet radiation (UVR) from natural and artificial sources

UVR is the most important risk factor for the development of MN [5, 6, 11, 13, 45, 55–57]. It is estimated that about 90 % of the MN cases are caused by UVR, mostly from sunlight [45].

4.1.1 Natural UVR source - sunlight

According to their biological effects, the UV range (200 – 400 nm) can be subdivided into three spectral regions: UVA (320 – 400 nm), UVB (290 – 320 nm) and UVC (200 – 290 nm) [58]. The UVC range reaching the earth is neglectable, as nearly all is absorbed by the ozone layer. This is important as the DNA absorption maximum with 260 nm lies within the UVC spectrum, which makes them highly mutagenic [59]. A large proportion (70 – 90 %) of UVB is also absorbed by the stratosphere [60]. Therefore about 5 % of the electromagnetic spectrum that reaches the earth is comprised by UVR [58, 60] with a radiation spectrum ranging from 290 – 400 nm [60]. On a summer´s day, the terrestrial UVR comprises about 94 % of UVA and 6 % of UVB [58].

The wavelengths of sunlight can penetrate variably deep into the different layers of the skin and can be absorbed there by different cellular biomolecules. UVA can reach the dermal layer of the skin whereas UVB penetrates the epidermis [61]. UVA as well as UVB cause DNA damage via different mechanisms, with UVB being absorbed directly by nuclear DNA, and UVA damaging DNA indirectly via reactive oxygen species (ROS) [42]. Both result in carcinogenesis [44], but in MN pathogenesis the exact role is yet to be clarified [61]

UVA makes up the prominent part of UVR and penetrates deeper into the skin, but is less genotoxic in comparison to UVB [62]. Although UVA is poorly absorbed by DNA, it causes indirect damage to DNA via endogenous UVA chromophores that trigger the formation of ROS. Those chromophores are still not fully characterized [63], potential candidates contained in the skin are among others flavins, porphyrins and melanin [42, 63]. Oxidation of nucleotide bases affects the DNA by promoting mispairing, which leads to mutagenesis. The transversion of the purine base guanine (G) to the pyrimidine base thymine (T) is a well-known mutation caused by ROS. This amounts to the oxidation of guanine (at the eighth position) which causes the formation of 8-hydroxy-2'-

deoxyguanine (8-oxo-dG). 8-oxo-dG often pairs with adenine (A) instead of cytosine (C), and this substitution mutates a G/C pair into an A/T pair. To avoid oxidative mutagenesis, the base excision repair (BER) pathway can reverse oxidative damage in DNA [44].

UVB is higher in energy than UVA. It damages DNA by direct absorption of UV-photons by pyrimidine bases [44, 61], which leads to the formation of two major and highly mutagenic photoproducts [44], cyclobutane pyrimidine dimers (CPDs) and pyrimidine (6-4)-pyrimidone photoproducts (6-4PPs) [44, 61]. CPDs are more abundant in formation, whereas 6-4PPs are more mutagenic [42]. One day´s sun exposure results in up to 10^5 UV-photoproducts in every keratinocyte exposed [64]. The UV-induced photoproducts lead to a bulky lesion that distort the DNA helix, can impair transcription and block DNA replication [65]. The nucleotide excision repair (NER) pathway identifies and repairs CPDs and 6-4PPs [62] as well as other bulky DNA lesions [44]. If unrepaired, photoproducts can result most frequently in C > T and CC > TT transition mutations [65, 66] (also known as UV fingerprint mutations [65]).

UVR-induced ROS can furthermore trigger different inflammatory pathways (e.g. MAPK, AKT/PKB, JAK-2 and STAT-3) which upregulate COX-2-mediated PGE_2 production leading to tumor progression. In MN, COX-2 is associated with DNA damage, tumor survival, resistance to apoptosis, immune resistance, invasiveness and metastasis [67].

4.1.2 Artificial UVR sources

Besides from sunlight, people may also be exposed to UVR from artificial sources by various lamps at home (e.g. for cosmetic purposes) or at work (e.g. for research, medical or industrial purposes), but the main source for artificial UVR arises from tanning devices [68]. Modern tanning beds mainly operate in the UVA range, only a small proportion (< 5 %) lies in the UVB range –which corresponds to the normal ratio of UVA to UVB on a sunny day [68]. Yet tanning devices are designed to provide rapid tan, so the emitted UVR-doses are accordingly high [69]. The UVA intensity in tanning beds is 10 – 15 times higher than the UVA radiation at midday sun [70]. As a consequence, these UVA doses received per unit of time during one tanning session are higher than those received during sunbathing or daily life [60]. In the year 2009, WHO´s International Agency for Research on Cancer (IARC) classified UV-emitting tanning devices (sunbeds) as Group 1 carcinogens to humans [71]. People using a sunbed at least once in their lives are at 20 % higher risk for MN than individuals never having used such a device, and each additional annual session adds approximately another 2 % of risk [72]. The first use of tanning beds before the age of 35 increases the risk for developing MN significantly to 75 % [60].

4.1.3 Vitamin D and cancer

On the one hand UVR is a potential environmental factor for MN [5, 6, 11, 13, 45, 55–57], on the other hand it is required for the synthesis of Vitamin D [44, 61, 73, 74]. 10 % of the fat-soluble Vitamin D is derived from exogenous sources (diet and supplements), whereas 90 % is synthesized endogenously in the skin at UVB exposure. Nevertheless, as mentioned above, UVR is associated with skin cancer including MN [74]. The optimal trigger for Vitamin D synthesis is a sub-erythemal dose of UVR, whereas longer UV exposure only results in linearly increased DNA damage but not in a higher Vitamin D level [69]. A common phenomenon after the diagnosis of MN is sun avoidance, which leads to a deficiency of Vitamin D [75]. Yet the correlation between Vitamin D and MN is not clarified [74, 76]. Recent studies suggest that MN patients show suboptimal levels of Vitamin D [75–77] and therefore bear a higher risk for MN as well as a worse prognosis [75, 77]. It is therefore recommendable to keep a good balance between sun exposure and sun protection [74].

4.2 Socioeconomic status and lifestyle (including occupation)

Individuals with higher Socioeconomic status (SES), especially those who are highly educated, have an increased risk for developing MN, while having at the same time a decreased mortality rate [78]. A hypothesis for this could be that this population is more regardful in consulting a dermatologist. Lower SES individuals on the other hand get MN diagnosis at a later-stage and therefore have higher mortality rates – maybe because they have less vigilance concerning MN risk [78].

Lifestyle risk factors associated with the development of MN are among others obesity (BMI – obese persons bear an almost 4-fold risk for MN) [57], marital status (unmarried and widowed persons tend to a lifestyle associated with a greater risk), the use of tanning beds and recreational UV exposure (as mentioned above) as well as occupation [78].

Occupation also may play a decisive role in the development of MN. Different professional fields have specific occupational risk factors like agricultural and manufacturing workers, electronics workers, lithographs, printers, airline pilots and cabin crew [79]. Airline pilots and crew members for example have about twice the risk to develop MN [80, 81], pilots also are at twice the risk to die from MN as the general population [80].

4.3 Sex and Age

In the US, the probability for the white population to develop MN is about 1.5-times higher when you are male than when you are female (calculations based on [24]). In EU-27, however, it is only 1.1 times higher (calculation based on [23]).

In Europe, the incidence for MN has increased tremendously over the last few years in adults over 60, especially in men [11]. Younger and middle-aged people are more affected (with a linearly rise between 25 to 50 years [25], with a peak at 65 [27] – about two thirds of all new cases being diagnosed at the age of 55 to 84, and a mean age of 65 [82]. Women predominate until the age of 40, whereas at the age of 75 men´s incidence is 3 times higher [25]. Compared to male MN patients, female patients exhibited a survival advantage, lower risk of progression and a decreased probability to develop nodal and visceral metastasis [83]. The median time for women to develop distant metastasis was significantly later (7.5 months) compared to men [84].

According to parts of the body, MN in women prevails at the limbs (57 %), in men on the trunk (43 %) [85]. Generally speaking, MN arises at younger ages at less sun exposed sites like the trunk and limbs, at older ages at parts of the body that are more exposed like face, neck and ears (especially in men also scalp) [6].

4.4 Skin type (phototype) and geographical location

Phototype and geographical place of residence are two key risk factors in MN development [86]. The highest incidences of MN observed can be found with predominantly fair skinned people [13] (mostly Caucasians of Fitzpatrick phototypes I and II [86]) living in areas of the world with very high UV radiation [7, 13], such as Australia and New Zealand (about 50 cases of MN per 100,000 each year), followed by North America (in lower latitudes, about 30 cases per 100,000 each year). In both North America and Europe at higher latitudes the MN incidence has risen steadily during the last decades. [13]. In Europe, the highest incidence rates occur in Northern European countries, whereas Southern European countries are not affected to such degrees. The reason for this might be the higher pigmentation of the skin and the rather chronic sun exposure at southern countries [25].

In Brazil, the largest country of South America, there is a statistically significant correlation between European ancestry (geographically grouped together as stemming from Central Europe and Latin Europe, but especially Germany or Italy) and a higher risk for developing MN. Being of indigene ancestry, on the other hand, seems to have a protective effect [87].

If you compare the US data of the cancer statistics for African American 2022 [24] concerning African Americans and the white population and their incidence for MN, the incidence rate is approximately 33 times higher in white men and about 27 times higher in white women than in their African American counterparts.

In South Africa there are about 81 % Black Africans and approximately 8 % White African population. For the White African population, the probability to develop MN is about 20 times higher compared to the Black African population. This protection is ascribed to the higher epidermal melanin with black people that acts as an endogenous sun protection factor of approximately 13.4 [88].

4.5 Immunosuppression

Immunosuppression can be triggered by UVR – which is called “photoimmunology” [89, 90] or by immunomodulating drugs (including both immunosuppressants and systematic corticosteroids to prevent organ transplantation reaction or to treat autoimmune diseases) [91]. Immunosuppressed persons (e.g. solid organ transplant patients, SOTP) are at an increased risk to develop MN [91–94]. Generally, in this group the risk for developing MN is more than 2 times higher compared to the general population. With some SOTP subgroups like renal transplant patients the risk is about 2.5, in liver and heart transplant patients about 5 times higher than in the background population This higher MN risk in the last subgroup may be based on more intense immunosuppressive therapies [92]. If you look at the risk to develop non-keratinocyte skin cancers in SOTPs, MN constitutes the most common cancer with 61.8 % [95].

4.6 Family history of MN

The term “familial melanoma” is used when two or more first degree family members (such as parents, children or siblings), or three or more relatives on the same side of the family (independent of the degree of relationship) have developed MN [96]. About 5 - 10 % of all MN cases appear in families [13, 97–99].

Affected genes for familial MN are above all CDKN2A, which is the major high penetrance susceptibility gene and is identified in 20 – 40 % of all cases. Mutations in other predisposition genes like CDK4, BAP1, MITF, POT1, ACD, TERF2IP, and TERT are uncommon and only explain further 10 % of familial MN. Nevertheless about 50 % of all incidents in MN families remain unexplained concerning the underlying genetic susceptibility [97] and seem to carry private mutations [13].

Individuals out of families with a MN history show a 74 % increased risk for the development of MN compared to individuals with no family history. Affected families have

a 94 % increased risk for MN on the trunk (abdomen, upper and lower back, buttock, hip, shoulder, and thigh) and an 83 % increased risk for MN on the upper and lower extremities. This is independent of mole count and pigmentary traits. The personal risk to develop MN within a family with positive history is 3 to 8 times higher. True genetic susceptibility may not always be the reason for a positive family history of MN, similar behavior within a family, for example concerning UV protection or recreational habits, may lead to MNs resulting from chronical sun exposure [100].

4.7 Number of Nevi

The term “nevi” is synonymously used with “moles”, “melanocytic nevi”, “common nevi” or “pigmented skin lesion” within different papers [3, 19, 28, 82, 88, 101–105] – in this thesis they will be termed consistently as “nevi”.

Nevi are benign lesions [3, 102] and form pigmented clusters or nests of round (non-dendritic) melanocytes [104] leading to dark spots on the skin because of the tendency of the melanocytes to retain melanin [3]. Benign nevi show cytological and architectural features (symmetry and circumscription) that distinguish them from MNs. Dependent on where they can be found they are junctional (within the epidermis), dermal (within the dermis) or compound (within both epidermis and dermis) [104].

Nevi are viewed as markers [103] and precursors [19, 103] for an increased MN-risk and the number of nevi constitutes a highly important risk factor for the development of MN. An individual with a high density of nevi (101 – 120 nevi) bears an almost seven-fold likelihood for MN than people with very few nevi (0 – 15 nevi) [19]. The percentage of MNs associated with pre-existent nevi ranges from 20-50 % [102, 103, 106–108], but most nevi are stable and regress rather than progress. Therefore it is not recommended to preventatively excise them [14]. The estimated risk for a single nevus to progress into MN is very low but increases with age. It ranges from 1:200,000 for both sexes until the age of 40 and peaks with men older than 60 (1:33,000) per year [103].

The number of atypical (dysplastic) nevi also accounts for an independent and highly significant risk factor. Compared with persons lacking atypical nevi, the existence of any atypical nevus bears a 10-fold risk for the development of MN [19].

Nevi can be congenital (present at birth) or acquired (appear later) [109, 110]. Congenital nevi are present with 1 % of newborn babies, but in rare cases can occur between the 1st and 24th month [111], whereas acquired nevi mostly appear in childhood and adolescence [112]. Hereditary factors as well as sun exposure play a decisive role for the development of acquired nevi, especially in early childhood [105, 112].

Generally, men are reported to exhibit more nevi than women, the reason for this being the average body area of men (2.1 m^2) that is greater than that of females (1.7 m^2). Thus, the density of nevi (about 40 nevi per m^2) between sexes does not differ fundamentally [113].

Nevi are very common (most individuals have 5 – 20 nevi) and may vary concerning shape, size and color. Therefore, it is important to recognize those changes as normal or as abnormal alterations that may indicate MN [105]. For this reason, the ABCDE criteria (first published as ABCD rules in 1985 [114] and extended to ABCDE in 2004 [115]) were established as a simple tool for both laypersons and general practitioners. The ABCDE criteria comprise **A**symmetry (no symmetric shape), **B**orders (irregular borders), **C**olor (multiple colors), **D**iameter (> 6 mm) and **E**volving (in shape, color, size, surface or symptoms. If any of these symptoms arise, people are advised to see a dermatologist for further examination (dermoscopy or bioscopy, or both) [115]

5 Mechanotransduction in cancer and metastasis

In the tissue microenvironment, living cells are permanently exposed to physical/mechanical (e.g. tensional and shear forces) and chemical (e.g. cytokines and growth factors) signals [116]. Mechanical cues stem from the surroundings (such as neighboring cells), blood flow, or pressure from interstitial spaces [117]. Through mechanotransduction (MTD) cells can respond to mechanical stimuli by converting a physical input into a specific intracellular biochemical signal [116, 118, 119]. Cellular responses depend on how the forces are sensed by the cell, on cellular context, or on the cell type [117]. This process, on the one hand, is important to maintain normal cell functions like cell adhesion, proliferation, migration, and survival, but on the other hand it promotes the progression of diseases like cancer [120].

Forces from the cell environment (exerted on cells or exercised by cells) are typically first experienced on the cell surface and are sensed there by a group of specialized molecules named mechanosensors [117]. Cells show a broad variety of mechanosensory structures including force-sensitive ion channels (e.g. Piezo ion channel family [121, 122]) and receptors (e.g. cell adhesion molecules like integrins in focal adhesions, and cadherins in adherens junctions [119, 123]) [117, 119].

5.1 Ion channels: MTD and cancer

Ion channels are pore-forming, proteinaceous transmembrane channels that enable ions to pass through the plasma membrane. Through physical or chemical stimuli, the state of the channel pore can change from resting-closed to activated-open [124]. Mechanically activated ion channels are directly activated by physical forces. Representatives of this kind of ion channels are for example the non-selective cation channels Piezo1 and Piezo2 [121]. After the mechanical activation of the non-selective ion channels, a combination of cations (e.g. Ca^{2+}) passes through the open pore down their electrochemical gradient resulting in a depolarization of the cell [124] and in an intracellular increase of the ubiquitous second messenger cation, Ca^{2+} [125]. Ca^{2+} can diffuse over larger cellular regions and modulate many signaling pathways [124] some of which are involved in cancer metastasis like cell migration, intravasation, angiogenesis and proliferation [125]. In MN for example, calcium signaling is involved in tumorigenesis and progression [126]. Thus, ion channels are able to convert local mechanical events into global cellular occurrences [124].

5.1.1 Piezo channel

The largest known pore forming multimeric ion channels comprise the Piezo channel family (Piezo1 and Piezo2) that are made up of three individual subunits composed of about 2,500 amino acids each [121]. The gating of Piezo channels can be triggered by several mechanical stimuli acting on the plasma membrane and comprising shear stress, stretching, poking, membrane tension, and suction [127] or via drugs (e.g. selectively activated by Yoda-1) [128]. Piezo1 (formerly known as Fam38A [129]) is responsible for the transduction of forces applied internally or externally and is expressed primarily in non-neural cell types (for example, Piezo1 is abundant in cells of the skin sensitive to mechanical stimuli [127]).

Piezo2 (formerly known as Fam38B [129]), on the other hand, is expressed in some specialized mechanosensory structures and in sensory neurons. It is important for proprioception (sensing the position of limbs in space and the ability to balance) and for sensory processes like the detection of (light) touch [121].

Piezo channels are upregulated in several types of cancer [130–133], primarily of epithelial origin [127], for example Piezo 1 is overexpressed in melanoma [134]. In MN, Piezo1 promotes proliferation, invasion [134], migration [135], metastasis, transvascular migration, and distant metastasis. It acts as an oncogene by activating the PI3K/AKT/mTOR signaling pathway, and its upregulation is correlated with poor survival [134].

5.2 Integrins in focal adhesion: MTD, cancer and adhesion

Focal adhesions are cell anchoring connections [121] which physically link the actin cytoskeleton to the ECM mediated through integrins [120].In mammalians, integrins are a group of 24 distinct subtypes of bidirectional (“inside-out” and “outside-in”), transmembrane, αβ heterodimer, adhesive receptors [136] and also function as mechanosensors [137]. Each integrins consist of an α- and a β-subunit and their non-covalent [138] αβ association out of 18 α- and 8 β-subunits form the distinct integrins [136].This leads to their different affinities to the corresponding extracellular ligand [139] (ECM protein [120]), for example collagen, fibronectin or fibrinogen [120, 139]. Each integrin is composed of three domains: a large extracellular domain and a small cytoplasmatic tail domain, which are connected by a single transmembrane domain [140]. Once the ligation of integrins with ECM proteins has taken place, numerous intracellular structural proteins (like talin and paxillin) and signaling proteins (like Src family kinases (SKFs) and focal adhesion kinase (FAK) [141]) are recruited [120] at their

cytoplasmic tails and form a so-called “adhesome [142]”. The newly formed adhesome establishes a link to the actin cytoskeleton (for example, the recruited talin has a binding site for vinculin, which again binds to the actin cytoskeleton [120]) and initiates integrin signaling [142], like the Ras-ERK, PI3K/AKT, and YAP/TAZ pathways [141, 143] – the latter is part of the Hippo pathway [144, 145]. Actin is also connected with the nucleus envelope by LINC (linker of nucleoskeleton and cytoskeleton) [119]. Thus, integrins act as both: a physical anchor (they mediate cell adhesion) and a bidirectional signaling hub to regulate the response of the cell [141]. Also, Piezo 1 is linked to the integrin system of the cell. It helps epithelial cells to maintain integrin activation, as Piezo1 expression leads to R-Ras relocation to the endoplasmic reticulum, stimulating the calpain signaling, which increases the integrin affinity, ligand binding and cell adhesion [146].

Integrins and integrin mediated processes play an important role in nearly every phase of cancer progression like cancer initiation and proliferation, invasion, migration, metastasis, and drug resistance [141, 143]. Integrins regulate the expression of matrix metalloproteinases (MMPs like MMP-9), which are increased in invasive MN. MMPs are responsible for the degradation of the basement membrane and the surrounding ECM proteins (e.g. collagen, fibronectin). This process is crucial for the invasion and progression of tumor cells [147]. An increased expression of integrin β3 in MN leads to a switch of the indolent radial growth phase (RGP) to the aggressive vertical growth phase (VGP) which is the most critical step in MN progression. The VGP MN cells show detachment from neighboring KC and invade and proliferate in the dermis after degradation of the basement membrane [148]. This invasion through the basement membrane is the differentiating step from a pre-cancerous neoplasm to malignant cancer [29]. With an enforced expression of β3, the β3 subunit and endogenous αv form a functional complex (αvβ3) which increases the malignant phenotype [148]. In addition, it was shown that αvβ3 integrin expression leads to a higher elasticity of MN cells [149]. The specific integrin expression on circulating MN cells determines the metastasis to different organs. Metastasis to the lungs, for example, is probable when melanoma cells express integrin β3, whereas with integrin β1 expression lymph node metastasis is likely [150].

5.3 Cadherins in adherens junction: MTD, cancer and adhesion

Adherens junctions (AJ) are adhesion complexes that anchor cells to other cells (cell-cell adhesion) [117] in a zipper-like structure and function as signal hubs, both mediated through cadherins [151]. Cadherins are a large superfamily of cell surface proteins, which can be divided into different subtypes, the best studied of which are the classic

cadherins. Classic cadherins are transmembrane, Ca^{2+}-dependent, homophilic, cell-adhesion molecules that mediate cell-cell adhesion, signaling and the anchoring of the cytoskeleton [152]. Based on phylogenetic relationships, the classic cadherins can be further divided into type I (e.g. E-cadherin, N-cadherin, R-cadherin [152]) and type II (e.g. VE-cadherin [152]) cadherins [153]. The classic cadherins consist of three domains: a repeated extracellular domain and a cytoplasmatic tail domain, which are connected by a single-pass transmembrane anchoring domain [154]. The extracellular region, containing the adhesive function, is composed of five extracellular cadherin (EC) domains [155], with Ca^{2+} binding sites at each interdomain junction [156]. Ca^{2+} binds together the EC domains, forming stiff and rod-like proteins [152] that physically connect the extracellular parts of the cadherins of neighboring cells [151] and form a trans-dimer [157], thus mediating direct cell-cell interaction [151]. Intracellularly, catenins (α-catenin, β-catenin and p120-catenin) are the main cytoplasmatic binding partners for cadherins [158]. On the cytoplasmatic tail, there are two non-overlapping and divers binding domains [159]: the juxtamembrane domain that binds to p120-catenin, and a catenin-binding domain binding to β-catenins [151]. This cadherin-β-catenin complex then binds to α-catenin [158], which then either binds directly the actin filament or indirectly via other actin-binding proteins (e.g. vinculin, ZO1, α-actinin) linking the cadherins physically [152] and functionally [159] to the actin cytoskeleton [152, 159]. Thus, via adherens junctions, the cytoskeletons of adjacent cells are connected and are part of a linear chain [155] to transmit mechanical signals between cells [157] in a bidirectionally regulated way which modulates and is modulated by the actin cytoskeleton [159]. Through their binding partners, cadherins can modulate various different signaling pathways like Hippo, RhoA GTPases, and Wnt pathways [160]. Via the cadherin-β-catenin complex, Piezo channels interact with the actin cytoskeleton. Disruption of E-cadherin or β-catenin in this complex leads to defective Piezo 1 mediated function [161].

Another mechanism for epithelial tumor cells to metastasize is epithelial-to-mesenchymal transition (EMT) [162]. This is a process, in which the non-motile epithelial cells switch to a motile mesenchymal phenotype activated by transcription factors like Twist and Snail, stemming from different signaling pathways as TGF-β and Wnt pathways [31]. This influences cell morphology and contributes to metastasis [163]. Subsequently, in EMT a process occurs that is called “cadherin switching”, a switch in adhesion molecules [140] which upregulates N-cadherin (mesenchymal adhesion protein [164]) and downregulates E-cadherin (epithelial adhesion protein [164]). This leads to a dissociation of cell-cell junctions (AJ for example), and to migration and invasion in cancer [165]. Drug resistance in cancer can also be induced by EMT, the

specific mechanisms are still a subject of research and may be different in various cancer types [166]. EMT can be observed in various types of cancer [167–169]. In MN, due to the fact that MN are derived from neural crest cells and are not *per se* of epithelial origin, cells undergo an “EMT-like transition”, a phenotypical switch with similarities to EMT, the cadherin switching for example [164]. MC and KC lose their connection, which is the initial step for the metastatic cascade [49].

5.4 Cholesterol: MTD, cholesterol-rich structures and cancer

As a fundamental border, the plasma membrane (PM) separates the cell from its environment [170]. When mechanical forces reach the PM, it functions as a scaffold platform that modulates signaling [145]. The PM is an asymmetric bilayer formed by a high amount of transmembrane proteins, carbohydrates and lipids like glycerophospholipids, sphingolipids and cholesterol [170].

Cholesterol is a highly hydrophobic [171] four-ring structure (sterol) molecule which is enriched in the PM [172] where it regulates the membrane fluidity, maintains the structure integrity [173], modulates rigidity and permeability [171], influences the membrane proteins function [174], and makes up 20 – 25 % of the overall lipid molecules. Cholesterol originates from two sources: de novo synthesis and dietary intake with a ratio of about 70:30 [172]. Almost all mammalian cells (e.g. melanocytes [175]) are able to perform the de novo synthesis of cholesterol [171], which is mediated by the mevalonate pathway and starts with acetyl CoA. The rate-limiting enzyme in this pathway is HMG-CoA reductase which catalyzes the conversion of HMG-CoA into mevalonate [172]. Statins, for example Lovastatin, are able to inhibit HMG-CoA reductase and therefore block the de-novo synthesis of cholesterol [176].

Cancer cells are fast-proliferating cells and therefore need a great amount of cholesterol for membrane biosynthesis and other functions [177]. The increased cholesterol demand is satisfied through reprogramming cholesterol metabolism, for example by enhancing de novo synthesis, which is upregulated in many cancers [171]. In melanoma, for example, increased expression of cholesterol synthesis genes correlates with poor patient survival [178]. Cholesterol contributes to cancer growth, development, migration, and invasion [171, 179].

Cholesterol also influences MTD and plays an important role in the PM as well as structures being connected with it:

In the PM, Piezo 1 is associated as clusters and its activation is linked with the “force-from-lipid” model [180] where membrane tension alters lipid-protein interaction and triggers channel gating [121]. Lipids like cholesterol play an important role for all membrane-embedded proteins and can influence their function, especially mechanically gated ion channels such as Piezo 1, where the local membrane concentration of cholesterol modulates the activity of this ion channel [181]. Drug depletion of cholesterol for example reduced Piezo 1 channel sensitivity and decelerated activation. This indicates the interplay between Piezo 1 -mediated MTD and cholesterol [180].

Other structures in the PM are the cholesterol-rich caveolae which exhibit mechanoprotective properties (they buffer changes in the PM tension), function as a MTD signal (they translocate to the nucleus to deliver stress information, e.g. UV-induced stress), and crosstalk with MTD pathways (Hippo pathway, for example) and the actin cytoskeleton (for more details concerning the latter see [182]) [145].

5.5 Adhesion and cancer

The two major adhesive structures, focal adhesions and adherens junctions, are engaged in bidirectional mechanical crosstalk. They show various similarities, like mechanosensing mechanisms, mechanotransduction pathways, structures and links to the cytoskeleton, the role of which in mechanical crosstalk is unclear. Strong adhesion of the cell-cell junctions decreases the adhesion to the ECM, so both adhesion structures influence each other inversely [183]. Cell adhesion (cell-cell and cell-ECM) is fundamental for cellular morphology, survival, differentiation, migration, proliferation, and is also pivotal for tissue integrity [184]. Any changes [185] or downregulation [184] in the adhesion molecule system leads to detachment of cancer cells from their primary site and invasion through neighboring tissues [184, 185]. Prostaglandins influence cell-cell contacts, their formation and disassembly. If cadherin adhesive connections are stimulated by prostaglandins, the cell-cell connections are lost [186]. The loss of adhesion molecules means invasiveness, an important characteristic of MN [67]. Cancer cells become increasingly motile, degrade the ECM [151], intravasate into the circulation (lymphatic system or blood stream) and form metastases at distant sites [184]. Thus, in cancer progression and metastasis, cell adhesion molecules have a significant part [187].

It also has to be mentioned that there exists a bidirectional crosstalk between cancer cells and the tumor microenvironment which enhance the progression of tumor malignancy and metastasis [188], for more details see also [162, 189]

Taken together, MTD through integrins, cadherins, cholesterol structures and Piezo, as well as cell adhesion molecules play an important role in cancer progression and metastasis. Therefore, therapies try to intervene in these processes.

5.6 Drugs for the manipulation of the MTD apparatus

5.6.1 Lovastatin

Lovastatin is a hydrophobic natural compound of the fungus *Aspergillus terreus* and belongs to the group of statins. It is clinically used to treat hypercholesterolemia. Like all statins, it inhibits the rate-limiting enzyme of the cholesterol de-novo-synthesis, HMG-CoA reductase [176], see 5.4. Besides their cholesterol lowering effects, statins minimize the activation of MMPs [190], significantly inhibit cell proliferation, induce apoptosis [179, 191], inhibit invasion and angiogenesis [191]. Lovastatin for example promotes apoptosis and inhibits proliferation in different kinds of cancer [191] such as MN [192]. In MN, Lovastatin furthermore reduces cell growth, angiogenesis [193] and inhibits invasion and migration in a dose-dependent matter [192]. Statins such as Lovastatin are also used in combination therapy with anti-cancer drugs, where they show synergistic effects to master drug resistance [191]. These effects are also observed in murine MN cell lines [194].

5.6.2 Yoda-1

Yoda-1 is a synthetic small molecule selectively activating both human and murine Piezo 1 channels [195] which leads to Ca^{2+} influx [196], see 5.1. It lowers the mechanical threshold of the channel activation by serving as a molecular wedge [128]. Yoda-1 also mimics the effect of constant laminar shear stress on endothelial cells in static cultures [197], inhibits epidermal growth factor (EGF)-induced macropinocytosis. in human epidermoid carcinoma cells [196] and decreases the expression of MMPs in human osteoarthritis chondrocytes [198].

5.6.3 Celecoxib

One of the hallmarks of cancer is inflammation [199], that predisposes to cancer development and supports tumorigenesis at all stages [200].

Prostaglandin E_2 (PGE_2) represents an inflammatory factor that reacts to pain, inflammation and immune response [201]. It is a downstream metabolic product of the proinflammatory enzyme cyclooxygenase-2 (COX-2) from the so-called COX-2/PGE_2 pathway [202]. In this pathway, COX (consisting of the two isoforms COX-1 and COX-2)

catalyzes the rate limiting step in the biosynthesis of PGE_2 from arachidonic acid (AA) [201, 203].

COX-2 plays an important role in cancer development and progression (e.g. promotes cell proliferation, inhibits cell apoptosis, stimulates angiogenesis, influences cell adhesion), is responsible for drug resistance [67, 204] and is highly expressed in various cancer tissues [201, 205, 206] such as MN [207]. In MN, COX-2 induces MMP 2 and 14 (responsible for ECM degradation, vascular mimicry, and tumor invasion), tumor progression and chemoresistance [67]. PGE_2 reduces apoptosis, increases metastasis and angiogenesis, as well as tumor growth and invasion, suppresses anti-tumor immunity [208] and plays an important role in carcinogenesis of MN [67]. Taken together, the COX-2/PGE_2 signaling axis plays an important role in cancer development [201, 205].

COX, especially COX-2 and therefore the COX-2/PGE_2 pathway, can be suppressed for example by selective NSAIDs (non-steroidal anti-inflammatory drugs) like Celecoxib (CXB) [209] which binds COX-2 about 375-fold more selectively than COX-1 [210]. This specific COX-2 inhibitor is clinically used mainly for the therapy of inflammatory diseases (e.g. inflammatory musculoskeletal conditions [211], rheumatoid arthritis, and osteoarthritis [210]) [201]. In cancer, CXB inhibits the migration and invasion of cancer cells [201, 212], makes cancer cells more susceptible towards radiation therapy [212], significantly reduces the response of multidrug resistance [201], and promotes the lethal effect of chemotherapeutic drugs [201, 213].

As a single agent, CXB shows significant growth inhibition as well as apoptosis in MN which both seem to be independent of COX-2 expression [214]. A low dose of CXB alone (50 nM) also shows antineoplastic effects [215]. Additive anti-tumor capabilities were observed in combining CXB with rapamycin (an mTOR antagonist) by inhibition of proliferation [214], as well as an increase in MN cell sensitivity to trametinib (a MAP kinase inhibitor), which promotes the therapeutic treatment response [215]. Combined with plumbagin (which suppresses STAT3, AKT/mTOR and NF-κB) CXB exerts a synergistic effect against MN cells by inhibiting COX-2 and STAT3 [216].

Taken together, the effect of CXB on the one hand relies on the inhibition of the COX-2/PGE_2 pathway, and on the other hand there exist COX-2 independent ways [217]. The anti-tumor action of CXB is still needed to be further explored [213].

6 Aim of the thesis and experimental layout

This thesis is an attempt to get a better understanding of the molecular mechanisms sustaining the progression of melanoma, one of the deadliest forms of all skin cancers, as described above.

The principles and processes of MTD are tightly linked to the development of metastasis. Since the key structures of adhesion (e.g. integrins in FA) and other structures as force-sensitive ion channels (like the Piezo family) also act as mechanosensors, they have a proven impact on the development of MN metastasis. Drugs that manipulate and intervene with the pathways connected to these structures might provide precious insights into molecular mechanism of action sustaining the progression of melanoma and open in this way new perspectives in cancer therapy – in this thesis, the three selected drugs, namely celecoxib, lovastatin and Yoda-1, which are meant to manipulate crucial aspects of melanoma mechanical competence, targeting the cell membrane from different molecular pathways.

To evaluate the effect of the different drugs, a de-adhesion assay was established. This assay was then performed with two xenograft derived MN cell lines, the cutaneous MN cell line (YDFR-C) and the brain metastatic MN cell line (YDFR-CB), after a static incubation of 24 hours with one of the selected drugs in a concentration of 1µM each. The main goal was to investigate the impact on the morphology and de-adhesion process of the cells – the latter being crucial for metastasis. The question arising was, if the YDFR-C cells were more readily detaching from a stiff substrate than the YDFR-CB cells – cells that had already once detached from their original site and had undergone and adapted to the physiological stress of the metastatic cascade - and how the different drugs influenced this behavior and mechanosensitive processes.

In addition, a quantitative total protein profiling of both cell line (YDFR-C and YDFR-CB) in every condition (treated or control) was performed via mass spectrometry-based proteomics. A number of up- and downregulated proteins of interest were selected, and the results were compared to each other to investigate differences and changes in both, conditions and cell lines.

With this experimental setup, we tried to get a better understanding about the different medication impacts on MN cells, their interplay with mechanosensory structures, how the cells respond to these different kinds of manipulation, and thus taking another step forward in our understanding of MN as well as towards future therapeutic approaches.

7 Material and Methods

7.1 Cell culture, materials and instruments used, and preparation of reagents

Here the used MN cell lines are briefly described, their general handling, the routinely used reagents and materials, the preparation of the reagents used for the analyses, as well as the instruments used during the preparation of the assays, and define their denomination or abbreviation used in this chapter:

7.2 Cell culture

Both human cancer cell lines, the cutaneous melanoma cell line (YDFR-C) and the brain metastatic melanoma cell line (YDFR-CB), were briefly described and for more detailed information cross linked in Neuditschko et al., 2020 [218]. These cells were cultivated in RPMI 1640 (1X) medium (Gibco™, Thermo Fisher Scientific) which contains L-glutamine, glutathione and high concentrations of vitamins, but no lipids, proteins or growth factors. This medium uses a sodium bicarbonate buffer system (2.0 g／L) with a Phenol Red Indicator. It was supplemented with 10 % (v/v) heat inactivated foetal Bovine Serum (Sigma-Aldrich), and 1 % (v/v) Penicillin G and Streptomycin (Sigma-Aldrich). The medium was aliquoted in 50 mL polypropylene Screw Cap Tubes (Sarstedt AG & Co. KG) and stored at 4 °C at the fridge (Liebherr). This fully supplemented and aliquoted RPMI (1x) medium is denominated “fully supplemented RPMI medium” from now on. Cells were grown in cap filtered T25 standard polysterene tissue culture flasks with treated surface for adherent cells with a 25 cm^2 growth area (Sarstedt AG & Co. KG) and will be denominated from now on “T25 culture flasks”. They were incubated in a humidified incubator (Panasonic Healthcare or Thermo Fisher Scientific) at 37 °C and 5% CO_2 (these conditions are denominated “standard conditions” from now on). The cell viability was checked during the week every day based on visual observation with a cell culture microscope (Olympus-Lifescience) and sub-cultured based on a recurring rhythm every 3rd or 4th day - at the latest, with an 80 % confluence. For the assays, cells were passaged 20 times maximum. To maintain sterile working conditions during work on the cell cultures, during drug treatment, during the preparation of reagents as well as during different stages of aliquoting (drugs, reagents), all procedures were executed in a laminar flow hood (Thermo Fisher Scientific) – a fact that will be taken for given and will subsequently no longer be mentioned.

7.2.1 Determination of cell number

Cell numbers were always determined with the MOXI Z Mini Automated Cell Counter (Orflo Technologies) and the belonging MOXI Z (Type M) Cassettes (Orflo Technologies). For this, 100 µL cell suspension was applicated into the designed opening on the MOXI Z (Type M) Cassette. Thereupon the cell number was counted automatically by the MOXI Z Mini Automated Cell Counter. From now on this process will be termed “determination of cell numbers with MOXI cell counter”.

7.2.2 Preparation of drug stock solution

Depending on the solubility of the powdery drugs Lovastatin (Enzo Life Sciences), Yoda-1 (Sigma-Aldrich) and Celecoxib (Sigma-Aldrich), DMSO (Carl Roth) was used to prepare the stock solutions with the highest possible concentration (depending on the solubility product). Thereby, stock solutions with the following concentrations could be achieved:

Table 2: stock solutions of the used drugs

drug	solved in	final concentration
Celecoxib	DMSO	100 mM
Lovastatin	DMSO	20 mM
Yoda-1	DMSO	30 mM

For easier handling, the different stock solutions were intermediately diluted, aliquoted and stored at the freezer (Liebherr) at -20 °C.

7.2.3 Preparation of drug media

For each drug, a separate drug medium was prepared on the day of the drug treatment. For this, 5 mL of fully supplemented RPMI medium was provided in a 15 mL Falcon Tube. Afterwards, 5 µl and 50 µl each were removed from the tube and 5 µl of the diluted drug, as well as 50 µl LC-MS grade H_2O (Sigma-Aldrich) added.

Water was added because of another drug (PKA) which had to be diluted in autoclaved bi-distilled H_2O and was part of the original experiment layout, but is not subject of this thesis. Thus, drug media with the requested drug concentration (Celecoxib 1 µM, Lovastatin 1 µM, Yoda-1 1 µM) and the same parts of DMSO and H_2O respectively were achieved.

7.2.4 Trypsin for the de-adhesion assay

The enzyme´s function is to retract the spread-out adherent cell at the bottom of the cell culture vessel after a short delay to a rounded shape. This process is called de-adhesion or detachment [219]. The enzyme selected was trypsin, which cleaves between the carboxyl acid group and the amino group of the adjacent amino acid inside the peptide bond, predominantly between arginine or lysine [220]. It shows an enzyme activity of about 3,500 BAEE U/mL, as the de-adhesion of both cell-lines (YCDF-C and YDFR-CB) sets in delayed in time. This retardation allowed a better tracking of the cells and the onset and development of the ongoing de-adhesion process could be monitored more easily. To improve the handling and reproducibility of the de-adhesion assay, an adequate amount of trypsin with the above-mentioned enzyme activity was produced out of trypsin powder (Gibco™, Thermo Fisher Scientific), 99% EDTA (Carl Roth), PBS (10X) and in autoclaved bi-distilled H_2O as follows:

In a 500 mL autoclaved Duran laboratory bottle (DURAN®) 50 mL PBS (10X), 450 mL autoclaved bi-distilled H_2O, 77.832 mg 99 % EDTA and 2.0719 g trypsin powder were mixed on ice, pH value (7.1) verified (VWR), sterile filtered (Sarstedt AG & Co KG), aliquoted 1.2 mL each in reaction tubes (Sarstedt AG & Co KG) and stored at -20 °C (Liebherr) until used for the experiments.

In addition, DPBS (1X) (Gibco™, Thermo Fisher Scientific) was aliquoted and stored at +4 °C (Liebherr) until used for the de-adhesion experiments.

7.2.5 General preparations for the experiments

For the deadhesion assay, cells were seeded in TC 35 standard polysterene tissue culture dishes for adherent cells with a 9.4 cm^2 growth area (Sarstedt AG & Co. KG, “T35 culture dishes”). For the analysis of proteomics, cells were seeded in a standard polysterene 6-well cell culture plate for adherent cells (Sarstedt AG & Co. KG).

7.3 Cell passaging

The cells were cultivated exclusively in T25 culture flasks under standard conditions, the following information and volume indications always refer to those flasks.

For the cell passaging, the fully supplemented RPMI medium, modified Dulbecco’s Phosphate–Buffered Saline (DPBS, without calcium chloride and magnesium chloride, DPBS Gibco™, Thermo Fisher Scientific) and Trypsin-EDTA solution 0,25% (Sigma-Aldrich) were warmed up in a water bath (VWR International) to 37 °C.

First, the medium was removed and the cells were washed with 5mL warmed up DPBS. Then the cells were incubated with 2 mL warmed up Trypsin-EDTA solution and placed

for 3 minutes in the incubator-chamber at standard conditions. The enzyme was disabled by adding 4mL warmed up fully supplemented RPMI medium and the whole solution was carefully suspended 3 to 4 times. Then the solution was transferred into a 15 mL Falcon Tube (Sarstedt AG & Co. KG) and placed into a tempered (23 °C) centrifuge (Thermo Fisher Scientific) and centrifuged for 5 minutes at 220 x g. After having removed the supernatant, the cell pellet was resuspended in 5mL warmed up fully supplemented RPMI medium. The cells were seeded in a ratio of 1:5 into T25 culture flasks, each endowed with 4 mL warmed up fully supplemented RPMI medium. Finally, the cells were cultured under standard conditions.

7.4 Experimental workflow

From cell seeding to experiment is a three days´ process (for a short overview see Figure 5):

- day 1: cell seeding (80,000 cells)
- day 2: drug treatment (Celecoxib, Lovastatin, Yoda-1)
- day 3: experiment (de-adhesion assay or proteomic analysis)

7.4.1 Day 1: Cell seeding

In short, cells (YCFR-C and YDFR-CB) were cultured as mentioned in 7.2 Cell culture. After the determination of the cell number with MOXI cell counter, 80,000 cells per each condition were seeded in T35 culture dishes for the de-adhesion assay and for proteomics analysis in 6-well plates.

In detail, the procedure is the same as described in 7.3 Cell passaging, including the resuspension of the cell pellets in 5 mL warmed up fully supplemented RPMI medium. Then 500 µl cell suspension were transferred to a reaction tube (Sarstedt AG & Co KG) for the cell counting with the MOXI cell counter (as described in 7.2.1). Meanwhile, the remaining 4.5 mL cell suspension was stored in the incubator at standard conditions.

Based on these results and depending on the experiment, 80,000 cells per cavity were seeded, for the de-adhesion assay in TC 35 standard culture dishes, for the analysis of proteomics in a 6-well plate. After seeding, each cavity was filled up with warmed up fully supplemented RPMI medium to the volume of 2 mL and cultivated for 24 hours at standard conditions.

7.4.2 Day 2: Drug treatment

For the drug treatment, the used fully supplemented RPMI medium of the cells seeded the day before was replaced by 2 mL drug medium (see 7.2.3). The cells were then incubated for 24 hours under standard conditions.

7.4.3 Day 3: Experiments

After the cells had been incubated with the drugs for 24 hours, they were ready for the following experiments:

- De-adhesion assay (7.4.3.1)
- Proteomic analysis (7.4.3.2)

7.4.3.1 De-adhesion assay

In short: during the de-adhesion assay, the adhesion of the cells after trypsinization is tracked over a defined period of time and is illustrated visually at certain time intervals. The measurements obtained were used for further calculations. De-adhesion followed a sigmoidal curve and divided into 3 phases (see Figure 6):

- a lagged initiation of de-adhesion (trypsin detaches FA contacts between surface and cell [221])
- quickly proceeding cell contraction (until rounding of the cells [221])
- which finally ended in a plateau phase (with no further changes in cell size)

The paper of Sen and Kumar, 2009 [219] was taken as a model to establish the de-adhesion assay.

In detail, before the de-adhesion assay could be started, diverse settings concerning hard- and software of the microscope had to be adjusted (objective lens: 20-fold magnification; software [Olympus cellSens Entry]: total magnification 20 x1, calibration X and Y 110 nm per pixel; entitling of the assay as well as automated saving of the pictures). Furthermore, a tempered water bath (37 °C) and a laboratory bucket filled with ice were prepared.

For the handling of the de-adhesion assay, a recurring 6-minute cycle had proven successful. One cycle was designed as follows:

At the beginning, a T35 culture dish was taken from the incubator and the drug medium removed and discarded. The cells were washed with 1 mL warmed up prepared DPBS (vortexed), the DPBS was then also discarded. An appropriate area with a confluence of about 40 – 60 % was selected under the microscope and a picture was taken (t = 0 s). From then on, the T35 culture dish did not have to be moved.

The assay started by adding 1 mL warmed up prepared trypsin – vortexed slightly and pipetted at the brink of the T35 culture dish, with the time being measured with a stopwatch from the moment the enzyme was added. Every 5 second a picture was taken at 20-fold magnification and thus the progression of the de-adhesion was recorded. After 180 seconds, the assay was completed with 36 pictures taken, altogether 37 pictures with the first picture at t = 0 s. The time span of 180 seconds proved suitable for the assay to guarantee that with both cell lines (YDFR-C and YDFR-CB) the de-adhesion process was completed with regard to all drug treatment variants (see 7.2.3).

To keep the conditions the same and thus to improve the reproducibility of the experiments, both the prepared trypsin and the prepared DPBS were kept in the water bath (37 °C) for 6 minutes (this corresponded with one complete cycle of the assay) and were replaced by a cold one to be preheated after removal. The temperature of the water bath was controlled by an additional thermometer and was kept constant at 37 °C. The 6-minutes assay cycle (as mentioned above) was kept continuously and was monitored with a stopwatch. For the de-adhesion assay, trypsin with specific enzyme activity was produced (prepared trypsin), aliquoted and stored at -20 °C until usage (see 7.2.4). The order of the different conditions was randomized with each assay to limit experimental bias. If with the first de-adhesion assay the condition “Celecoxib 1 µM” was analyzed at first rank for example, it was placed at a different rank with the next. The cells in the petri dishes remained in the incubator at standard conditions and were only removed when being used.

7.4.3.1.1 Evaluation of the pictures with ImageJ

In short: during the de-adhesion assays, the de-adhesion of the cells was photographed in a period of 180 seconds every 5 seconds after trypsinization. So, the progression of the de-adhesion could be recorded in 37 pictures and be analyzed graphically by the openly available software ImageJ.

At the beginning of the analysis, the picture t = 0 s (the actual state at the time the assays start) was uploaded and the scaling properties of the picture (they could be read from the software of the microscope during the assay) were entered in the evaluation software ImageJ (0.11 µm per pixel). Afterwards, an outside party not engaged in the experiments picked 10 cells evenly distributed over the whole picture in a Z-layout, so that the personal bios of the investigator who was familiar with the expected behavior of the cells was bypassed (see Figure 4).

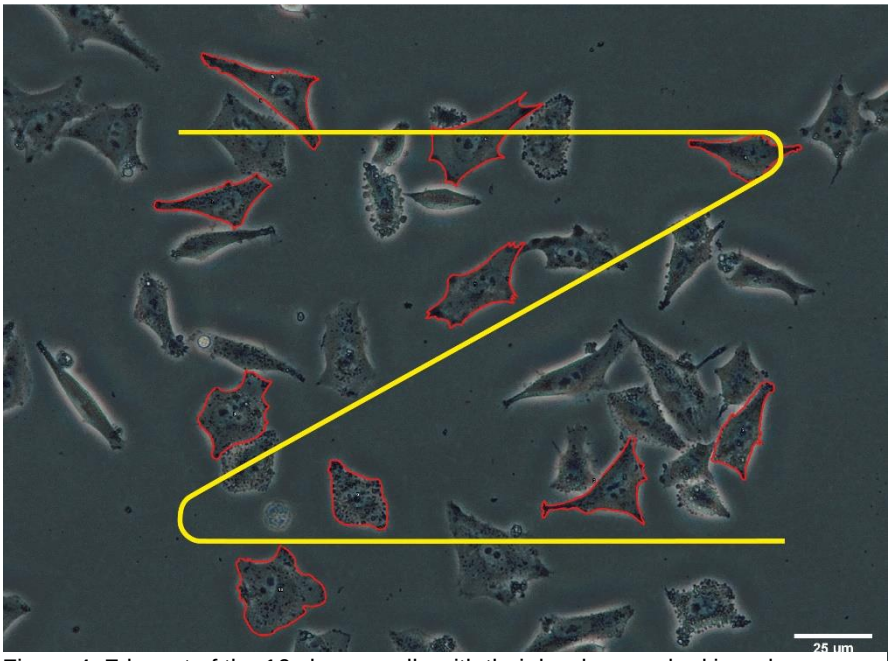

Figure 4: Z-layout of the 10 chosen cells with their borders marked in red

Thereupon the pictures were magnified to 150 %, the borders of the preselected cells were marked freehand on a Surface Pro laptop with touchscreen by means of a surface pen and were tracked as ROI (region of interest) during the whole assay. For this, the pictures t = 0 s, t = 5 s and then in intervals of 10 seconds t = 15 s … until t = 175 s and at last t = 180 s were used respectively. The interval of 5 seconds both at the beginning and the end of the assay had the reason to delineate the curve progression of the de-adhesion process more subtly.

After having marked the last cell in the active picture, the program ImageJ calculated the preset parameters: area, center of mass, and shape description (circularity, aspect ratio, roundness, solidity). These data were transferred into an excel-file and the beforehand marked cells were saved as a ROI file. For a rough overview of how the image analysis by ImageJ could be like, see [222].

So, the development of the de-adhesion for each of the 10 marked cells in one de-adhesion assay could be displayed graphically as a curve through 20 measuring points and form the basis for further calculations.

7.4.3.1.2 Calculations and statistic evaluation

The data from the ImageJ analysis saved as an excel file (see 7.4.3.1.1) were transferred to Origin software and formed the basis for further calculations, statistical analysis and graphic presentations.

7.4.3.1.2.1 Cell describing parameters and spider web charts

The cell describing parameters were calculated automatedly by ImageJ with the following underlying formulas.

Circularity (also called form factor or compactness), is a size-independent [223] and dimensionless parameter [224] which indicates mathematically the closeness to a perfect circle [225]. The values range from 1 and 0 [224], with 1 being a perfect circle [226], a smaller value denoting a more spindle-shaped cell [227] and 0 describing a straight line [228]. Schöchlin et al. [228] suggested a circularity classification as follows: round (circularity values greater equal 0.8 to smaller 1), oval (circularity greater equal 0.6 to 0.8), elongated (circularity value greater equal 0.35 to 0.6), and spindled (circularity greater 0 to 0.35). It is important to note that this classification is based on nuclear shapes [228].

$$\text{Circularity} = \frac{4\pi \cdot \text{Area}}{\text{Perimeter}^2}$$

Aspect ratio (AR) is the ratio of the cellular major to minor axes and describes how elongated cells are [226], with the value 1 being a perfect circle and a rise in AR meaning an increase of deformation [229].

$$\text{Aspect Ratio} = \frac{\text{Major Axis Length}}{\text{Minor Axis Length}}$$

Cell roundness is described by the ratio of “area” to “long axis” [230]. It is similar to circularity but non-sensitive to irregular borders [225] – the parameter is normalized to 1, with 1 representing a circle [230].

$$\text{Roundness} = \frac{4 \cdot \text{Area}}{\pi \cdot \text{Major Axis Length}^2}$$

Cell solidity is the ratio of the cell area and its convex hull area and is used to measure the density of a cell (or cellular construct), with 1 describing a solid object. Values <1 correspond to irregular boundaries or concavities of the object [223].

$$\text{Solidity} = \frac{\text{Area}}{\text{Convex Hull Area}}$$

For the graphical representation of the data in spider web charts, the cell describing parameters were edited so that they all took on a value between 1 and 10 and fitted into the spider web charts. These parameters were edited as follows: Area was divided by 100, circularity, roundness and solidity was multiplied by 10.

7.4.3.1.2.2 Calculations of the normalized area

The area data collected were at first normalized on the basis of this formula:

$$\mathrm{Area}_{(\mathrm{normalized})} = \frac{\mathrm{A}_{(\mathrm{start})} - \mathrm{A}_{(\mathrm{t})}}{\mathrm{A}_{(\mathrm{start})} - \mathrm{A}_{(\mathrm{end})}}$$

in which $A_{(start)}$ represents the area at the beginning of the assay (t = 0 s), $A_{(end)}$ the area at the end of the assay (t = 180 s) and $A_{(t)}$ representing the area at any time chosen (t = x s). Thereby the area values (μm^2) were transformed in unit-free values between 0 and 1, with 0 being the area at the start of the assay (t = 0 s) and therefore the biggest area and 1 being the smallest area at the end of the assay (t = 180 s).

Normalization of the area was conducted so that instrumental parameters (e.g. magnification) and units were omitted, as well as the area curve progression into a sigmoidal curve was achieved.

7.4.3.1.2.3 Statistic evaluation

For the statistical analysis of the de-adhesion assay, the normalized data were used to perform a dose-response analysis (DRA) and thereupon the obtained data were statistically analyzed with a two-sample t-test or ANOVA.

It is important to mention that for the DRA function the following formula (already implemented in the Origin software) is used:

$$\mathrm{y} = \mathrm{A}_1 + \frac{\mathrm{A}_2 - \mathrm{A}_1}{1 + 10^{[(\mathrm{LOGx0} - \mathrm{x}) \cdot \mathrm{p}]}}$$

with A_1 being the lower (bottom) asymptote, A_2 the upper (top) asymptote, p being the hill slope and LOGx0 the center (turning point of the curve). For both A_1 (fixed value = 0) and A_2 (fixed value = 1) predetermined values were assigned, as the normalized area values always range between 0 and 1 (see 7.4.3.1.2.2)

As a result of the DRA one receives effective time (ET) values, in this case ET_{20}, ET_{50}, and ET_{80}. The half maximal effective time (ET_{50}) value represents a point of time (in seconds) at which the curve of the normalized area has covered 50 % (half the way) between the minimum and maximum response – the other subscripted numbers represent the points of time of respective curve progressions (20 or 80 %).

7.4.3.2 Proteomics (proteome profiling)

In short: the treated cells were subdivided into a cytoplasmatic and a nucleus fraction, lysed and proteins were precipated in ethanol. After storage at -20 °C in the freezer, the precipates for the mass spectrometric analysis (proteome profiling) were prepared and afterwards measured.

7.4.3.2.1 Cell lysis: cytoplasmatic fraction (CYT) and nucleus fraction (NE)

In short: cell lysis by shear force (physically based) and receipt of the cytoplasmatic isolate (supernatant) after centrifugation. The remaining pellet was lysed reagent based after resuspension and the nuclear extract was received after centrifugation. Both fractions were alcoholically (ethanol) precipitated.

The cell fractionation and the disruption of these fractions was performed with the “cell fractionation Standard Operating Protocol (SOP) for adherent cells (updated version 2016-10-26)” which is established in the research group of Prof. Gerner. This was operated in detail as follows:

Before SOP was performed, the treated cells were photographed with the microscope (Carl Zeiss Microscopy GmbH). All work was conducted on ice, the reagents used (see 7.5.3) were put on ice and the centrifuge (Thermo Fisher Scientific) was cooled down to 4 °C. To receive the cytoplasmatic fraction (synonymously cytoplasmatic isolate), the medium was discarded, the cells were washed twice with 1 mL cold PBS (Sigma-Aldrich) each, and this washing solution was again discarded. After adding 1 mL cold lysis buffer, the adherent cells were scrapped off using a cell scraper (the same cell scraper was used for biological replicates). The cell suspension was transferred into a new 15 mL falcon tube with the aid of a syringe and needle (the same were used for biological replicates) and was then lysed by shear forces at the wall of the falcon tube. This process was repeated 10 times, until the cell lysis was completed (the progress of the lysis was microscopically screened via dropping and fixing the cell lysate on a cover slip). Afterwards the cell lysate was placed into a cooled centrifuge and centrifuged for 5 minutes at 2,227 x g. In a new 15 mL falcon tube with 4 mL prepared ice-cold ethanol (EtOH, 99 %, Austro Alco) the supernatant (cytoplasmatic isolate) was transferred and precipated. This falcon tube was sealed with Parafilm and kept with the top up at -20 °C in the freezer – and will be called cytoplasmatic fraction (CYT) from now on.

To receive the nucleus fraction (synonymously nuclear extract), the remaining pellet in the falcon tube was dried up carefully with tissue paper and thus the cytoplasmatic isolate was removed. Afterwards the pellet was re-suspended in 100 µL TE-NaCl and incubated on ice for 10 minutes. Then 900 µL TE-NP40 lysismix were added, vortexed and

incubated for another 15 minutes. Thereupon the falcon tube was placed into a cooled centrifuge and centrifuged for 5 minutes at 2,227 x g. In a new 15 mL falcon tube with 4 mL prepared ice-cold EtOH the supernatant (nuclear extract) was transferred and precipated. This falcon tube was sealed with Parafilm and kept with the top up at -20 °C in the freezer - and will be termed nuclear fraction (NE) from now on.

7.4.3.2.2 Further sample processing and determination of protein concentration

In short, precipated proteins were collected by centrifugation at 5,000 x g for 30 minutes, protein pellets were re-solubilized after drying in Protifi® lysis buffer with subsequent determination of the protein concentration with BCA-assay.

In detail, the protein fractions were stored in the freezer (-20 °C) for at least 24 hours before centrifugation. The falcon tubes were centrifuged in a cooled (4 °C) centrifuge for 30 minutes at 5,000 x g. The supernatant was discarded, and the pellet was dried in a two-stage process at room temperature. For it, the falcon tubes were first dried top down on tissue paper for 20 minutes and then top up for further 30 minutes in vacuum (desiccator). The dried pellets of each fraction were then dissolved overnight in different amounts of Protifi® lysis buffer. The next day, the sample solution was transferred into a labelled 2 mL reaction tube, the protein concentration was determined with a BCA-assay (see 7.4.3.2.2.1) and stored at -20 °C in the freezer until further processing and protein digestion.

Proteolytic digestion of the samples and LC-MS/MS analysis were performed by the team of Prof. Gerner according to the protocols published in [231].

7.4.3.2.2.1 BCA assay (bicinchoninic acid assay)

The bicinchoninic acid assay (BCA assay) was developed in 1985 by Smith et al. [232] for the quantitative determination of the protein concentration and is a combination of the biuret reaction and bicinchoninic acid (BCA) as detection system. There, at first step, the containing proteins reduce under alkaline conditions (triggered either by susceptible amino acids, such as cysteine (Cys), tyrosine (Tyr) and tryptophan (Trp), or by peptide bonds) Cu^{2+} to Cu^{+}. At the second step, Cu^{+} interacts with two molecules BCA forming a purple and stabile complex that absorbs light. The absorption maximum of this complex is at a wavelength of 562 nm. Thereby the protein concentration can be determined quantitatively by means of a calibration standard straight (the ratio of reduced Cu^{2+} to the amount of proteins in the sample is the same) [233].

The BCA assay was performed according to the standard BCA assay protocol by choosing 6 calibration standards to cover a concentration range of 0 – 5 µg BCA. Samples as well as calibration standards were prepared in reaction tubes following below-mentioned pipetting scheme (Table 3). These reaction tubes were placed in a prewarmed (60 °C) thermomixer (Eppendorf AG) and shaken at 1,100 rpm for 30 minutes in the dark. Afterwards 200 µL each were transferred into a 96-well cell culture plate (Sarstedt AG & Co KG) and absorption was measured with a microplate reader (Thermo Fisher Scientific) at 562 nm. The protein concentration was determined quantitatively by means of the calibration standard straight.

Table 3: pipetting scheme of the BCA assay

	BSA (1µg / µL)	**LC-MS grade H_2O**	**Protifi® lysis buffer**	**standard working reagent**	**sample**
Standard 0	0 µL	9 µL	1 µL	200 µL	0 µL
Standard 1	1 µL	8 µL	1 µL	200 µL	0 µL
Standard 2	2 µL	7 µL	1 µL	200 µL	0 µL
Standard 3	3 µL	6 µL	1 µL	200 µL	0 µL
Standard 4	4 µL	5 µL	1 µL	200 µL	0 µL
Standard 5	5 µL	4 µL	1 µL	200 µL	0 µL
Sample	0 µL	9 µL	1 µL	200 µL	1 µL

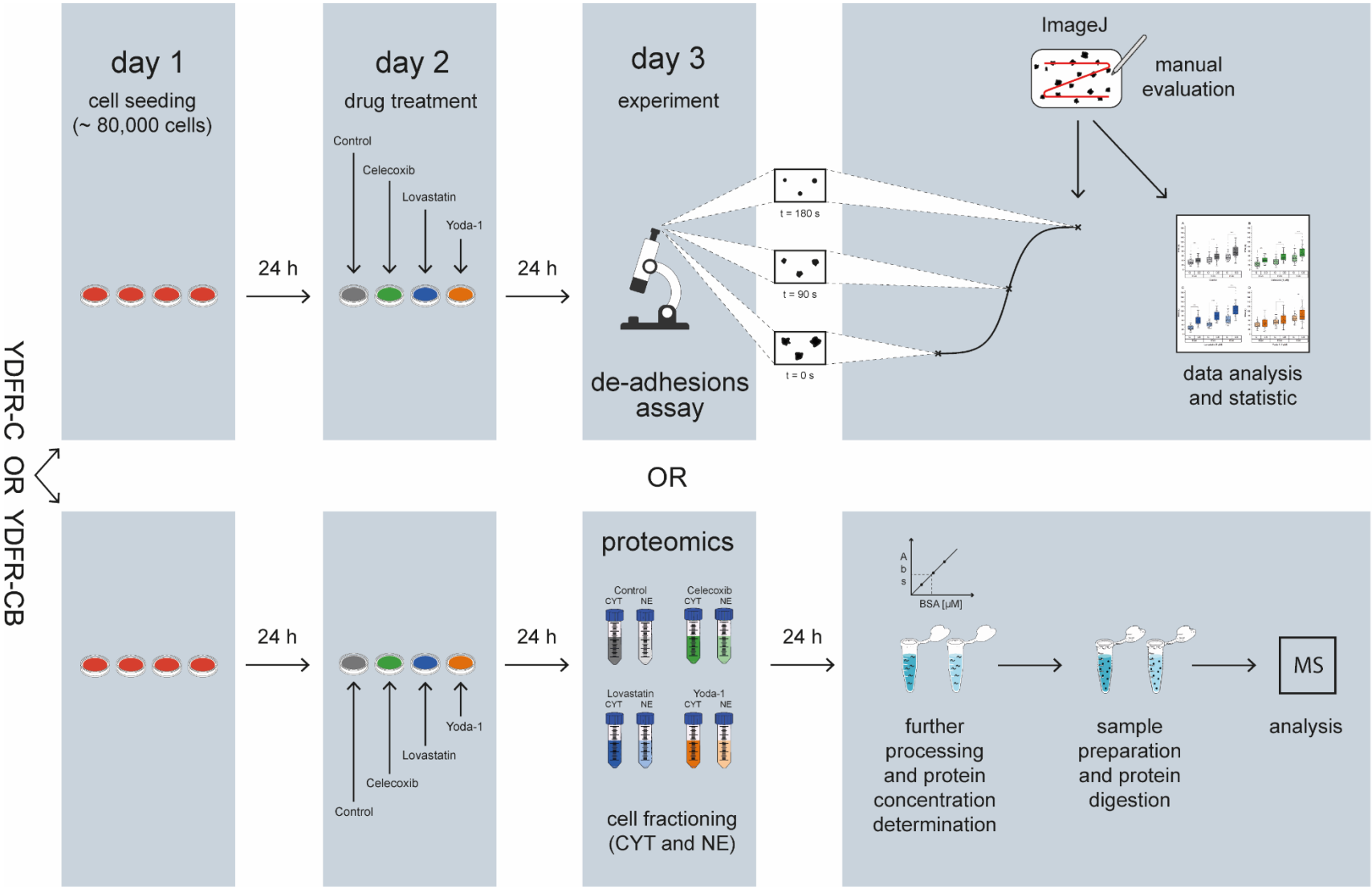

Figure 5: Experimental layout

7.5 Materials

7.5.1 Chemicals and reagents

Chemicals/reagents	Company
Celecoxib	Sigma-Aldrich
Cell freezing Medium-DMSO	Sigma-Aldrich
Dimethylsulfoxide (DMSO) ≥ 99.5 %	Carl Roth GmbH
Dulbecco's phosphate buffered saline (DPBS), -$CaCl_2$, -$MgCl_2$	Gibco^{M}, Thermo Fisher Scientific
Ethanol, 99 %	Austro Alco
Ethanol, absolute, 99.8 %	Thermo Fisher Scientific,
Ethylenediaminetetraacetic acid (EDTA) ≥ 99 %	Carl Roth GmbH
Fetal bovine Serum (FBS)	Sigma-Aldrich
LC-MS grade H2O	Sigma-Aldrich
Lovastatin	Enzo Life Science
PBS (phosphate buffer saline)	Sigma-Aldrich
Penicillin G - Streptomycin	Sigma-Aldrich
PPC (Phosphatase Inhibitor Cocktail)	Sigma-Aldrich
RPMI 1640 (1X) Medium (L-Glutamin und Glutathion)	Gibco^{TM}, Thermo Fischer Scientific
Trypsin powder 1:250	Gibco^{TM}, Thermo Fisher Scientific
Trypsin-EDTA-Solution, 0.25 %	Sigma-Aldrich
Yoda-1	Sigma-Aldrich

7.5.2 Consumption materials and instruments

Instruments/materials	Type	Company
6-well cell culture plate for adherent cells		Sarstedt AG & Co KG
96-well cell culture plate, polystyrene, standard		Sarstedt AG & Co KG
Autoclave	Systec DX-150	Systec GmbH
Balance	Adventurer® Analytical AX224	Mettler-Toledo
	DeltaRange® Microbalance XP 26	Mettler-Toledo
	ML204 NewClassic Analytical Balance	Mettler-Toledo

Cell counter	MOXI Z Mini Automated Cell Counter	Orflo Technologies
	MOXI Z Type M Cassettes	Orflo Technologies
Cell culture dish (TC35 polysterene) for adherent cells, 9.4 cm^2 growth area		Sarstedt AG & Co KG
Cell culture flask T-25 (cap filtered, for adherent cells)		Sarstedt AG & Co KG
Centrifuge	Megafuge™ 16R	Thermo Fisher Scientific
DURAN® Laborflasche (100 mL, 250 mL, 500 mL, 1000 mL)		DURAN Group GmbH
Falcon tube (15 mL, 50 mL)		Sarstedt AG & Co KG
Fridge/Freezer	Liebherr Premium and Comfort (4 °C, -20 °C)	Liebherr
Fume Hood		Prutscher Laboratory Systems GmbH
Incubator	MCO-170AICUV, CO_2	Panasonic Health Care
	Heracell 150i CO_2	Thermo Fisher Scientific
Laminar flow hood	Heraseafe™	Thermo Fisher Scientific
Microplate reader	Multiskan GO Microplate Spectrophotometer	Thermo Fisher Scientific
Microscopy	Olympus CKX53, Objectives: LCAchN 20X/0,40 IPC, CAchN 10X/ 0,25 IPC, UPlan FLW 4X/0,13 IPC	Olympus Life Science GmbH
	Inverted microscope Axiovert 40C, Objectives: A-Plan 5X/0,12 Ph0, A-Plan 10X/0,25 Ph1; Ocular: PL 10X/18	Carl Zeiss Microscopy GmbH
	LSM confocal, ELYRA-systems PS 1, Objectives: Plan-Neofluar 10X/0,30, Plan-Apochromat 63X/1,4 oil, Plan-Apochromat 100X/1,46 oil	Carl Zeiss Microscopy GmbH
	Primo Vert Inverted Microscope	Carl Zeiss Microscopy GmbH
Multi Step pipette	Handy Step®	Brand GmbH &Co KG

Nitrile gloves (powder free)		Kimberly Clark GmbH
pH-meter (Benchtop)		VWR International
Pipette tips (5000 µL), non sterile		Eppendorf AG
Pipette tips (10 µL, 200 µL, 1000 µL), non sterile		Sarstedt AG & Co KG
Reaction tubes (0.5 mL, 1.5 mL, 2.0 mL)		Sarstedt AG & Co KG
Serological pipette (1 mL, 5 mL, 10 mL, 25 mL)		Sarstedt AG & Co KG
Sterile filter	Filtropur V50 vacuum filtration with 0.2 µm pore size	Sarstedt AG & Co KG
Thermomixer	Eppendorf ThermoMixer®	Eppendorf AG
Vacuum Filtration Unit, 500 mL, PES, 0.2 µm	Filtropur V50	Sarstedt AG & Co KG
Vortex	Lab Dancer S40	IKA®-Werke GmbH & Co. KG
Water bath	vwb 12	VWR International

7.5.3 Prepared reagents for proteomics analysis

Reagents	Components
Fraction puffer	10 mM NaCl 10 mM HEPES/NaOH (pH 7.4) 1 mM EGTA (ethylene glycol bis(2-aminoethyl) tetraacetic acid) 3.5 mM MgCl2 0.25 M sucrose 0.5 % (v/v) Triton X-100
Lysis buffer	Fraction buffer with 1:100 PPC and 1:100 PMSF (PPC and PMSF was added shortly before use)
Protifi® lysis buffer	8 M Urea 50 mM tetraethylamoniumbromid (TEAB) 5 % /v/v) sodium dodecyl sulfat (SDS) pH 7.55
PSMF (phenylmethylsulfonyl fluoride)	1.742 g per 100 mL Isopropanol

Reagent A (BCA-Assay)	186 mM sodium carbonat 26 mM bicinchoninic acid disodium salt hydrate 113 mM sodium bicarbonat 8 mM sodium tatrat pH 11.25 (adjusted by using 3 M sodium hydroxide)
Reagent B (BCA-Assay)	200 mM copper sulfate pentahydrate
Standard working reagents (BCA-Assay)	reagent A : reagent B = 50:1 is prepared shortly before use
TE-NaCl buffer	10 mM Tris/HCl 1 mM EDTA 0.5 M NaCl
TE-NP40	10 mM Tris/HCl 1 mM EDTA 0.5 % (v/v) NP-40
TE-NP40 lysis mix	TE-NP40 with 1:100 PPC and 1:100 PMSF (PPC and PMSF was added shortly before use)

7.5.4 Prepared reagents for de-adhesion assay

Reagents	Components
500 mL Trypsin-EDTA in PBS (1X), pH = 7.1, sterile filtered	0.53 mM 99% EDTA 2.0719 g Trypsin powder 1:250

8 Results

8.1 De-adhesion assay

The de-adhesion assay starts with the adding of pre-warmed trypsin which leads to a lagged initiation (phase 1), a contraction of the spread cells until rounding (phase 2), and finally to a plateau phase with no further changes in cell size (phase 3). During this process, the cell area is diminishing. An exemplification curve with representative photographs of how the cells behave during the assay is presented in Figure 6. This effect could be observed in both cell lines (YDFR-C and YDFR-CB) and in every condition (control, CXB, Lovastatin, and Yoda-1).

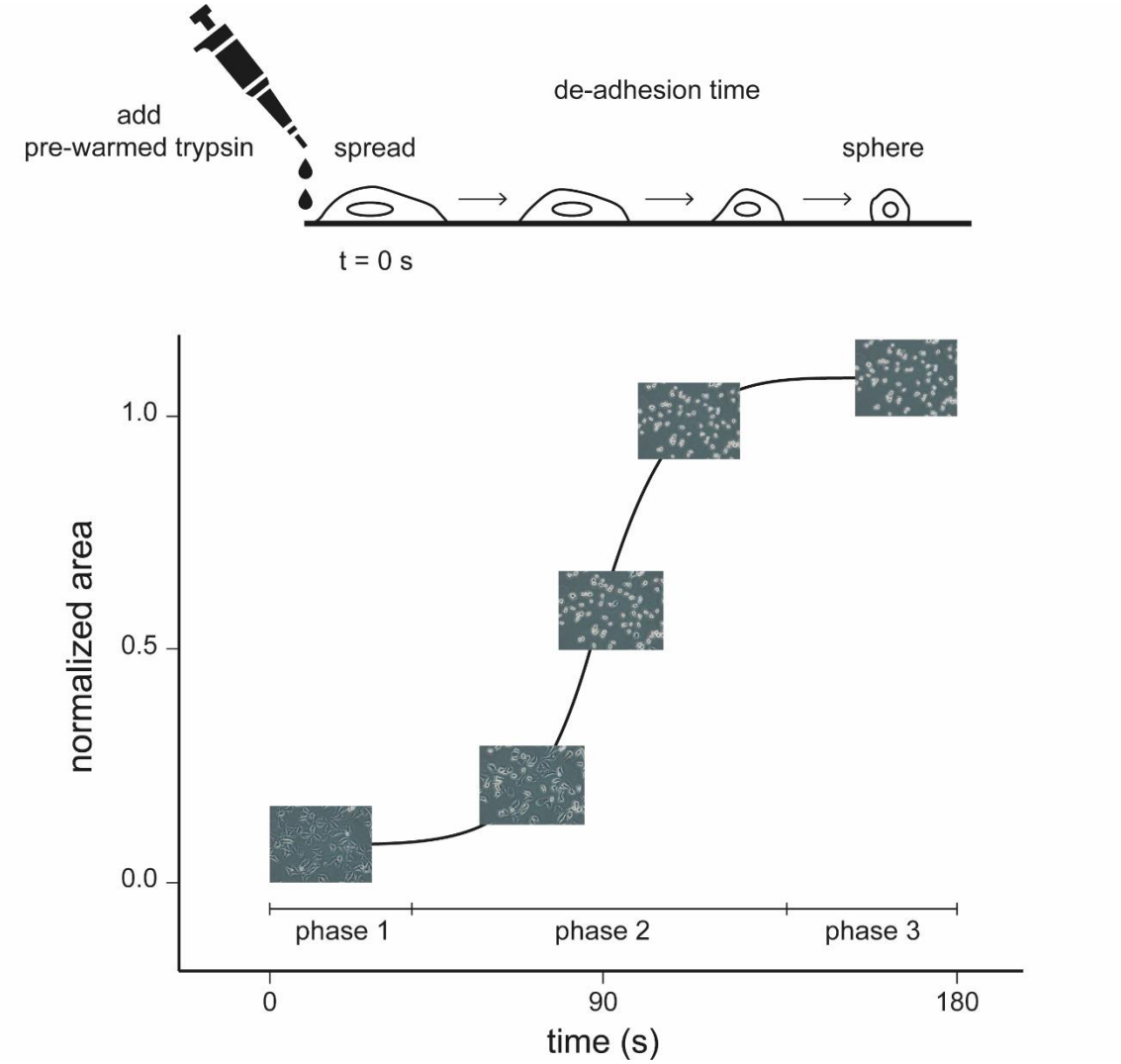

Figure 6: Exemplification curve and overview of the de-adhesion assay

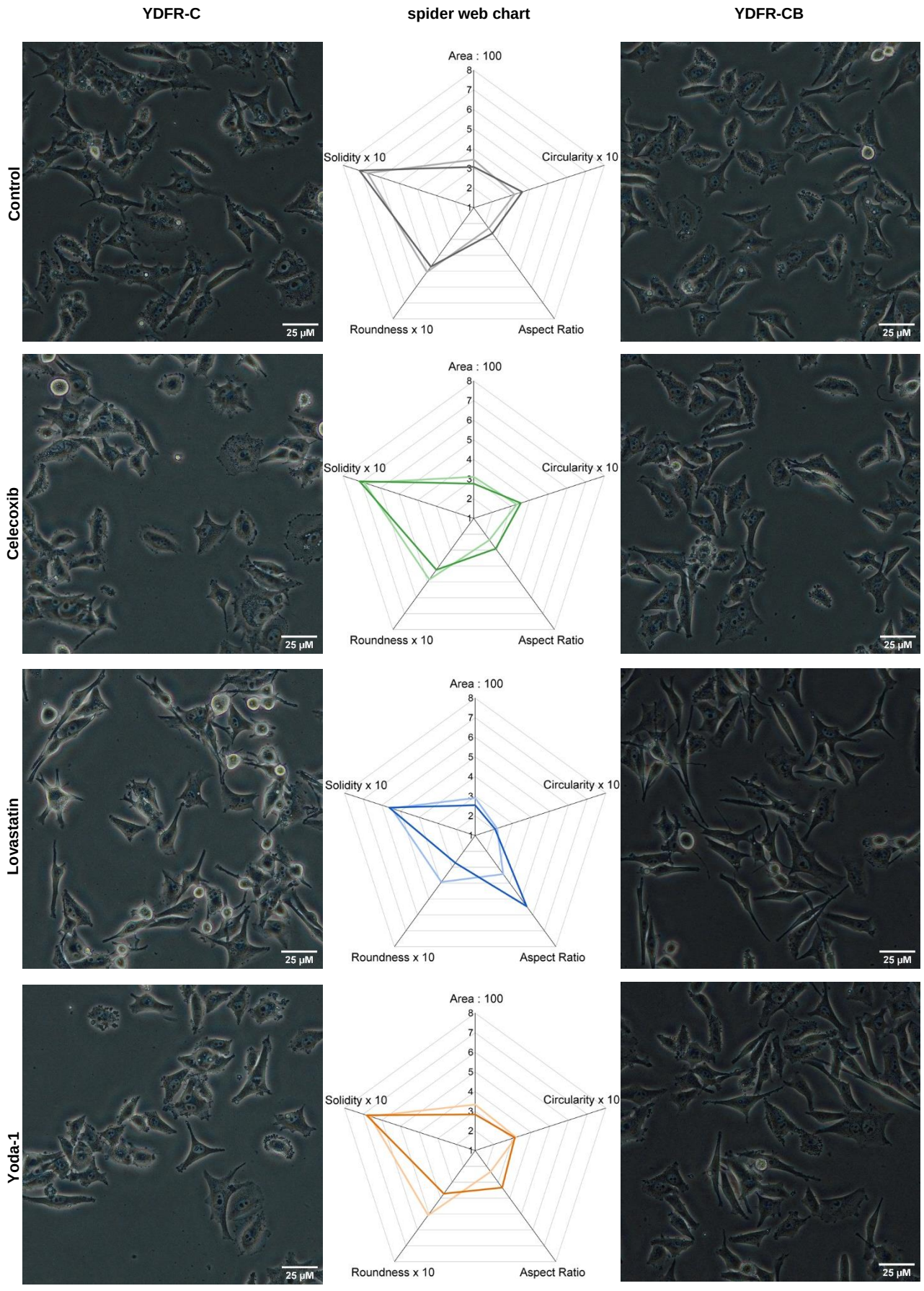

Figure 7: Evaluation of cell morphology from YDFR-C (left) and YDFR-CB (right) cell line after 24 h static incubation with and without drug treatment (1 µM) before the de-adhesion assay (t = 0 s).
spider web chart: Cell area, circularity, aspect ratio, roundness and solidity data are mean values of n ≥ 50 selected cells from ≥5 independet experiments. Data quantification with ImageJ software, statistic calculations with Origin software. light coloured: YDFR-C; dark coloured: YDFR-CB;

After a static incubation of 24 hours, the MN cells from both cell lines showed a similar growth pattern and appearance. Their borders ranged from oblong elliptic, wide-spread star shaped, bulbous round to corrugated, some showing trapezoid or triangular like shapes. The lovastatin-treated cells however showed long drawn-out, spindle-shaped appearance, thin excrescences and partly spiky star-shaped borders with a lower tendency for wide-spread cell areas (see Figure 7).

On an average, the YDFR-C cell lines (both control and all drug treatments) showed a greater area compared to their YDFR-CB cell line counterparts, but statistically there was significant evidence (p=0.05) for that only with Yoda-1-treated cells. Interestingly, despite the fact that the mean area values differed significantly only in Yoda-1, the values of the mean area varied strongly within YDFR-C and YDFR-CB in every group (drug treatment and control). The area ratio of C:CB were very similar (see Table 4), with Yoda-1 area ratio setting itself apart slightly.

There was no significant difference in the cell area within the particular cell line (YDFR-C or YDFR-CB) comparing the drug treatments with their corresponding controls, except for the Lovastatin treatment with differences in both cell lines: In the YDFR-C cell line (p=0.05) and in the YDFR-CB cell line (p=0.01), the area differed significantly from the control. This supports the marked visual differences in morphology of Lovastatin-treated cells mentioned above (all results are listed in Table 4).

Table 4: Compendium of the morphological data collected

treatment	cell line	number of cells	mean area (μm^2)	area ratio (C:CB)
Control	YDFR-C	60	344.37 ± 162.63	1,12
	YDFR-CB	70	307.79 ± 103.68	
Celecoxib 1 µM	YDFR-C	60	311.41 ± 105.42	1,12
	YDFR-CB	50	276.95 ± 80.82	
Lovastatin 1 µM	YDFR-C	60	291.07 ± 109.87 *	1,14
	YDFR-CB	50	254.28 ± 93.74 **	
Yoda-1 1 µM	YDFR-C	60	333.77 ± 130.89	1,18
	YDFR-CB	50	283.71 ± 87.02	

Results are expressed as mean values ± SD, significances of each area (treatment and corresponding control counterpart) were tested with a two-sample t-test. Significant differences in the cell areas in the particular cell lines (YDFR-C and YDFR-CB) comparing drug treatment with their corresponding controls are indicated as * with $p<0.05$ and ** with $p<0.01$. Data quantification with ImageJ software, statistic calculations with Origin software.

When comparing both cell lines (YDFR-C vs. YDFR-CB) within the same group (control or drug treatment) concerning the other measured cell shape describing parameters, circularity, aspect ratio (AR), roundness, and solidity (summarized in Table 5), there was no significant difference within the control-group. Within the CXB-group there appeared a difference of p=0.05 in AR, with Lovastatin a difference of 0=0.001 in AR and p=0.01 in roundness, and within the Yoda-1-group both AR and roundness differed with p=0.001.

Table 5: cell shape describing parameters

treatment	cell line	number of cells	Circularity	Aspect Ratio	Roundness	Solidity
Control	C	60	0.32 ± 0.13	2.30 ± 1.01	0.51 ± 0.18	0.67 ± 0.14
	CB	70	0.36 ± 0.14	2.62 ± 1.43	0.47 ± 0.20	0.71 ± 0.12
Celecoxib 1 µM	C	60	0.33 ± 0.12	2.36 ± 1.07	0.49 ± 0.17	0.69 ± 0.13
	CB	50	0.35 ± 0.11	2.91 ± 1.51	0.42 ± 0.18	0.71 ± 0.12
Lovastatin 1 µM	C	60	0.22 ± 0.10***	3.43 ± 2.07***	0.40 ± 0.20**	0.55 ± 0.14***
	CB	50	0.21 ± 0.12***	5.46 ± 3.20***	0.27 ± 0.20***	0.56 ± 0.16***
Yoda-1 1 µM	C	60	0.32 ± 0.12	2.34 ± 1.03	0.51 ± 0.20	0.66 ± 0.13
	CB	50	0.31 ± 0.10*	3.34 ± 1.55*	0.37 ± 0.18**	0.68 ± 0.11

Results are expressed as mean values ± SD, significances of each parameter (treatment and corresponding control counterpart) were tested with a two-sample t-test. Significant differences in the cell parameters in the particular cell lines (YDFR-C and YDFR-CB) comparing drug treatment with their corresponding controls are indicated as * with p<0.05 and ** with p<0.01. Data quantification with ImageJ software, statistic calculations with Origin software.

When comparing drug treatment versus control within the two cell lines YDFR-C or YDFR-CB with these other cell shape describing parameters mentioned above, it became apparent that CXB-treated cells in neither of the two cell lines differed from their respective controls. The Yoda-1-treated cells showed a significant difference in the parameters circularity (p=0.05), AR (p=0.05), and roundness (p=0.01) within the YDFR-CB cell line compared to their corresponding controls. The biggest impact on the cell morphology of both cell lines showed the treatment with Lovastatin, where all measured cell shape describing parameters differed significantly (p=0.001) from those of the respective controls. Solely the parameter roundness of the YDFR-C cell line exhibited a p=0.01 significant difference to the control. For a better overview, the Lovastatin specific results are summarized in Figure 8.

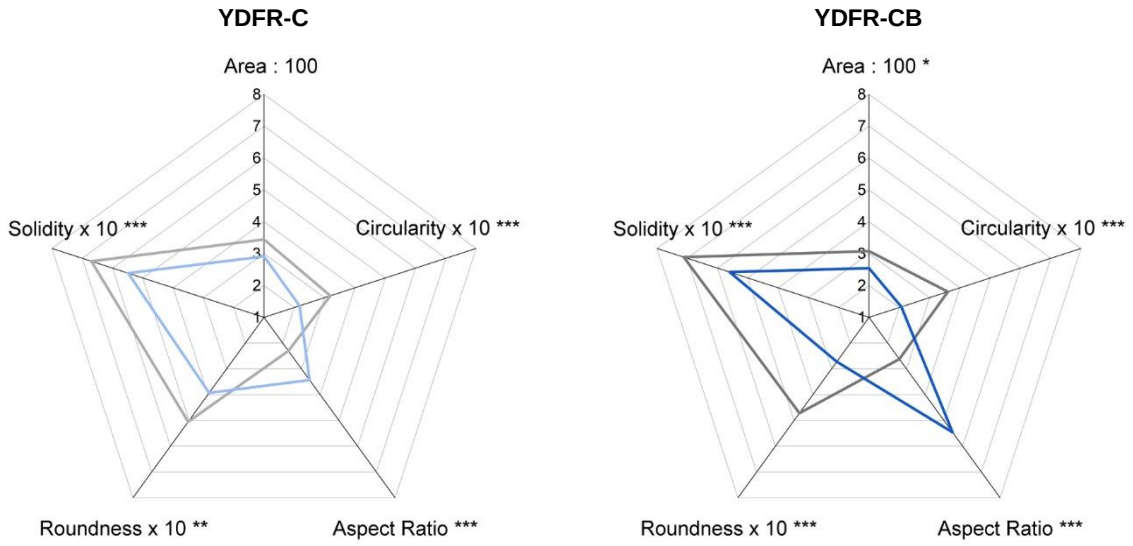

Figure 8: Impact of Lovastatin treatment on the cell morphology
Comparison of the cell morphology treated with Lovastatin (*blue*) and untreated cells (control – *grey*) in YDFR-C (*left*) and YDFR-CB (*right*) cell lines. Significant differences are indicated as * with $p<0.05$, ** with $p<0.01$ and *** with $p<0.001$, tested with an ANOVA. Data quantification with ImageJ software, statistic calculations with Origin software.

During the de-adhesion assay, the visual observation was made that the YDFR-C cell line showed a faster reaction to the added trypsin than the YDFR-CB cell line in both control and drug-treated cells. This observation also presents itself in the graphic summary of the de-adhesion assay (see Figure 9). There the curve progression of every condition for both cell lines of each de-adhesion assay is depicted as mean values of the normalized area ± standard deviation (SD) versus time (s).

To verify this observation statistically, the ET (effective time)-values were calculated from a DRA for each analyzed cell for each cell line (YDFR-C and YDFR-CB) and condition (control and drug treatment). The abscissa data (time axis) had to be adjusted by adapting it logarithmically before the sigmoidal fitting for the DRA function could be performed. The adapted curve progressions (mean values of the normalized area ± SD versus logarithm of time) are illustrated as a representative example in Figure 10. After the sigmoidal fitting for the DRA function, the so obtained ET-values of each cell for both cell lines (YDFR-C and YDFR-CB) and every condition (control and drug-treated cells) could be obtained and their mean values ± SD are listed in Figure 13b.

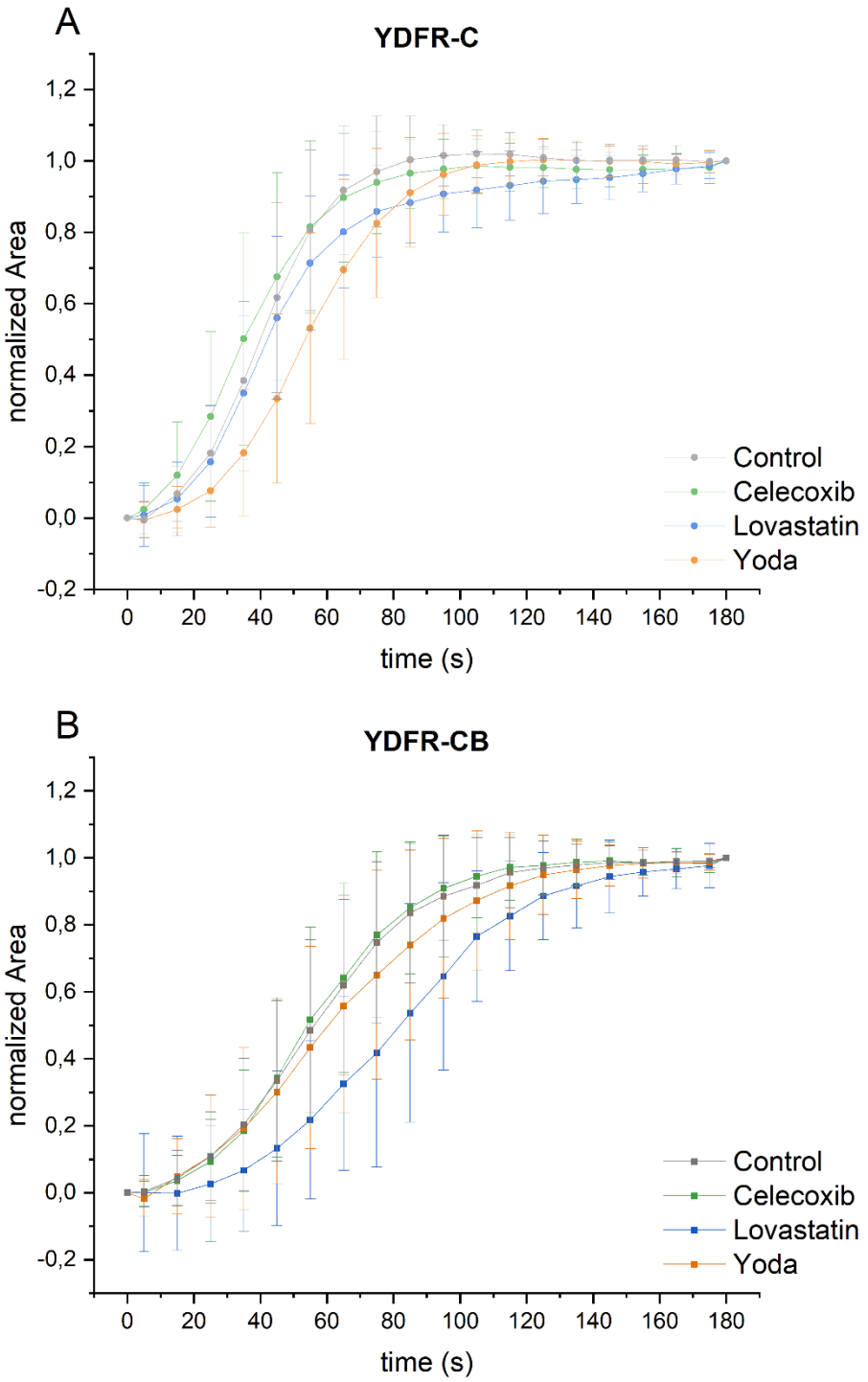

Figure 9: Curve progression of the summarized results of the DAA.
A and B: Results are the normalized area vs time (s) expressed as mean values ± SD. Control and drug treated YDFR-C cell lines (**A**) show faster detachment than their YDFR-CB cell line counterparts (**B**). Data quantification with ImageJ software, statistic calculations and graphical design with Origin software.

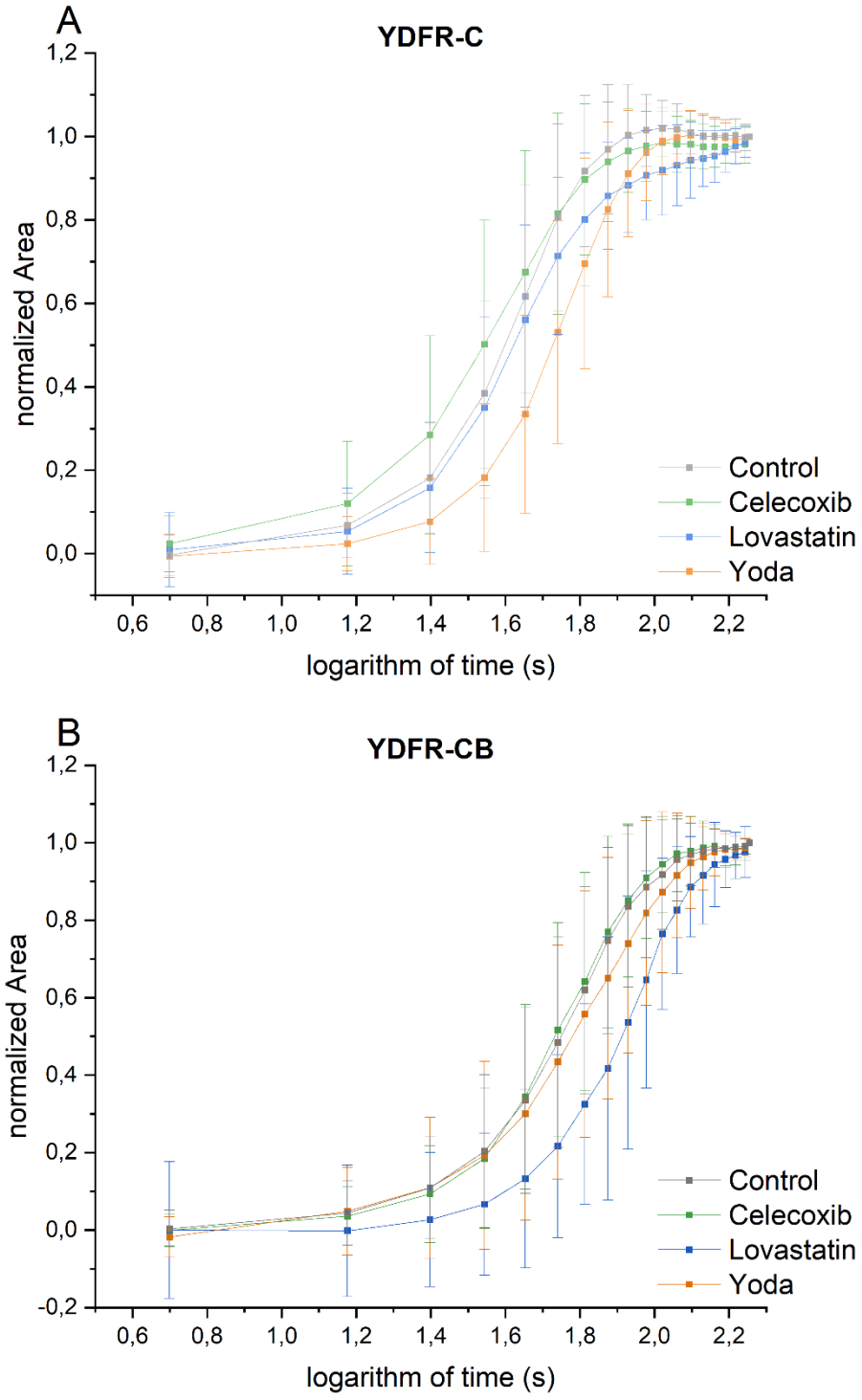

Figure 10: Representative example for the adjustment of the time axis for the DRA
A and B: show the adapted curve progressions (mean values of the normalized area ± SD versus logarithm of time). Data quantification with ImageJ software, statistic calculations and graphical design with Origin software.

To get a better overview over the data distribution, the so gained single values of each cell from each assay were depicted in Figure 11 as box blot diagram.

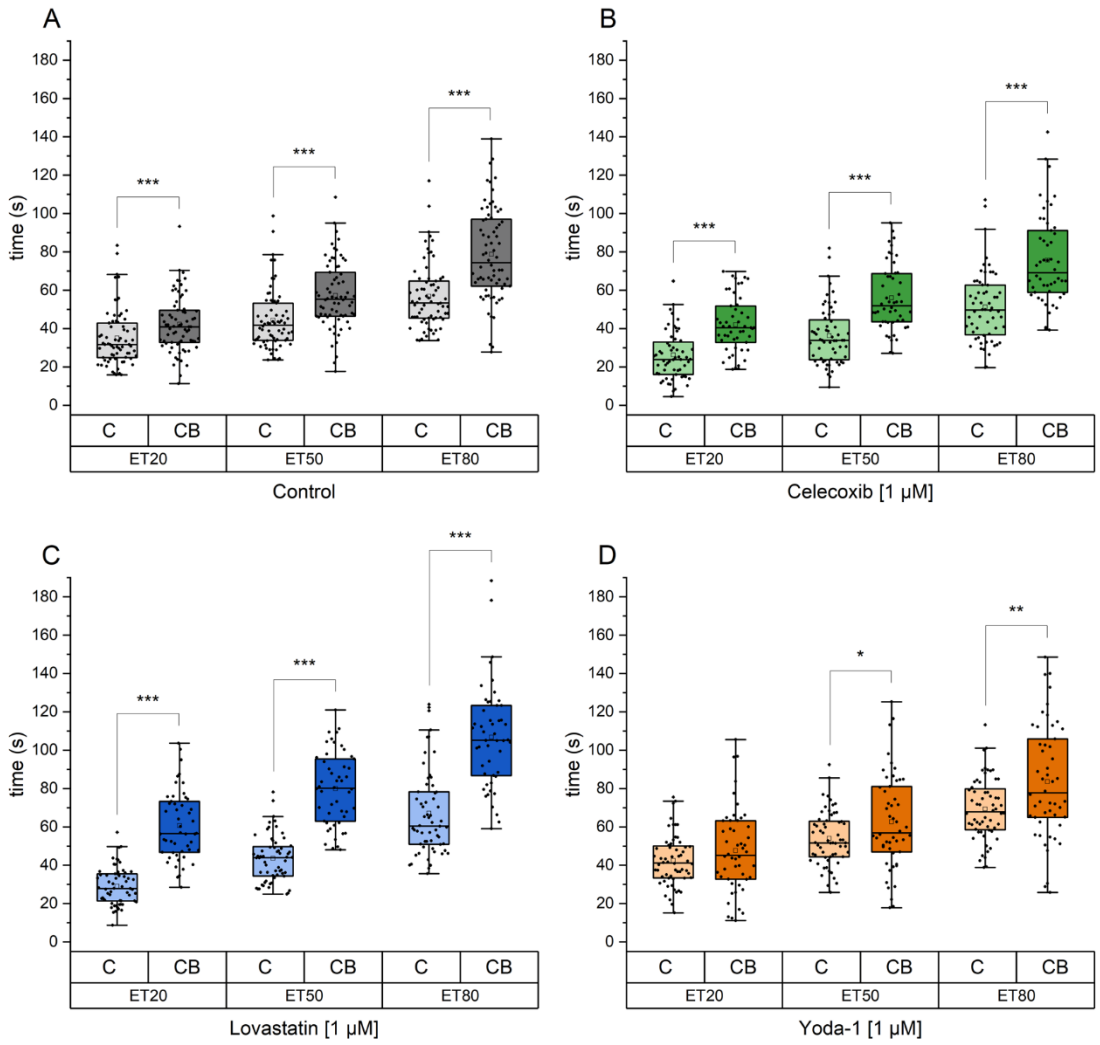

Figure 11: Comparison of ET-values of the YDFR- C and YDFR-CB cell lines
Presentation of all single ET-values in their particular response to their de-adhesion behavior. Results are the ET-values of the normalized area versus time (s) expressed as mean values ± SD. Significances of each ET-value (YDFR-C and YDFR-CB cell line) were tested with a two-sample t-test. Significant differences are indicated as * with $p<0.05$, ** with $p<0.01$ and *** with $p<0.001$.

The ET-values (ET_{20}, ET_{50}, and ET_{80}) of the YDFR-CB cell line of each condition (control or drug treatment) were compared to the corresponding ET-values of the YDFR-C cell line with the appropriate condition with the aid of a two-sample t-test. The visual observation mentioned above was widely confirmed:

All YDFR-C cell lines in every condition (control and drug treatment) showed a significantly faster de-adhesion process compared to their corresponding YDFR-CB cell line (see Figure 11 for detailed significance level), exempt Yoda-1 ET_{20}, that did not demonstrate significant difference. For better illustration, the progression of the ET-values was described in a line graph (without SD) in Figure 13a.

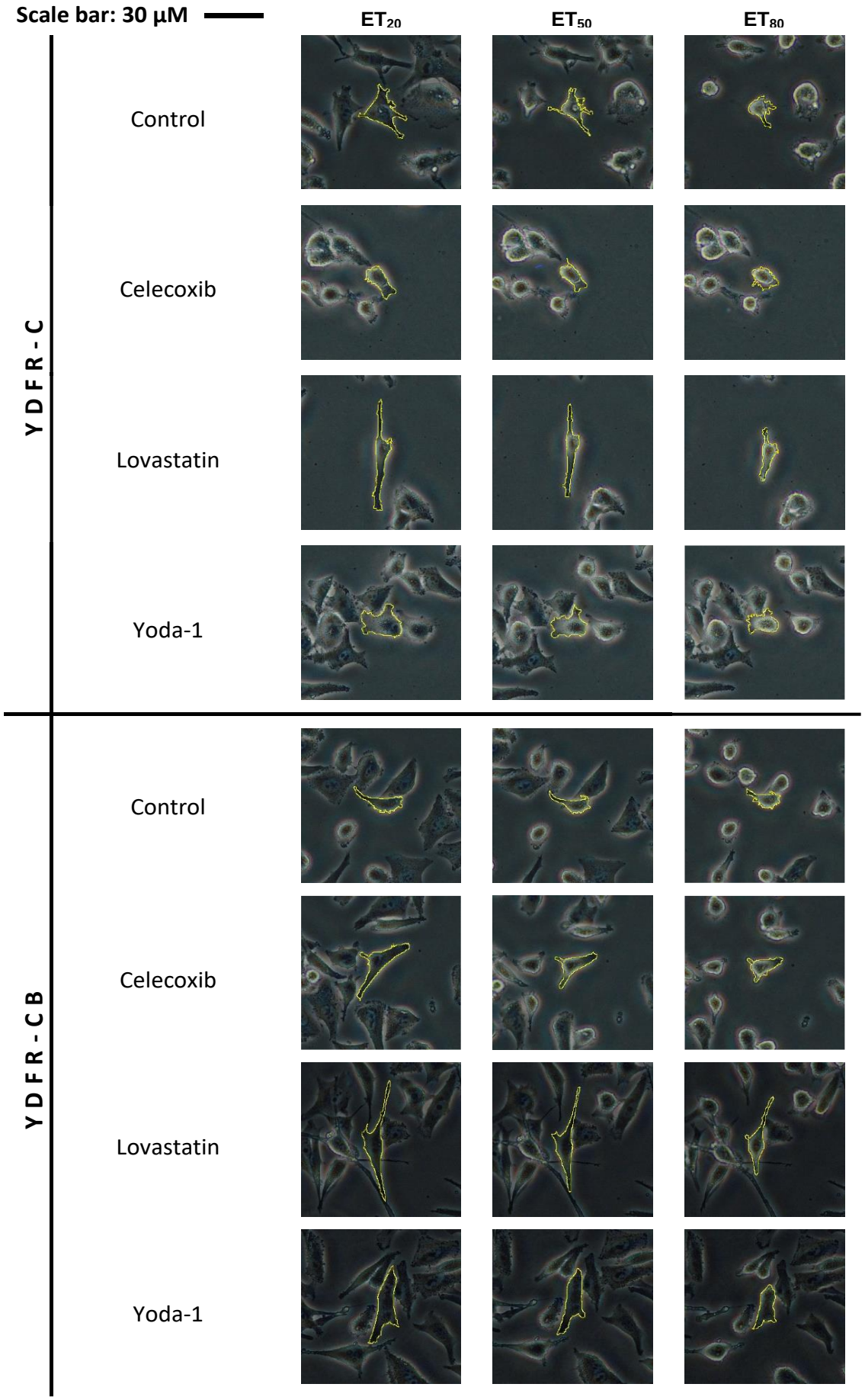

Figure 12: Overview over the de-adhesion behavior and changes in morphology of representatively chosen cells.
Tracking of the de-adhesion process and therefore of the transformation (rounding) of the different treated and untreated cells in YDFR-C and YDFR-CB cell lines at defined points of time (ET_{20}, ET_{50} and ET_{80}). Cell borders are marked in yellow. Data quantification with ImageJ software.

To follow the morphological changes of the different cells graphically, representative photographs of the cells (during the de-adhesion assays a photo was taken every 5 s, see also 7.4.3.1) at the points in time closest to the actual ET-values (ET_{20}, ET_{50}, and ET_{80}) were summarized in Figure 12. The cell borders were marked yellow with the ImageJ software, so that the de-adhesion behavior of the chosen cell could be traced more easily. A distinct rounding and thus diminution of the cell area during the de-adhesion process (before detachment the cells contract and round) could be observed. The mean values ± SD of the ET-values of each cell for both cell lines (YDFR-C and YDFR-CB) and every condition (control and drug-treated cells) are listed in Figure 13b.

The ET-values (ET_{20}, ET_{50}, and ET_{80}) of each condition (CXB, Yoda-1 and Lovastatin) was compared to the ET counterparts of the corresponding control within the same cell line (either YDFR-C or YDFR-CB) to observe possible significant changes in the de-adhesion process during drug treatment. This was performed with a two-sample t-test, the results are also listed in Figure 13b:

The drug treatments had the following impact on the time response of the de-adhesion process within the YCFR-C cell line. CXB treatment accelerated the initial de-adhesion process (ET_{20}) by about 5 s ($p=0.05$) on an average. The remaining curve progression at ET_{50} and ET_{80} however did not differ significantly from the control. Lovastatin treatment had no significant impact on the de-adhesion process both at ET_{20} and ET_{50}, yet at ET_{80} it showed a highly significant ($p=0.001$) deceleration, by about 14 s compared with the control. Yoda-1 treatment had the greatest impact on the YDFR-C cell lines. It decelerated de-adhesion most significantly ($p=0.001$) throughout the whole process, at an average of about 11 s at ET_{20}, 13 s at ET_{50} and about 16 s at ET_{80} compared with the control.

The YDFR-CB cell line, however, displayed other responses after drug treatment. Neither CXB nor Yoda-1 treatment had an impact on the de-adhesion process (ET_{20}, ET_{50}, and ET_{80}) compared with the control. Lovastatin treatment, on the other hand, decelerated de-adhesion most significantly ($p=0.001$) throughout the whole process, at an average of about 18 s at ET_{20}, about 22 s at ET_{50} and 28 s at ET_{80}. For better illustration, these results are summarized as a line graph (without SD) in Figure 13a.

A

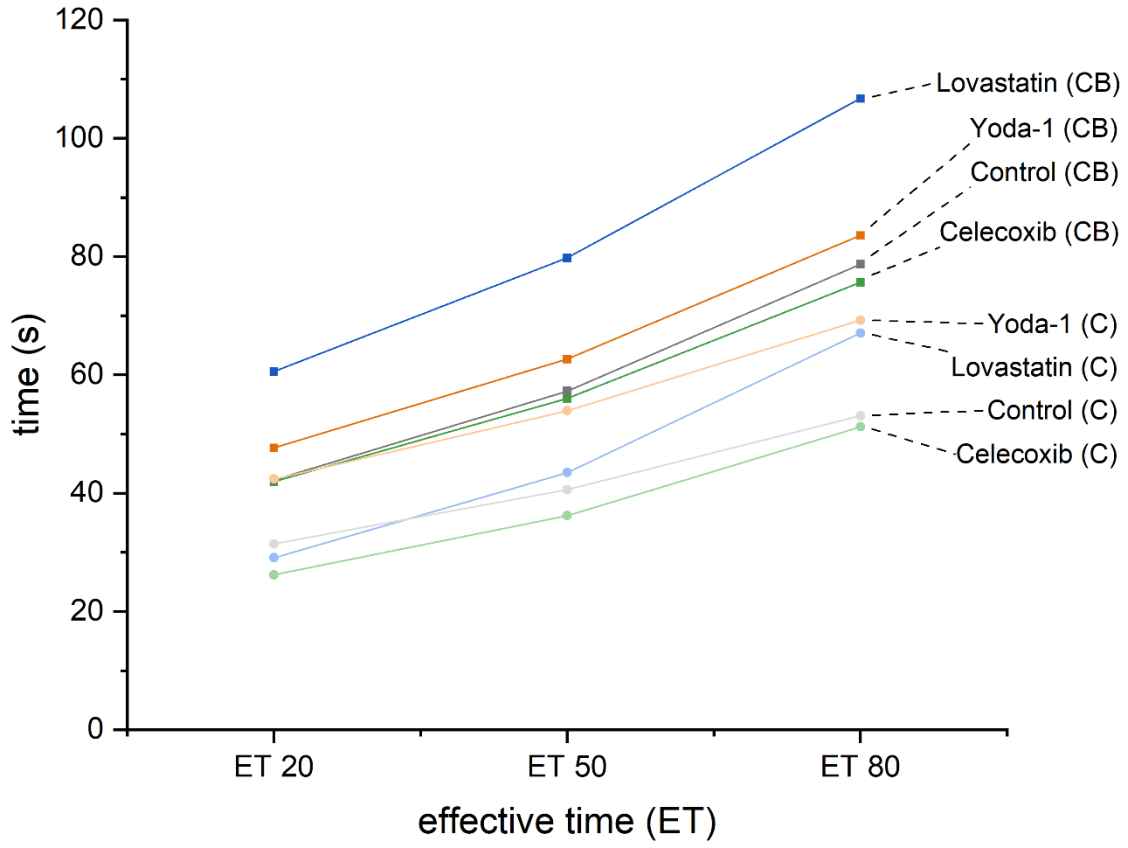

B

treatment	cell line	number of cells	mean ET_{20} values (in s)	mean ET_{50} values (in s)	mean ET_{80} values (in s)
Control	C	60	31.42 ± 11.20	40.59 ± 11.84	53.06 ± 13.82
	CB	70	42.20 ± 14.69	57.25 ± 17.47	78.72 ± 24.13
Celecoxib [1µM]	C	60	26.18 ± 13.27 *	36.21 ± 15.19	51.19 ± 18.39
	CB	50	41.98 ± 14.34	56.00 ± 17.24	75.67 ± 23.48
Lovastatin [1µM]	C	60	29.08 ± 9.76	43.45 ± 12.15	67.05 ± 22.24 ***
	CB	50	60.58 ± 17.91 ***	79.81 ± 19.04 ***	106.72 ± 26.52 ***
Yoda-1 [1µM]	C	60	42.36 ± 13.19 ***	53.93 ± 13.98 ***	69.25 ± 16.01 ***
	CB	50	47.63 ± 21.91	62.65 ± 24.88	83.56 ± 29.61

Figure 13: Overview of ET-value trends and ET values of all cell lines and treatments
A: Graphical representation of the time response through the calculated ET-values (listed in **B**)
B: Results are the ET-values of the normalized area versus time (s) expressed as mean value ± SD. Significances of each ET-value (treatment and corresponding control counterpart) were tested with a two-sample t-test. Significant differences are indicated as * with $p<0.05$ and *** with $p<0.001$.

8.2 Proteomics analysis

The total proteome profiling was performed with biological triplicates via mass spectrometry-based proteomics. From the received MS data, 18 proteins were selected out of the 15 most up-regulated and 15 most down-regulated proteins of each condition (untreated control, CXB, Lovastatin, and Yoda-1) and were divided into 5 classes. The results of this analysis were illustrated in a heatmap (Figure 14).

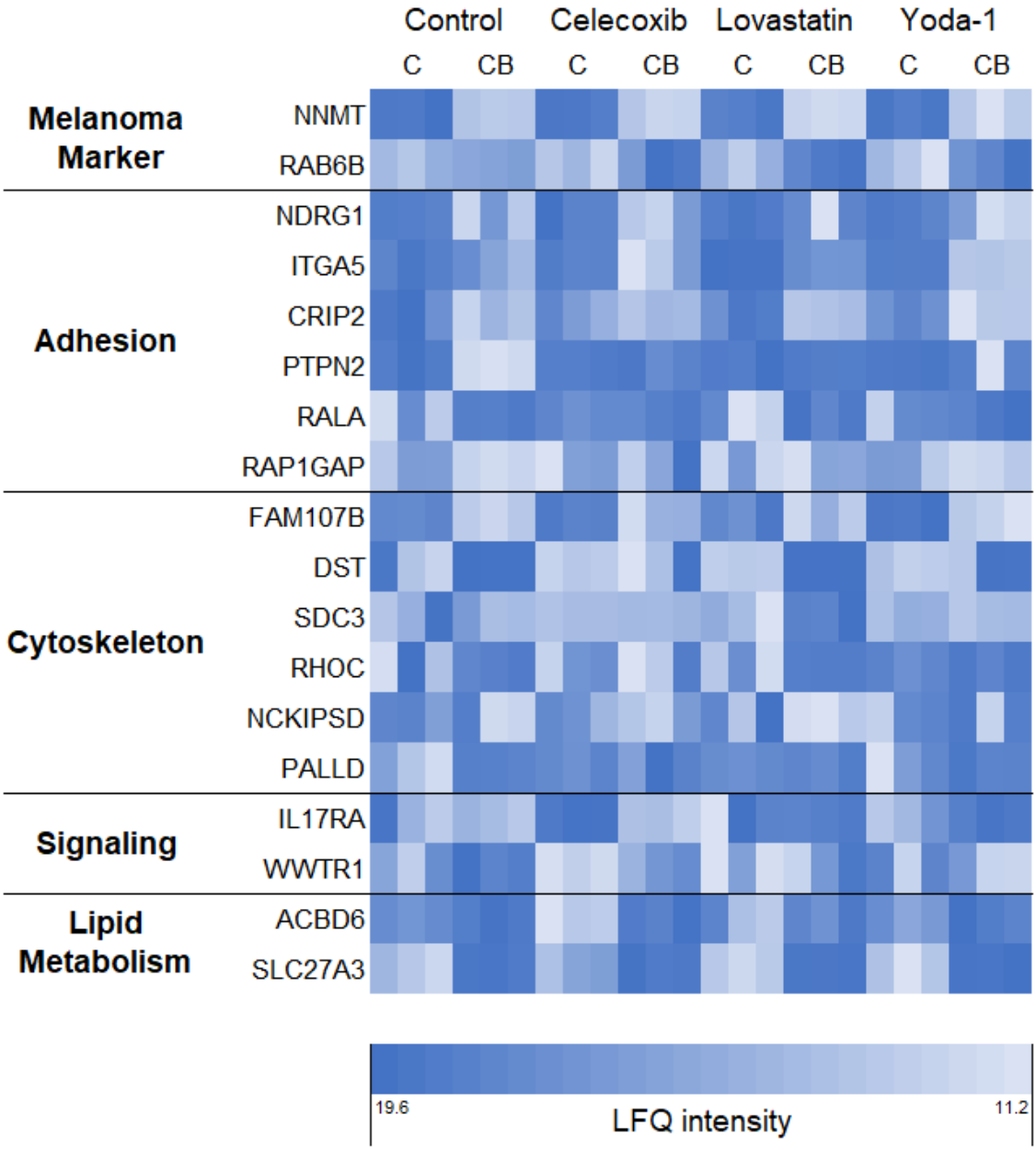

Figure 14: Heatmap of the selected proteins from the total protein analysis
The biological triplicates of the 18 selected proteins were divided into 5 classes and presented in the heatmap with their LFQ intensity. The scalebar visualizes the highest LFQ intensity (19.6, dark blue) at the left and the lowest LFQ intensity (11.2, light blue) at the right side of the bar and represents the colors and LFQ intensities in the heatmap.

For the classification into the five classes mentioned above the quoted papers were used as a basis:

- **Melanoma marker:** NNMT [234, 235], RAB6B [236, 237]
- **Adhesion:** NDRG1 [238], ITGA5 [239, 240], CRIP2 [241], PTPN2 [241], RALA [241], RAP1GAP [242]
- **Cytoskeleton:** FAM107B [243], DST [244], SDC3 [245], RHOC [246], NCKIPSD (also known as SPIN90 [247]) [248] , PALLD [249];
- **Signaling:** IL17RA [250], WWTR1 [251]
- **Lipid metabolism:** ACBD6 [252], SLC27A3 (also known as FATP3 [253]) [254]

With the MN marker, especially NNMT has to be mentioned which is up-regulated in the control of the YDFR-C cell line, but down-regulated in the corresponding YDFR-CB control. This tendency continues after drug treatment as well. RAB6B only shows a slight up-regulation in YDFR-CB control compared to the YDFR-C control. This up-regulation in the YDFR-CB cell line is enhanced with drug treatments within each group (CXB, Lovastatin, Yoda-1). Concerning the adhesion proteins, ITGA5 is up-regulated in the YDFR-C control compared to the corresponding YDFR-CB control – a tendency that persist after drug treatment. RAP1GAP appears to be down-regulated in all conditions (control, CXB, Lovastatin, Yoda-1) and cell lines (YDFR-C and YDFR-CB). With proteins associated with lipid metabolism, SLC27A3 is down-regulated in YDFR-C control compared to the corresponding YDFR-CB control. This tendency continues after drug treatment as well. The cytoskeleton protein DST appears to be down-regulated in the YDFR-C control and up-regulated in the corresponding YDFR-CB control. This tendency changes only after CXB treatment where the corresponding YDFR-CB cell line shows no up-regulation.

9 Discussion

Metastasis is the major reason for treatment failure and the high mortality rate of cancer. The deadliest form of all skin cancers is MN, which arises from the malignant transformation of melanocytes. De-adhesion is the key event in metastasis and represents the first step in the metastatic cascade. This thesis focuses on morphological and proteomic alterations of two human MN cell lines, the cutaneous MN cell line YDFR-C and the brain metastatic cell line YDFR-CB originating from the same patient, regarding their de-adhesion behavior and in how far different drugs on the one hand influence this behavior and on the other hand influence mechanosensitive processes. For this, the cell-describing parameters were determined by means of a morphometric analysis. A de-adhesion assay was established and performed to analyze the de-adhesion behavior of the above-mentioned MN cell lines, as well as an MN signature was characterized by proteomics.

9.1 Morphometric analysis

9.1.1 Cell describing parameters and morphological changes

Changes in cell morphology occurred during EMT [163]. The question arose, if with MN and its EMT-like switch it also comes to changes in the morphological parameters and if the drugs used for treatment might have a certain influence on them. Especially the visible deviation during cell culturing with Lovastatin (see 8.1) offered motivation to further investigate this item. Figure 7 presents examples of microscopic pictures with their belonging spider web charts outlining the selected 5 cell shape describing parameters (area, circularity, aspect ratio, roundness, and solidity).

Under qualitative visual observation, there was no noticeable difference between the two control cell lines (untreated YDFR-C and YDFR-CB) concerning cell appearance. The morphometric characterization of the cells also showed no significant difference with both control cell lines concerning the cell describing parameters. The same results were presented in another study which, among other things, compared the morphology of 4 different MN cell lines including YDFR-C and YDFR-CB [218]. Notably, three parameters (area, circularity, and roundness) were collected equally in both papers. The results in relation to each other (YDFR-C vs. YDFR-CB) as shown in the spider web charts are about the same, but the numeric values – especially with area – differ greatly, possibly in relation to different correction values used in the two studies.

After having thus defined the morphology of both untreated cell lines (YDFR-C and YDFR-CB), the question arose, in how far the 24-hour static treatment with the different drugs affected the cell shape describing parameters:

CXB showed no significant impact on the cell morphology (in both cell lines, YDFR-C vs. YDFR-CB). Visually as well, the two cell lines did not differ from each other or from the corresponding control. A possible explanation for this could be that maybe the imaging technique used showed no sufficient accuracy concerning the analysis of the effects of CXB on the morphology of the cells. Venkatesan et al. [255] used for the comparison of methods three techniques, phase contrast microscopy, high resolution confocal laser fluorescence microscopy and atomic force microscopy. Thereby they could demonstrate that using the phase contrast microscopy no significant changes in morphology with CXB-treated cells (for 24 hours) were discernable, whereas with the other two microscope techniques mentioned above a morphologic difference was observed [255].

Lovastatin triggered the most significant change on cell morphology, already visually a considerable difference compared to the control could be seen (spindle shaped appearance, see also 8.1). Shellman et al. reported morphological changes (rounded and detached cells) in with 1 and 4 µM Lovastatin treated human MN cell lines after 72 hours incubation [256], whereas Song et al. observed cell rounding, elongation, cell-cell separation and detachment with PTM and PCB cells after 24 hour treatment with 15 and 30 µM Lovastatin [257]. The marked visual difference also appeared with the cell describing parameters, which differed significantly from the corresponding control in both cell lines (YDFR-C and YDFR-CB). If you used the circularity classification of Schöchlin et al. [228], Lovastatin-treated cells would be classified as distinctly spindled in both cell lines. A significantly increased AR as well hints at a spindle like cell shape.

EMT influences cell morphology, contributes to metastasis [163], and, during its progression, a significant increase in cellular AR could be observed [258]. This hints at a spindled shaped morphology, which is a hallmark of EMT as well [259]. Taken together, with the initiation of EMT, cell morphology changes and cells become more spindle shaped as well as more motile, which is the initial step of the metastatic cascade (also described in 5.3). On the basis of these morphologic observations, it could be hypothesized that Lovastatin contributes to the metastatic potential of MN cells because of the increased spindle like cell shape (significant reduction of circularity with simultaneous significant increase in AR).

Furthermore, Lovastatin is the only one of the three drugs used to show a significantly lower cell area in both cell lines (compared to the corresponding control) after a 24 hour static incubation. Menter et al. described in his experiment with another hydrophobic statin (10 µM Simvastatin) an inhibition of cell growth after 24 hours of treatment [260]. Such an inhibition of cell growth is possibly also an explanation for the significantly lower area of the Lovastatin-treated cells.

Yoda-1 mimics constant shear stress in static cultures by activating pharmacologically Piezo 1 channels [197]. The cell lines treated with Yoda-1 were the only cell lines showing a difference in area between YDFR-C vs. YDFR-CB. The treated YDFR-C cell line grew significantly compared to the treated YDFR-CB cell line, about 17 % on an average.

Similar to Lovastatin, the YDFR-CB cell line tended to a spindled morphologic change with Yoda-1 treatment, which again showed as a significant reduction in circularity as well as a significant increase in AR compared to the corresponding control. These observations correspond to Liu et al. [227] who examined the morphologic response of fluid shear stress to osteoblasts. After an exposure of one hour with a magnitude of 1.9 Pa they observed the same morphologic changes (reduction of circularity and rise in AR) as response to shear stress [227].

The EC_{50} concentration of Yoda-1 on purified Piezo 1 proteins lies within a range of 10 – 50 µM [128]. To activate the Piezo 1 channel, Yoda-1 at a moderate concentration of 1 µM was used. At this concentration, the cutaneous YDFR-C cells showed no difference in any of the morphologic parameters concerning their control, but the brain metastatic YDFR-CB cell line did, as mentioned above. It seems as if cells which had once before experienced shear stress (during their metastatic journey through the circulation) showed a strong morphologic response already in low doses of Yoda-1.

Finally it has to be mentioned that, if you apply the circularity classification of Schöchlin et al. [228], (see 7.4.3.1.2.1), Lovastatin treatment in both cell lines (YDFR-C and YDFR-CB) showed a circularity clearly ranging within the band width of the class “spindled”, whereas all other conditions (control, CXB and Yoda-1) in both cell lines moved round the upper margin between “spindled” and “elongated”. It is important to note that this classification is based on nuclear shapes and therefore may not be used for the classification of cell shapes. Nevertheless, the morphology of MN cells has already been described as triangular or spindled [261].

9.1.2 De-adhesion behavior

MN is a kind of cancer with high capacity for metastasis [262] and metastasis is always accompanied by a loss of adhesion [263]. The question arose if tumor cells from a primary site (cutaneous) would bring about a quicker de-adhesion response than secondary tumors (brain metastasis) and in how far different drugs influence this behavior. To date, no literature in reply of this question could be found. For investigation, corresponding cell lines of cutaneous (YDFR-C) and brain metastatic (YDFR-CB) cells shared same genetic ancestry.

By means of de-adhesion assays it could be demonstrated that there was a significant difference between the YDFR-C and the YDFR-CB cell lines (both as untreated control). This became evident in all three examined phases (ET_{20}, ET_{50}, and ET_{80}) during the course of de-adhesion. At an average, the difference in time amounts to about 11 s (ET_{20}), about 17 s (ET_{50}) and about 15 s (ET_{80}). The YDFR-CB cell line showed a delayed de-adhesion process after trypsinization.

As described in chapter 7.4.3.1, a morphological change discernable on the photos only started in the second phase of the assay with quick proceeding of cell contraction (until rounding of the cells [221]), as in the first phase only the FA contacts between cell and surface were detached by trypsin [221] which led to a lagged initiation of de-adhesion. The significant delay of the de-adhesion process of the YDFR-CB compared to the YDFR-C cell line supports the conclusion that adhesion is more pronounced in this cell line. In a recent study, it could be verified, that in MN brain metastases the PI3K/AKT pathway was upregulated [264]. This pathway modulates e.g. attachment in metastatic cells [265], a fact that could explain this observations.

After having characterized the de-adhesion profiles and behaviors of both untreated cell lines (YDFR-C and YDFR-CB), the question arose, how the 24-hour static treatment with the different drugs affected the de-adhesion properties *per se*:

With Lovastatin treatment, only the YDFR-CB cell line showed a significant impact on the three examined phases (ET_{20}, ET_{50}, and ET_{80}) during the course of de-adhesion compared to the corresponding control. Thereby, Lovastatin delayed the de-adhesion process in this cell line after trypsinization on an average of about 18 s (ET_{20}), about 22 s (ET_{50}) and about 28 s (ET_{80}).

This observation is interesting, as an accelerated de-adhesion process (especially in the YDFR-C cell line) was anticipated, because statins – as reported in several papers [266–269] – decrease cell adhesion. However, the de-adhesion process did not differ significantly from the control within the first two phases (ET_{20} and ET_{50}), hence only at

the end of the assay (at ET_{80}) a significant delay of de-adhesion arose. As cholesterol is co-responsible for the membrane fluidity [172], a possible interpretation could be, that after a certain reduction of cell area the reduced motility of the membrane could influence the contraction process. This could also explain the significantly decelerated contraction process in der YDFR-CB cell line compared to its corresponding control. These results suggest that Lovastatin, against other scientific observations, strengthens adhesion in MN brain metastatic cells and has furthermore no impact on the adhesion behavior of cutaneous MN cells.

Yoda-1 treatment was the only drug treatment which flattened up the difference between both cell lines (YDFR-C vs. YDFR-CB) concerning the de-adhesion behavior at the beginning of the assay (ET_{20}). In all other treatments, the de-adhesion process (ET_{20}) set in significantly faster with YDFR-C cell lines in every condition (control, CXB, Lovastatin) than with YDFR-CB.

Furthermore, with Yoda-1 treatment, only the YDFR-C cell line showed a significant impact on the three examined phases (ET_{20}, ET_{50}, and ET_{80}) during the course of de-adhesion compared to the corresponding control. Thereby, Yoda-1 delayed the de-adhesion process in this cell line after trypsinization on an average of about 11 s (ET_{20}), about 13 s (ET_{50}) and about 16 s (ET_{80}).

This deceleration is so pronounced that there is no significant difference between YDFR-C Yoda-1-treated cell line and the untreated YDFR-CB control in the first two examined phases (ET_{20} and ET_{50}), and ET_{80} is only just different ($p=0.05$). These results show that the adhesion behavior seems to be contrary to morphology - it seems as if cells which had not experienced shear stress before showed a strong response concerning de-adhesion behavior with already low doses of Yoda-1.

The exact role of CXB in tumor protection is still unclear [213], its effect on de-adhesion also provides diverging results [186, 201, 204, 270, 271].

In our case, only the examined ET_{20} phase of the CXB-treated YDFR-C cell line showed a significant difference compared to the corresponding control. The de-adhesion process started on an average about 5 s earlier. The other two examined phases (ET_{50} and ET_{80}) showed no significant difference concerning de-adhesion time compared to the untreated YDFR-C control. These results suggest that CXB reduces the de-adhesion behavior of the YDFR-C cell line. Finally, it has to be mentioned that CXB treatment displayed the same trend in all ET-values (ET_{20}, ET_{50}, and ET_{80}), also in those bearing no statistical significance: the mean ET-values were always below those of the corresponding controls.

The trypsin de-adhesion assay has been performed by others and has been discussed in many papers [219, 221, 272, 273], but to the best of our knowledge so far nobody has yet addressed this specific topic, so that there has been no work on MN-cells (e.g. YDFR-C and/or YDFR-CB) by now. Solely one paper [273] has been found performing the trypsin de-adhesion assay with an MN cell line (among diverse breast cancer cell lines) – though the MN cell line used (MDA-MB-453) was defined in various other publications [274–277] as being a breast cancer cell line.

9.2 Proteomics

As can be seen from the heatmap, NNMT is up-regulated in the primary tumor (untreated YDFR-C control) and could thus function as a molecular bio marker for MN as suggested by Ganzetti at al. [235]. The second MN marker, RAB6B, shows a slight up-regulation in the YDFR-CB control compared to the corresponding YDFR-C control. This up-regulation in the YDFR-CB cell line increased after drug treatments (CXB, Lovastatin, Yoda-1). These results seem to support the pro-tumorgenetic functions of RAB6B [237] and could support the theory of Peng et al. that RAB6B could function as a prognostic marker [236], maybe also for MN.

A reduction in the expression of the adhesion molecule ITGA5 is associated with reduced adhesion [240]. ITGA5 is up-regulated in the YDFR-C control compared to the corresponding YDFR-CB control. Nevertheless, the results of the de-adhesion assay show that the YDFR-C cell line shows a faster de-adhesion response after

compared to the YDFR-C cell line (in the control group, see 9.1.2). RAP1GAP appears to be down-regulated in all conditions (control, CXB, Lovastatin, Yoda-1) and cell lines (YDFR-C and YDFR-CB), which in MN promotes cell survival, proliferation and migration [242]. SLC27A3 shows the same tendency with all drug treatments (CXB, Lovastatin, Yoda-1): down-regulation in the YDFR-C cell line and up-regulation in the corresponding YDFR-CB cell line. Interestingly, this also applies with Lovastatin, that influences lipid metabolism. The cytoskeletal protein DST is associated with the identification of MN metastases [278]. In the used YDFR cell line, the brain metastatic cell line YDFR-CB (untreated control) showed an up-regulation of this protein, which could support the above-mentioned assumption.

Finally, the following should be mentioned critically:

Differences in morphology may have been discernable using different imaging/microscope techniques (e.g. see [255]).

2-D cell cultures might constitute a reductionist approach as they may not represent the tumor environment properly and may show an aberrant drug response [279]

The enzyme activity of the enzyme used determines the course of the de-adhesion assay, especially in phase one (see 7.4.3.1) where the enzyme detaches the FA contacts between cell and surface. Therefore, it would be worth considering including the enzyme activity into the calculations as a kind of parameter, as to be able to compare the results from other de-adhesion assays with each other, if needed.

The quality of the data depends on the personal, manual data analysis as well as the analysis device. In this case, always the same person evaluated the data by the same device for stringent conditions. Moreover, an independent evaluator not engaged in the experiments picked cells in a Z-layout (see 7.4.3.1.1) so that the personal selection bias of the investigator was bypassed. Furthermore, it was tried to keep the conditions for the 6-minutes assay circle the same by choosing a standardized procedure to improve the reproducibility of the experiments (see 7.4.3.1). For the de-adhesion assay, trypsin was produced specifically (see 7.2.4) and the processing order of the different conditions was varied with each assay (see 7.4.3.1). By these measures, it was tried to keep the conditions equal, to increase the reproducibility as well as to eliminate the personal bias.

10 Conclusion

In conclusion, this work could successfully demonstrate that the adhesion capacity in the metastatic YDFR-CB cell line is more pronounced (a significant delay of de-adhesion process) than in the cutaneous YDFR-C cell line.

The results suggest that Lovastatin, against other scientific observations, strengthens adhesion in brain metastatic YDFR-CB cells and has furthermore no impact on the adhesion behavior of cutaneous YDFR-C cells. This is the case despite of morphologic changes with increased spindle-like cell shape (significant reduction of circularity with simultaneous significant increase of aspect ratio) in both cell lines (YDFR-C and YDFR-CB) after treatment with Lovastatin.

The results of Yoda-1 treatment seem to be contrary concerning the adhesion behavior and the morphologic changes: Cells which had not experienced shear stress before (YDFR-C) showed a strong response concerning de-adhesion behavior (delayed the de-adhesion process in this cell line), whereas cells already having once before experienced shear stress (YDFR-CB) showed a strong morphological response (significant reduction of circularity and significant increase of aspect ratio).

The presented data showed that Celecoxib reduces the de-adhesion behavior of the YDFR-C cell line.

Furthermore, nicotinamide N-methyltransferase (NNMT) seems to function as a molecular biomarker for melanoma.

The thesis hopefully contributes to the ongoing research on melanoma, the deadliest of all skin cancers, and may promote future progress in this field.

11 List of figures

12 List of tables

13 References

1. Ciarletta, P., Foret, L., Ben Amar, M.: The radial growth phase of malignant melanoma: multi-phase modelling, numerical simulations and linear stability analysis. Journal of the Royal Society, Interface **8**(56), 345–368 (2011). doi: 10.1098/rsif.2010.0285
2. Narayanan, D.L., Saladi, R.N., Fox, J.L.: Ultraviolet radiation and skin cancer. International journal of dermatology **49**(9), 978–986 (2010). doi: 10.1111/j.1365-4632.2010.04474.x
3. Liu, Y., Sheikh, M.S.: Melanoma: Molecular Pathogenesis and Therapeutic Management. Molecular and cellular pharmacology **6**(3), 228 (2014)
4. Leonardi, G.C., Falzone, L., Salemi, R., Zanghì, A., Spandidos, D.A., Mccubrey, J.A., Candido, S., Libra, M.: Cutaneous melanoma: From pathogenesis to therapy (Review). International journal of oncology **52**(4), 1071–1080 (2018). doi: 10.3892/ijo.2018.4287
5. Eddy, K., Shah, R., Chen, S.: Decoding Melanoma Development and Progression: Identification of Therapeutic Vulnerabilities. Frontiers in oncology **10**, 626129 (2020). doi: 10.3389/fonc.2020.626129
6. Arnold, M., Singh, D., Laversanne, M., Vignat, J., Vaccarella, S., Meheus, F., Cust, A.E., Vries, E. de, Whiteman, D.C., Bray, F.: Global Burden of Cutaneous Melanoma in 2020 and Projections to 2040. JAMA dermatology **158**(5), 495–503 (2022). doi: 10.1001/jamadermatol.2022.0160
7. Laikova, K.V., Oberemok, V.V., Krasnodubets, A.M., Gal'chinsky, N.V., Useinov, R.Z., Novikov, I.A., Temirova, Z.Z., Gorlov, M.V., Shved, N.A., Kumeiko, V.V., Makalish, T.P., Bessalova, E.Y., Fomochkina, I.I., Esin, A.S., Volkov, M.E., Kubyshkin, A.V.: Advances in the Understanding of Skin Cancer: Ultraviolet Radiation, Mutations, and Antisense Oligonucleotides as Anticancer Drugs. Molecules (Basel, Switzerland) **24**(8) (2019). doi: 10.3390/molecules24081516
8. Rebecca, V.W., Somasundaram, R., Herlyn, M.: Pre-clinical modeling of cutaneous melanoma. Nature communications **11**(1), 2858 (2020). doi: 10.1038/s41467-020-15546-9
9. Conforti, C., Zalaudek, I.: Epidemiology and Risk Factors of Melanoma: A Review. Dermatology practical & conceptual **11**(Suppl 1), e2021161S (2021). doi: 10.5826/dpc.11S1a161S
10. Lattmann, E., Levesque, M.P.: The Role of Extracellular Vesicles in Melanoma Progression. Cancers **14**(13) (2022). doi: 10.3390/cancers14133086

11. Garbe, C., Amaral, T., Peris, K., Hauschild, A., Arenberger, P., Basset-Seguin, N., Bastholt, L., Bataille, V., Del Marmol, V., Dréno, B., Fargnoli, M.C., Forsea, A.-M., Grob, J.-J., Hoeller, C., Kaufmann, R., Kelleners-Smeets, N., Lallas, A., Lebbé, C., Lytvynenko, B., Malvehy, J., Moreno-Ramirez, D., Nathan, P., Pellacani, G., Saiag, P., Stratigos, A.J., van Akkooi, A.C.J., Vieira, R., Zalaudek, I., Lorigan, P.: European consensus-based interdisciplinary guideline for melanoma. Part 2: Treatment - Update 2022. European journal of cancer (Oxford, England : 1990) **170**, 256–284 (2022). doi: 10.1016/j.ejca.2022.04.018
12. Elder, D.E., Massi, D., Scolyer, R.A., Willemze, R., editors (2018): WHO classification of skin tumours, 4th edn. IARC Press, Lyon (2018)
13. Wild CP, Weiderpass E, Stewart BW, editors (2020): World Cancer Report:. Cancer research for cancer development. International Agency for Research on Cancer (IARC), Lyon (2020)
14. Elder, D.E., Bastian, B.C., Cree, I.A., Massi, D., Scolyer, R.A.: The 2018 World Health Organization Classification of Cutaneous, Mucosal, and Uveal Melanoma: Detailed Analysis of 9 Distinct Subtypes Defined by Their Evolutionary Pathway. Archives of pathology & laboratory medicine **144**(4), 500–522 (2020). doi: 10.5858/arpa.2019-0561-RA
15. Ferrara, G., Argenziano, G.: The WHO 2018 Classification of Cutaneous Melanocytic Neoplasms: Suggestions From Routine Practice. Frontiers in oncology **11**, 675296 (2021). doi: 10.3389/fonc.2021.675296
16. Scolyer, R.A., Long, G.V., Thompson, J.F.: Evolving concepts in melanoma classification and their relevance to multidisciplinary melanoma patient care. Molecular oncology **5**(2), 124–136 (2011). doi: 10.1016/j.molonc.2011.03.002
17. Swetter, S.M., Tsao, H., Bichakjian, C.K., Curiel-Lewandrowski, C., Elder, D.E., Gershenwald, J.E., Guild, V., Grant-Kels, J.M., Halpern, A.C., Johnson, T.M., Sober, A.J., Thompson, J.A., Wisco, O.J., Wyatt, S., Hu, S., Lamina, T.: Guidelines of care for the management of primary cutaneous melanoma. Journal of the American Academy of Dermatology **80**(1), 208–250 (2019). doi: 10.1016/j.jaad.2018.08.055
18. Rajkumar, S., Watson, I.R.: Molecular characterisation of cutaneous melanoma: creating a framework for targeted and immune therapies. British journal of cancer **115**(2), 145–155 (2016). doi: 10.1038/bjc.2016.195
19. Gandini, S., Sera, F., Cattaruzza, M.S., Pasquini, P., Abeni, D., Boyle, P., Melchi, C.F.: Meta-analysis of risk factors for cutaneous melanoma: I. Common and atypical naevi. European journal of cancer (Oxford, England : 1990) **41**(1), 28–44 (2005). doi: 10.1016/j.ejca.2004.10.015

20. Rebecca, V.W., Sondak, V.K., Smalley, K.S.M.: A brief history of melanoma: from mummies to mutations. Melanoma research **22**(2), 114–122 (2012). doi: 10.1097/CMR.0b013e328351fa4d
21. Sung, H., Ferlay, J., Siegel, R.L., Laversanne, M., Soerjomataram, I., Jemal, A., Bray, F.: Global Cancer Statistics 2020: GLOBOCAN Estimates of Incidence and Mortality Worldwide for 36 Cancers in 185 Countries. CA: a cancer journal for clinicians **71**(3), 209–249 (2021). doi: 10.3322/caac.21660
22. Siegel, R.L., Miller, K.D., Fuchs, H.E., Jemal, A.: Cancer statistics, 2022. CA: a cancer journal for clinicians **72**(1), 7–33 (2022). doi: 10.3322/caac.21708
23. Dyba, T., Randi, G., Bray, F., Martos, C., Giusti, F., Nicholson, N., Gavin, A., Flego, M., Neamtiu, L., Dimitrova, N., Negrão Carvalho, R., Ferlay, J., Bettio, M.: The European cancer burden in 2020: Incidence and mortality estimates for 40 countries and 25 major cancers. European journal of cancer (Oxford, England : 1990) **157**, 308–347 (2021). doi: 10.1016/j.ejca.2021.07.039
24. Giaquinto, A.N., Miller, K.D., Tossas, K.Y., Winn, R.A., Jemal, A., Siegel, R.L.: Cancer statistics for African American/Black People 2022. CA: a cancer journal for clinicians **72**(3), 202–229 (2022). doi: 10.3322/caac.21718
25. Rastrelli, M., Tropea, S., Rossi, C.R., Alaibac, M.: Melanoma: epidemiology, risk factors, pathogenesis, diagnosis and classification. In vivo (Athens, Greece) **28**(6), 1005–1011 (2014)
26. Goon, P., Banfield, C., Bello, O., Levell, N.J.: Skin cancers in skin types IV-VI: Does the Fitzpatrick scale give a false sense of security? Skin health and disease **1**(3), e40 (2021). doi: 10.1002/ski2.40
27. Michielin, O., van Akkooi, A.C.J., Ascierto, P.A., Dummer, R., Keilholz, U.: Cutaneous melanoma: ESMO Clinical Practice Guidelines for diagnosis, treatment and follow-up†. Annals of oncology : official journal of the European Society for Medical Oncology **30**(12), 1884–1901 (2019). doi: 10.1093/annonc/mdz411
28. Uong, A., Zon, L.I.: Melanocytes in development and cancer. Journal of cellular physiology **222**(1), 38–41 (2010). doi: 10.1002/jcp.21935
29. Hapach, L.A., Mosier, J.A., Wang, W., Reinhart-King, C.A.: Engineered models to parse apart the metastatic cascade. NPJ precision oncology **3**, 20 (2019). doi: 10.1038/s41698-019-0092-3
30. Wang, S., Ye, T., Li, G., Zhang, X., Shi, H.: Margination and adhesion dynamics of tumor cells in a real microvascular network. PLoS computational biology **17**(2), e1008746 (2021). doi: 10.1371/journal.pcbi.1008746

31. Novikov, N.M., Zolotaryova, S.Y., Gautreau, A.M., Denisov, E.V.: Mutational drivers of cancer cell migration and invasion. British journal of cancer **124**(1), 102–114 (2021). doi: 10.1038/s41416-020-01149-0
32. Fujii, T., Shimizu, T., Katoh, M., Nagamori, S., Koizumi, K., Fukuoka, J., Tabuchi, Y., Sawaguchi, A., Okumura, T., Shibuya, K., Fujii, T., Takeshima, H., Sakai, H.: Survival of detached cancer cells is regulated by movement of intracellular Na+,K+-ATPase. iScience **24**(5), 102412 (2021). doi: 10.1016/j.isci.2021.102412
33. Fares, J., Fares, M.Y., Khachfe, H.H., Salhab, H.A., Fares, Y.: Molecular principles of metastasis: a hallmark of cancer revisited. Signal transduction and targeted therapy **5**(1), 28 (2020). doi: 10.1038/s41392-020-0134-x
34. Meirson, T., Gil-Henn, H., Samson, A.O.: Invasion and metastasis: the elusive hallmark of cancer. Oncogene **39**(9), 2024–2026 (2020). doi: 10.1038/s41388-019-1110-1
35. Ju, R.J., Stehbens, S.J., Haass, N.K.: The Role of Melanoma Cell-Stroma Interaction in Cell Motility, Invasion, and Metastasis. Frontiers in medicine **5**, 307 (2018). doi: 10.3389/fmed.2018.00307
36. Gershenwald, J.E., Scolyer, R.A., Hess, K.R., Sondak, V.K., Long, G.V., Ross, M.I., Lazar, A.J., Faries, M.B., Kirkwood, J.M., McArthur, G.A., Haydu, L.E., Eggermont, A.M.M., Flaherty, K.T., Balch, C.M., Thompson, J.F.: Melanoma staging: Evidence-based changes in the American Joint Committee on Cancer eighth edition cancer staging manual. CA: a cancer journal for clinicians **67**(6), 472–492 (2017). doi: 10.3322/caac.21409
37. Izraely, S., Witz, I.P.: Site-specific metastasis: A cooperation between cancer cells and the metastatic microenvironment. International journal of cancer **148**(6), 1308–1322 (2021). doi: 10.1002/ijc.33247
38. Salvati, L., Mandalà, M., Massi, D.: Melanoma brain metastases: review of histopathological features and immune-molecular aspects. Melanoma management **7**(2), MMT44 (2020). doi: 10.2217/mmt-2019-0021
39. Teixido, C., Castillo, P., Martinez-Vila, C., Arance, A., Alos, L.: Molecular Markers and Targets in Melanoma. Cells **10**(9) (2021). doi: 10.3390/cells10092320
40. Holmes, D.: The cancer that rises with the sun. Nature **515**(7527), S110-1 (2014). doi: 10.1038/515S110a
41. Shain, A.H., Bastian, B.C.: From melanocytes to melanomas. Nature reviews. Cancer **16**(6), 345–358 (2016). doi: 10.1038/nrc.2016.37
42. Markiewicz, E., Idowu, O.C.: DNA damage in human skin and the capacities of natural compounds to modulate the bystander signalling. Open biology **9**(12), 190208 (2019). doi: 10.1098/rsob.190208

43. Cui, R., Widlund, H.R., Feige, E., Lin, J.Y., Wilensky, D.L., Igras, V.E., D'Orazio, J., Fung, C.Y., Schanbacher, C.F., Granter, S.R., Fisher, D.E.: Central role of p53 in the suntan response and pathologic hyperpigmentation. Cell **128**(5), 853–864 (2007). doi: 10.1016/j.cell.2006.12.045
44. D'Orazio, J., Jarrett, S., Amaro-Ortiz, A., Scott, T.: UV radiation and the skin. International journal of molecular sciences **14**(6), 12222–12248 (2013). doi: 10.3390/ijms140612222
45. Sun, X., Zhang, N., Yin, C., Zhu, B., Li, X.: Ultraviolet Radiation and Melanomagenesis: From Mechanism to Immunotherapy. Frontiers in oncology **10**, 951 (2020). doi: 10.3389/fonc.2020.00951
46. Gelmi, M.C., Houtzagers, L.E., Strub, T., Krossa, I., Jager, M.J.: MITF in Normal Melanocytes, Cutaneous and Uveal Melanoma: A Delicate Balance. International journal of molecular sciences **23**(11) (2022). doi: 10.3390/ijms23116001
47. Yun, W.J., Kim, E.-Y., Park, J.-E., Jo, S.Y., Bang, S.H., Chang, E.-J., Chang, S.E.: Microtubule-associated protein light chain 3 is involved in melanogenesis via regulation of MITF expression in melanocytes. Scientific reports **6**, 19914 (2016). doi: 10.1038/srep19914
48. Costin, G.-E., Hearing, V.J.: Human skin pigmentation: melanocytes modulate skin color in response to stress. FASEB journal : official publication of the Federation of American Societies for Experimental Biology **21**(4), 976–994 (2007). doi: 10.1096/fj.06-6649rev
49. Brás, M.M., Radmacher, M., Sousa, S.R., Granja, P.L.: Melanoma in the Eyes of Mechanobiology. Frontiers in cell and developmental biology **8**, 54 (2020). doi: 10.3389/fcell.2020.00054
50. Kim, J.Y., Shin, J.Y., Kim, M.R., Hann, S.-K., Oh, S.H.: siRNA-mediated knock-down of COX-2 in melanocytes suppresses melanogenesis, 6 (2012)
51. Oren, M., Bartek, J.: The sunny side of p53. Cell **128**(5), 826–828 (2007). doi: 10.1016/j.cell.2007.02.027
52. Holcomb, N.C., Bautista, R.-M., Jarrett, S.G., Carter, K.M., Gober, M.K., D'Orazio, J.A.: cAMP-mediated regulation of melanocyte genomic instability: A melanoma-preventive strategy. Advances in protein chemistry and structural biology **115**, 247–295 (2019). doi: 10.1016/bs.apcsb.2018.10.008
53. Nasti, T.H., Timares, L.: MC1R, eumelanin and pheomelanin: their role in determining the susceptibility to skin cancer. Photochemistry and photobiology **91**(1), 188–200 (2015). doi: 10.1111/php.12335
54. Mitra, D., Luo, X., Morgan, A., Wang, J., Hoang, M.P., Lo, J., Guerrero, C.R., Lennerz, J.K., Mihm, M.C., Wargo, J.A., Robinson, K.C., Devi, S.P., Vanover, J.C.,

D'Orazio, J.A., McMahon, M., Bosenberg, M.W., Haigis, K.M., Haber, D.A., Wang, Y., Fisher, D.E.: An ultraviolet-radiation-independent pathway to melanoma carcinogenesis in the red hair/fair skin background. Nature **491**(7424), 449–453 (2012). doi: 10.1038/nature11624

55. Arisi, M., Zane, C., Caravello, S., Rovati, C., Zanca, A., Venturini, M., Calzavara-Pinton, P.: Sun Exposure and Melanoma, Certainties and Weaknesses of the Present Knowledge. Frontiers in medicine **5**, 235 (2018). doi: 10.3389/fmed.2018.00235
56. Cherepakhin, O.S., Argenyi, Z.B., Moshiri, A.S.: Genomic and Transcriptomic Underpinnings of Melanoma Genesis, Progression, and Metastasis. Cancers **14**(1) (2021). doi: 10.3390/cancers14010123
57. Cauci, S., Maione, V., Buligan, C., Linussio, M., Serraino, D., Stinco, G.: BsmI (rs1544410) and FokI (rs2228570) vitamin D receptor polymorphisms, smoking, and body mass index as risk factors of cutaneous malignant melanoma in northeast Italy. Cancer biology & medicine **14**(3), 302–318 (2017). doi: 10.20892/j.issn.2095-3941.2017.0064
58. Diffey, B.L.: Sources and measurement of ultraviolet radiation. Methods **28**(1), 4–13 (2002). doi: 10.1016/s1046-2023(02)00204-9
59. Timares, L., Katiyar, S.K., Elmets, C.A.: DNA damage, apoptosis and langerhans cells--Activators of UV-induced immune tolerance. Photochemistry and photobiology **84**(2), 422–436 (2008). doi: 10.1111/j.1751-1097.2007.00284.x
60. International Agency for Research on Cancer (IARC): Exposure to artificial UV radiation and skin cancer. IARC working group reports, vol. 1. International Agency for Research on Cancer, Lyon (2005)
61. Khan, A.Q., Travers, J.B., Kemp, M.G.: Roles of UVA radiation and DNA damage responses in melanoma pathogenesis. Environmental and molecular mutagenesis **59**(5), 438–460 (2018). doi: 10.1002/em.22176
62. Sample, A., He, Y.-Y.: Mechanisms and prevention of UV-induced melanoma. Photodermatology, photoimmunology & photomedicine **34**(1), 13–24 (2018). doi: 10.1111/phpp.12329
63. Brem, R., Macpherson, P., Guven, M., Karran, P.: Oxidative stress induced by UVA photoactivation of the tryptophan UVB photoproduct 6-formylindolo3,2-bcarbazole (FICZ) inhibits nucleotide excision repair in human cells. Scientific reports **7**(1), 4310 (2017). doi: 10.1038/s41598-017-04614-8
64. Hoeijmakers, J.H.J.: DNA damage, aging, and cancer. The New England journal of medicine **361**(15), 1475–1485 (2009). doi: 10.1056/NEJMra0804615

65. Budden, T., Davey, R.J., Vilain, R.E., Ashton, K.A., Braye, S.G., Beveridge, N.J., Bowden, N.A.: Repair of UVB-induced DNA damage is reduced in melanoma due to low XPC and global genome repair. Oncotarget **7**(38), 60940–60953 (2016). doi: 10.18632/oncotarget.10902
66. Noonan, F.P., Zaidi, M.R., Wolnicka-Glubisz, A., Anver, M.R., Bahn, J., Wielgus, A., Cadet, J., Douki, T., Mouret, S., Tucker, M.A., Popratiloff, A., Merlino, G., Fabo, E.C. de: Melanoma induction by ultraviolet A but not ultraviolet B radiation requires melanin pigment. Nature communications **3**, 884 (2012). doi: 10.1038/ncomms1893
67. Tudor, D.V., Bâldea, I., Lupu, M., Kacso, T., Kutasi, E., Hopârtean, A., Stretea, R., Gabriela Filip, A.: COX-2 as a potential biomarker and therapeutic target in melanoma. Cancer biology & medicine **17**(1), 20–31 (2020). doi: 10.20892/j.issn.2095-3941.2019.0339
68. International Agency for Research on Cancer (IARC) - Working Group on artificial ultraviolet (UV) light and skin cancer: The association of use of sunbeds with cutaneous malignant melanoma and other skin cancers: A systematic review. International journal of cancer **120**(5), 1116–1122 (2007). doi: 10.1002/ijc.22453
69. World Health Organization (WHO): Artificial Tanning Devices. Documents for Sale Ser. World Health Organization, Geneva (2017)
70. Autier, P.: Perspectives in melanoma prevention: the case of sunbeds. European journal of cancer (Oxford, England : 1990) **40**(16), 2367–2376 (2004). doi: 10.1016/j.ejca.2004.07.018
71. El Ghissassi, F., Baan, R., Straif, K., Grosse, Y., Secretan, B., Bouvard, V., Benbrahim-Tallaa, L., Guha, N., Freeman, C., Galichet, L., Cogliano, V.: A review of human carcinogens—Part D: radiation. The Lancet Oncology **10**(8), 751–752 (2009). doi: 10.1016/s1470-2045(09)70213-x
72. Boniol, M., Autier, P., Boyle, P., Gandini, S.: Cutaneous melanoma attributable to sunbed use: systematic review and meta-analysis. BMJ (Clinical research ed.) **345**, e4757 (2012). doi: 10.1136/bmj.e4757
73. Chhabra, G., Ndiaye, M.A., Garcia-Peterson, L.M., Ahmad, N.: Melanoma Chemoprevention: Current Status and Future Prospects. Photochemistry and photobiology **93**(4), 975–989 (2017). doi: 10.1111/php.12749
74. Ombra, M.N., Paliogiannis, P., Doneddu, V., Sini, M.C., Colombino, M., Rozzo, C., Stanganelli, I., Tanda, F., Cossu, A., Palmieri, G.: Vitamin D status and risk for malignant cutaneous melanoma: recent advances. European journal of cancer prevention : the official journal of the European Cancer Prevention Organisation (ECP) **26**(6), 532–541 (2017). doi: 10.1097/CEJ.0000000000000334

75. Bade, B., Zdebik, A., Wagenpfeil, S., Gräber, S., Geisel, J., Vogt, T., Reichrath, J.: Low serum 25-hydroxyvitamin d concentrations are associated with increased risk for melanoma and unfavourable prognosis. PloS one **9**(12), e112863 (2014). doi: 10.1371/journal.pone.0112863
76. Lombardo, M., Vigezzi, A., Ietto, G., Franchi, C., Iori, V., Masci, F., Scorza, A., Macchi, S., Iovino, D., Parise, C., Carcano, G.: Role of vitamin D serum levels in prevention of primary and recurrent melanoma. Scientific reports **11**(1), 5815 (2021). doi: 10.1038/s41598-021-85294-3
77. Timerman, D., McEnery-Stonelake, M., Joyce, C.J., Nambudiri, V.E., Hodi, F.S., Claus, E.B., Ibrahim, N., Lin, J.Y.: Vitamin D deficiency is associated with a worse prognosis in metastatic melanoma. Oncotarget **8**(4), 6873–6882 (2017). doi: 10.18632/oncotarget.14316
78. Jiang, A.J., Rambhatla, P.V., Eide, M.J.: Socioeconomic and lifestyle factors and melanoma: a systematic review. The British journal of dermatology **172**(4), 885–915 (2015). doi: 10.1111/bjd.13500
79. Fortes, C., Vries, E. de: Nonsolar occupational risk factors for cutaneous melanoma. International journal of dermatology **47**(4), 319–328 (2008). doi: 10.1111/j.1365-4632.2008.03653.x
80. Miura, K., Olsen, C.M., Rea, S., Marsden, J., Green, A.C.: Do airline pilots and cabin crew have raised risks of melanoma and other skin cancers? Systematic review and meta-analysis. The British journal of dermatology **181**(1), 55–64 (2019). doi: 10.1111/bjd.17586
81. Industrial Injuries Advisory Council (IIAC): Cutaneous malignant melanoma and occupational exposure to (natural) UV radiation in pilots and aircrew. UK Parliament Command Paper, session 2019/21, CP 216. Dandy Booksellers Ltd, Great Britain - London (2020)
82. Saginala, K., Barsouk, A., Aluru, J.S., Rawla, P., Barsouk, A.: Epidemiology of Melanoma. Medical sciences (Basel, Switzerland) **9**(4) (2021). doi: 10.3390/medsci9040063
83. Joosse, A., Vries, E. de, Eckel, R., Nijsten, T., Eggermont, A.M.M., Hölzel, D., Coebergh, J.W.W., Engel, J.: Gender differences in melanoma survival: female patients have a decreased risk of metastasis. The Journal of investigative dermatology **131**(3), 719–726 (2011). doi: 10.1038/jid.2010.354
84. Mervic, L.: Time course and pattern of metastasis of cutaneous melanoma differ between men and women, vol. 7 (2012)
85. Sacchetto, L., Zanetti, R., Comber, H., Bouchardy, C., Brewster, D.H., Broganelli, P., Chirlaque, M.D., Coza, D., Galceran, J., Gavin, A., Hackl, M., Katalinic, A.,

Larønningen, S., Louwman, M.W.J., Morgan, E., Robsahm, T.E., Sanchez, M.J., Tryggvadóttir, L., Tumino, R., van Eycken, E., Vernon, S., Zadnik, V., Rosso, S.: Trends in incidence of thick, thin and *in situ* melanoma in Europe. European journal of cancer (Oxford, England : 1990) **92**, 108–118 (2018). doi: 10.1016/j.ejca.2017.12.024

86. Bertrand, J.U., Steingrimsson, E., Jouenne, F., Bressac-de Paillerets, B., Larue, L.: Melanoma Risk and Melanocyte Biology. Acta dermato-venereologica **100**(11), adv00139 (2020). doi: 10.2340/00015555-3494
87. Bakos, L., Masiero, N.C.M.S., Bakos, R.M., Burttet, R.M., Wagner, M.B., Benzano, D.: European ancestry and cutaneous melanoma in Southern Brazil. Journal of the European Academy of Dermatology and Venereology : JEADV **23**(3), 304–307 (2009). doi: 10.1111/j.1468-3083.2008.03027.x
88. Norval, M., Wright, C.Y.: Cutaneous Melanoma: Etiology and Therapy. The Epidemiology of Cutaneous Melanoma in the White and Black African Population Groups in South Africa, Brisbane (AU) (2017)
89. Hart, P.H., Norval, M.: Ultraviolet radiation-induced immunosuppression and its relevance for skin carcinogenesis. Photochemical & photobiological sciences : Official journal of the European Photochemistry Association and the European Society for Photobiology **17**(12), 1872–1884 (2018). doi: 10.1039/c7pp00312a
90. Bernard, J.J., Gallo, R.L., Krutmann, J.: Photoimmunology: how ultraviolet radiation affects the immune system. Nature reviews. Immunology **19**(11), 688–701 (2019). doi: 10.1038/s41577-019-0185-9
91. Berge, L.A.M., Andreassen, B.K., Stenehjem, J.S., Heir, T., Karlstad, Ø., Juzeniene, A., Ghiasvand, R., Larsen, I.K., Green, A.C., Veierød, M.B., Robsahm, T.E.: Use of Immunomodulating Drugs and Risk of Cutaneous Melanoma: A Nationwide Nested Case-Control Study. Clinical epidemiology **12**, 1389–1401 (2020). doi: 10.2147/CLEP.S269446
92. Green, A.C., Olsen, C.M.: Increased risk of melanoma in organ transplant recipients: systematic review and meta-analysis of cohort studies. Acta dermato-venereologica **95**(8), 923–927 (2015). doi: 10.2340/00015555-2148
93. Robbins, H.A., Clarke, C.A., Arron, S.T., Tatalovich, Z., Kahn, A.R., Hernandez, B.Y., Paddock, L., Yanik, E.L., Lynch, C.F., Kasiske, B.L., Snyder, J., Engels, E.A.: Melanoma Risk and Survival among Organ Transplant Recipients. The Journal of investigative dermatology **135**(11), 2657–2665 (2015). doi: 10.1038/jid.2015.312
94. Kubica, A.W., Brewer, J.D.: Melanoma in immunosuppressed patients. Mayo Clinic proceedings **87**(10), 991–1003 (2012). doi: 10.1016/j.mayocp.2012.04.018

95. Sargen, M.R., Cahoon, E.K., Yu, K.J., Madeleine, M.M., Zeng, Y., Rees, J.R., Lynch, C.F., Engels, E.A.: Spectrum of Nonkeratinocyte Skin Cancer Risk Among Solid Organ Transplant Recipients in the US. JAMA dermatology **158**(4), 414–425 (2022). doi: 10.1001/jamadermatol.2022.0036
96. Bergman, W., Gruis, N.A.: Management of melanoma families. Cancers **2**(2), 549–566 (2010). doi: 10.3390/cancers2020549
97. Rossi, M., Pellegrini, C., Cardelli, L., Ciciarelli, V., Di Nardo, L., Fargnoli, M.C.: Familial Melanoma: Diagnostic and Management Implications. Dermatology practical & conceptual **9**(1), 10–16 (2019). doi: 10.5826/dpc.0901a03
98. Frank, C., Sundquist, J., Hemminki, A., Hemminki, K.: Risk of other Cancers in Families with Melanoma: Novel Familial Links. Scientific reports **7**, 42601 (2017). doi: 10.1038/srep42601
99. Lee, K.J., Janda, M., Stark, M.S., Sturm, R.A., Soyer, H.P.: On Naevi and Melanomas: Two Sides of the Same Coin? Frontiers in medicine **8**, 635316 (2021). doi: 10.3389/fmed.2021.635316
100. Wei, E.X., Li, X., Nan, H.: Having a first-degree relative with melanoma increases lifetime risk of melanoma, squamous cell carcinoma, and basal cell carcinoma. Journal of the American Academy of Dermatology **81**(2), 489–499 (2019). doi: 10.1016/j.jaad.2019.04.044
101. Bhatt, M., Nabatian, A., Kriegel, D., Khorasani, H.: Does an increased number of moles correlate to a higher risk of melanoma? Melanoma management **3**(2), 85–87 (2016). doi: 10.2217/mmt-2016-0001
102. Purdue, M.P., From, L., Armstrong, B.K., Kricker, A., Gallagher, R.P., McLaughlin, J.R., Klar, N.S., Marrett, L.D.: Etiologic and other factors predicting nevus-associated cutaneous malignant melanoma. Cancer epidemiology, biomarkers & prevention : a publication of the American Association for Cancer Research, cosponsored by the American Society of Preventive Oncology **14**(8), 2015–2022 (2005). doi: 10.1158/1055-9965.EPI-05-0097
103. Tsao, H., Bevona, C., Goggins, W., Quinn, T.: The transformation rate of moles (melanocytic nevi) into cutaneous melanoma: a population-based estimate. Archives of dermatology **139**(3), 282–288 (2003). doi: 10.1001/archderm.139.3.282
104. Colebatch, A.J., Scolyer, R.A.: Trajectories of premalignancy during the journey from melanocyte to melanoma. Pathology **50**(1), 16–23 (2018). doi: 10.1016/j.pathol.2017.09.002
105. Walter, F.M., Humphrys, E., Tso, S., Johnson, M., Cohn, S.: Patient understanding of moles and skin cancer, and factors influencing presentation in primary care: a qualitative study. BMC family practice **11**, 62 (2010). doi: 10.1186/1471-2296-11-62

106. Weatherhead, S.C., Haniffa, M., Lawrence, C.M.: Melanomas arising from naevi and de novo melanomas--does origin matter? The British journal of dermatology **156**(1), 72–76 (2007). doi: 10.1111/j.1365-2133.2006.07570.x
107. Pampena, R., Kyrgidis, A., Lallas, A., Moscarella, E., Argenziano, G., Longo, C.: A meta-analysis of nevus-associated melanoma: Prevalence and practical implications. Journal of the American Academy of Dermatology **77**(5), 938-945.e4 (2017). doi: 10.1016/j.jaad.2017.06.149
108. Pandeya, N., Kvaskoff, M., Olsen, C.M., Green, A.C., Perry, S., Baxter, C., Davis, M.B., Mortimore, R., Westacott, L., Wood, D., Triscott, J., Williamson, R., Whiteman, D.C.: Factors Related to Nevus-Associated Cutaneous Melanoma: A Case-Case Study. The Journal of investigative dermatology **138**(8), 1816–1824 (2018). doi: 10.1016/j.jid.2017.12.036
109. Bär, M.: Spitz and Reed nevi: acquired or congenital? Dermatology practical & conceptual **2**(3), 203a05 (2012). doi: 10.5826/dpc.0203a05
110. Endomba, F.T., Mbega, C.R., Tochie, J.N., Petnga, S.-J.N.: Giant congenital melanocytic nevus in a Cameroonian child: a case report. Journal of medical case reports **12**(1), 175 (2018). doi: 10.1186/s13256-018-1707-y
111. Tannous, Z.S., Mihm, M.C., Sober, A.J., Duncan, L.M.: Congenital melanocytic nevi: clinical and histopathologic features, risk of melanoma, and clinical management. Journal of the American Academy of Dermatology **52**(2), 197–203 (2005). doi: 10.1016/j.jaad.2004.07.020
112. Bauer, J., Garbe, C.: Acquired melanocytic nevi as risk factor for melanoma development. A comprehensive review of epidemiological data. Pigment cell research **16**(3), 297–306 (2003). doi: 10.1034/j.1600-0749.2003.00047.x
113. Echeverría, B., Bulliard, J.-L., Guillén, C., Nagore, E.: Indicators for the total number of melanocytic naevi: an adjunct for screening campaigns. Observational study on 292 patients. The British journal of dermatology **170**(1), 144–149 (2014). doi: 10.1111/bjd.12692
114. Friedman, R.J., Rigel, D.S., Kopf, A.W.: Early detection of malignant melanoma: the role of physician examination and self-examination of the skin. CA: a cancer journal for clinicians **35**(3), 130–151 (1985). doi: 10.3322/canjclin.35.3.130
115. Abbasi, N.R., Shaw, H.M., Rigel, D.S., Friedman, R.J., McCarthy, W.H., Osman, I., Kopf, A.W., Polsky, D.: Early diagnosis of cutaneous melanoma: revisiting the ABCD criteria. JAMA **292**(22), 2771–2776 (2004). doi: 10.1001/jama.292.22.2771
116. Uhler, C., Shivashankar, G.V.: Regulation of genome organization and gene expression by nuclear mechanotransduction. Nature reviews. Molecular cell biology **18**(12), 717–727 (2017). doi: 10.1038/nrm.2017.101

117. Swaminathan, V., Gloerich, M.: Decoding mechanical cues by molecular mechanotransduction. Current opinion in cell biology **72**, 72–80 (2021). doi: 10.1016/j.ceb.2021.05.006
118. Broders-Bondon, F., Nguyen Ho-Bouldoires, T.H., Fernandez-Sanchez, M.-E., Farge, E.: Mechanotransduction in tumor progression: The dark side of the force. The Journal of cell biology **217**(5), 1571–1587 (2018). doi: 10.1083/jcb.201701039
119. Romani, P., Valcarcel-Jimenez, L., Frezza, C., Dupont, S.: Crosstalk between mechanotransduction and metabolism. Nature reviews. Molecular cell biology **22**(1), 22–38 (2021). doi: 10.1038/s41580-020-00306-w
120. Seong, J., Wang, N., Wang, Y.: Mechanotransduction at focal adhesions: from physiology to cancer development. Journal of cellular and molecular medicine **17**(5), 597–604 (2013). doi: 10.1111/jcmm.12045
121. Murthy, S.E., Dubin, A.E., Patapoutian, A.: Piezos thrive under pressure: mechanically activated ion channels in health and disease. Nature reviews. Molecular cell biology **18**(12), 771–783 (2017). doi: 10.1038/nrm.2017.92
122. Uray, I.P., Uray, K.: Mechanotransduction at the Plasma Membrane-Cytoskeleton Interface. International journal of molecular sciences **22**(21) (2021). doi: 10.3390/ijms222111566
123. Chen, Y., Ju, L., Rushdi, M., Ge, C., Zhu, C.: Receptor-mediated cell mechanosensing. Molecular biology of the cell **28**(23), 3134–3155 (2017). doi: 10.1091/mbc.E17-04-0228
124. Nourse, J.L., Pathak, M.M.: How cells channel their stress: Interplay between Piezo1 and the cytoskeleton. Seminars in cell & developmental biology **71**, 3–12 (2017). doi: 10.1016/j.semcdb.2017.06.018
125. Dombroski, J.A., Hope, J.M., Sarna, N.S., King, M.R.: Channeling the Force: Piezo1 Mechanotransduction in Cancer Metastasis. Cells **10**(11) (2021). doi: 10.3390/cells10112815
126. Zhang, H., Chen, Z., Zhang, A., Gupte, A.A., Hamilton, D.J.: The Role of Calcium Signaling in Melanoma. International journal of molecular sciences **23**(3) (2022). doi: 10.3390/ijms23031010
127. Felice, D. de, Alaimo, A.: Mechanosensitive Piezo Channels in Cancer: Focus on altered Calcium Signaling in Cancer Cells and in Tumor Progression. Cancers **12**(7) (2020). doi: 10.3390/cancers12071780
128. Botello-Smith, W.M., Jiang, W., Zhang, H., Ozkan, A.D., Lin, Y.-C., Pham, C.N., Lacroix, J.J., Luo, Y.: A mechanism for the activation of the mechanosensitive Piezo1 channel by the small molecule Yoda1. Nature communications **10**(1), 4503 (2019). doi: 10.1038/s41467-019-12501-1

129. Song, S., Zhang, H., Wang, X., Chen, W., Cao, W., Zhang, Z., Shi, C.: The role of mechanosensitive Piezo1 channel in diseases. Progress in biophysics and molecular biology **172**, 39–49 (2022). doi: 10.1016/j.pbiomolbio.2022.04.006
130. Zhang, J., Zhou, Y., Huang, T., Wu, F., Liu, L., Kwan, J.S.H., Cheng, A.S.L., Yu, J., To, K.F., Kang, W.: PIEZO1 functions as a potential oncogene by promoting cell proliferation and migration in gastric carcinogenesis. Molecular carcinogenesis **57**(9), 1144–1155 (2018). doi: 10.1002/mc.22831
131. Yu, Y., Wu, X., Liu, S., Zhao, H., Li, B., Zhao, H., Feng, X.: Piezo1 regulates migration and invasion of breast cancer cells via modulating cell mechanobiological properties. Acta biochimica et biophysica Sinica **53**(1), 10–18 (2021). doi: 10.1093/abbs/gmaa112
132. Etem, E.Ö., Ceylan, G.G., Özaydın, S., Ceylan, C., Özercan, I., Kuloğlu, T.: The increased expression of Piezo1 and Piezo2 ion channels in human and mouse bladder carcinoma. Advances in clinical and experimental medicine : official organ Wroclaw Medical University **27**(8), 1025–1031 (2018). doi: 10.17219/acem/71080
133. Han, Y., Liu, C., Zhang, D., Men, H., Huo, L., Geng, Q., Wang, S., Gao, Y., Zhang, W., Zhang, Y., Jia, Z.: Mechanosensitive ion channel Piezo1 promotes prostate cancer development through the activation of the Akt/mTOR pathway and acceleration of cell cycle. International journal of oncology **55**(3), 629–644 (2019). doi: 10.3892/ijo.2019.4839
134. Zhang, S., Cao, S., Gong, M., Zhang, W., Zhang, W., Zhu, Z., Wu, S., Yue, Y., Qian, W., Ma, Q., Wang, S., Wang, Z.: Mechanically activated ion channel Piezo1 contributes to melanoma malignant progression through AKT/mTOR signaling. Cancer biology & therapy **23**(1), 336–347 (2022). doi: 10.1080/15384047.2022.2060015
135. Hung, W.-C., Yang, J.R., Yankaskas, C.L., Wong, B.S., Wu, P.-H., Pardo-Pastor, C., Serra, S.A., Chiang, M.-J., Gu, Z., Wirtz, D., Valverde, M.A., Yang, J.T., Zhang, J., Konstantopoulos, K.: Confinement Sensing and Signal Optimization via Piezo1/PKA and Myosin II Pathways. Cell reports **15**(7), 1430–1441 (2016). doi: 10.1016/j.celrep.2016.04.035
136. Hynes, R.O.: Integrins: Bidirectional, Allosteric Signaling Machines. Cell **110**(6), 673–687 (2002). doi: 10.1016/S0092-8674(02)00971-6
137. Wang, N.: Cellular adhesion: Instant integrin mechanosensing. Nature materials **16**(12), 1173–1174 (2017). doi: 10.1038/nmat5041
138. Slack, R.J., Macdonald, S.J.F., Roper, J.A., Jenkins, R.G., Hatley, R.J.D.: Emerging therapeutic opportunities for integrin inhibitors. Nature reviews. Drug discovery **21**(1), 60–78 (2022). doi: 10.1038/s41573-021-00284-4

139. Shattil, S.J., Kim, C., Ginsberg, M.H.: The final steps of integrin activation: the end game. Nature reviews. Molecular cell biology **11**(4), 288–300 (2010). doi: 10.1038/nrm2871
140. Janiszewska, M., Primi, M.C., Izard, T.: Cell adhesion in cancer: Beyond the migration of single cells. The Journal of biological chemistry **295**(8), 2495–2505 (2020). doi: 10.1074/jbc.REV119.007759
141. Cooper, J., Giancotti, F.G.: Integrin Signaling in Cancer: Mechanotransduction, Stemness, Epithelial Plasticity, and Therapeutic Resistance. Cancer cell **35**(3), 347–367 (2019). doi: 10.1016/j.ccell.2019.01.007
142. Strohmeyer, N., Bharadwaj, M., Costell, M., Fässler, R., Müller, D.J.: Fibronectin-bound α5β1 integrins sense load and signal to reinforce adhesion in less than a second. Nature materials **16**(12), 1262–1270 (2017). doi: 10.1038/nmat5023
143. Hamidi, H., Ivaska, J.: Every step of the way: integrins in cancer progression and metastasis. Nature reviews. Cancer **18**(9), 533–548 (2018). doi: 10.1038/s41568-018-0038-z
144. Zanconato, F., Battilana, G., Cordenonsi, M., Piccolo, S.: YAP/TAZ as therapeutic targets in cancer. Current opinion in pharmacology **29**, 26–33 (2016). doi: 10.1016/j.coph.2016.05.002
145. Del Pozo, M.A., Lolo, F.-N., Echarri, A.: Caveolae: Mechanosensing and mechanotransduction devices linking membrane trafficking to mechanoadaptation. Current opinion in cell biology **68**, 113–123 (2021). doi: 10.1016/j.ceb.2020.10.008
146. McHugh, B.J., Buttery, R., Lad, Y., Banks, S., Haslett, C., Sethi, T.: Integrin activation by Fam38A uses a novel mechanism of R-Ras targeting to the endoplasmic reticulum. Journal of cell science **123**(Pt 1), 51–61 (2010). doi: 10.1242/jcs.056424
147. Arias-Mejias, S.M., Warda, K.Y., Quattrocchi, E., Alonso-Quinones, H., Sominidi-Damodaran, S., Meves, A.: The role of integrins in melanoma: a review. International journal of dermatology **59**(5), 525–534 (2020). doi: 10.1111/ijd.14850
148. Hsu, M.-Y., Shih, D.-T., Meier, F.E., van Belle, P., Hsu, J.-Y., Elder, D.E., Buck, C.A., Herlyn, M.: Adenoviral Gene Transfer of β3 Integrin Subunit Induces Conversion from Radial to Vertical Growth Phase in Primary Human Melanoma. The American Journal of Pathology **153**(5), 1435–1442 (1998). doi: 10.1016/s0002-9440(10)65730-6
149. Lacaria, L., Lange, J.R., Goldmann, W.H., Rico, F., Alonso, J.L.: αvβ3 integrin expression increases elasticity in human melanoma cells. Biochemical and biophysical research communications **525**(4), 836–840 (2020). doi: 10.1016/j.bbrc.2020.02.156

150. Su, C.-Y., Li, J.-Q., Zhang, L.-L., Wang, H., Wang, F.-H., Tao, Y.-W., Wang, Y.-Q., Guo, Q.-R., Li, J.-J., Liu, Y., Yan, Y.-Y., Zhang, J.-Y.: The Biological Functions and Clinical Applications of Integrins in Cancers. Frontiers in pharmacology **11**, 579068 (2020). doi: 10.3389/fphar.2020.579068
151. Kaszak, I., Witkowska-Piłaszewicz, O., Niewiadomska, Z., Dworecka-Kaszak, B., Ngosa Toka, F., Jurka, P.: Role of Cadherins in Cancer-A Review. International journal of molecular sciences **21**(20) (2020). doi: 10.3390/ijms21207624
152. Gumbiner, B.M.: Regulation of cadherin-mediated adhesion in morphogenesis. Nature reviews. Molecular cell biology **6**(8), 622–634 (2005). doi: 10.1038/nrm1699
153. Oda, H., Takeichi, M.: Evolution: structural and functional diversity of cadherin at the adherens junction. The Journal of cell biology **193**(7), 1137–1146 (2011). doi: 10.1083/jcb.201008173
154. Shapiro, L., Weis, W.I.: Structure and biochemistry of cadherins and catenins. Cold Spring Harbor perspectives in biology **1**(3), a003053 (2009). doi: 10.1101/cshperspect.a003053
155. Leckband, D.E., Rooij, J. de: Cadherin adhesion and mechanotransduction. Annual review of cell and developmental biology **30**, 291–315 (2014). doi: 10.1146/annurev-cellbio-100913-013212
156. Cailliez, F., Lavery, R.: Cadherin mechanics and complexation: the importance of calcium binding. Biophysical journal **89**(6), 3895–3903 (2005). doi: 10.1529/biophysj.105.067322
157. Schoenit, A., Lo Giudice, C., Hahnen, N., Ollech, D., Jahnke, K., Göpfrich, K., Cavalcanti-Adam, E.A.: Tuning Epithelial Cell-Cell Adhesion and Collective Dynamics with Functional DNA-E-Cadherin Hybrid Linkers. Nano letters **22**(1), 302–310 (2022). doi: 10.1021/acs.nanolett.1c03780
158. Harris, T.J.C., Tepass, U.: Adherens junctions: from molecules to morphogenesis. Nature reviews. Molecular cell biology **11**(7), 502–514 (2010). doi: 10.1038/nrm2927
159. Brunton, V.G., MacPherson, I.R.J., Frame, M.C.: Cell adhesion receptors, tyrosine kinases and actin modulators: a complex three-way circuitry. Biochimica et biophysica acta **1692**(2-3), 121–144 (2004). doi: 10.1016/j.bbamcr.2004.04.010
160. Huang, H., Wright, S., Zhang, J., Brekken, R.A.: Getting a grip on adhesion: Cadherin switching and collagen signaling. Biochimica et biophysica acta. Molecular cell research **1866**(11), 118472 (2019). doi: 10.1016/j.bbamcr.2019.04.002
161. Wang, J., Jiang, J., Yang, X., Zhou, G., Wang, L., Xiao, B.: Tethering Piezo channels to the actin cytoskeleton for mechanogating via the cadherin-β-catenin

mechanotransduction complex. Cell reports **38**(6), 110342 (2022). doi: 10.1016/j.celrep.2022.110342

162. Maman, S., Witz, I.P.: A history of exploring cancer in context. Nature reviews. Cancer **18**(6), 359–376 (2018). doi: 10.1038/s41568-018-0006-7
163. Smith, B., Bhowmick, N.: Role of EMT in Metastasis and Therapy Resistance. JCM **5**(2), 17 (2016). doi: 10.3390/jcm5020017
164. Pedri, D., Karras, P., Landeloos, E., Marine, J.-C., Rambow, F.: Epithelial-to-mesenchymal-like transition events in melanoma. The FEBS journal **289**(5), 1352–1368 (2022). doi: 10.1111/febs.16021
165. Loh, C.-Y., Chai, J.Y., Tang, T.F., Wong, W.F., Sethi, G., Shanmugam, M.K., Chong, P.P., Looi, C.Y.: The E-Cadherin and N-Cadherin Switch in Epithelial-to-Mesenchymal Transition: Signaling, Therapeutic Implications, and Challenges. Cells **8**(10) (2019). doi: 10.3390/cells8101118
166. Las Rivas, J. de, Brozovic, A., Izraely, S., Casas-Pais, A., Witz, I.P., Figueroa, A.: Cancer drug resistance induced by EMT: novel therapeutic strategies. Archives of toxicology **95**(7), 2279–2297 (2021). doi: 10.1007/s00204-021-03063-7
167. Montanari, M., Rossetti, S., Cavaliere, C., D'Aniello, C., Malzone, M.G., Vanacore, D., Di Franco, R., La Mantia, E., Iovane, G., Piscitelli, R., Muscariello, R., Berretta, M., Perdonà, S., Muto, P., Botti, G., Bianchi, A.A.M., Veneziani, B.M., Facchini, G.: Epithelial-mesenchymal transition in prostate cancer: an overview. Oncotarget **8**(21), 35376–35389 (2017). doi: 10.18632/oncotarget.15686
168. Felipe Lima, J., Nofech-Mozes, S., Bayani, J., Bartlett, J.M.S.: EMT in Breast Carcinoma-A Review. Journal of clinical medicine **5**(7) (2016). doi: 10.3390/jcm5070065
169. Vu, T., Datta, P.K.: Regulation of EMT in Colorectal Cancer: A Culprit in Metastasis. Cancers **9**(12) (2017). doi: 10.3390/cancers9120171
170. Le Roux, A.-L., Quiroga, X., Walani, N., Arroyo, M., Roca-Cusachs, P.: The plasma membrane as a mechanochemical transducer. Philosophical transactions of the Royal Society of London. Series B, Biological sciences **374**(1779), 20180221 (2019). doi: 10.1098/rstb.2018.0221
171. Giacomini, I., Gianfanti, F., Desbats, M.A., Orso, G., Berretta, M., Prayer-Galetti, T., Ragazzi, E., Cocetta, V.: Cholesterol Metabolic Reprogramming in Cancer and Its Pharmacological Modulation as Therapeutic Strategy. Frontiers in oncology **11**, 682911 (2021). doi: 10.3389/fonc.2021.682911
172. Ikonen, E.: Cellular cholesterol trafficking and compartmentalization. Nature reviews. Molecular cell biology **9**(2), 125–138 (2008). doi: 10.1038/nrm2336

173. Zhang, J., Li, Q., Wu, Y., Wang, D., Xu, L., Zhang, Y., Wang, S., Wang, T., Liu, F., Zaky, M.Y., Hou, S., Liu, S., Zou, K., Lei, H., Zou, L., Zhang, Y., Liu, H.: Cholesterol content in cell membrane maintains surface levels of ErbB2 and confers a therapeutic vulnerability in ErbB2-positive breast cancer. Cell communication and signaling : CCS **17**(1), 15 (2019). doi: 10.1186/s12964-019-0328-4
174. Jaipuria, G., Ukmar-Godec, T., Zweckstetter, M.: Challenges and approaches to understand cholesterol-binding impact on membrane protein function: an NMR view. Cellular and molecular life sciences : CMLS **75**(12), 2137–2151 (2018). doi: 10.1007/s00018-018-2789-9
175. Pellerin, L., Carrié, L., Dufau, C., Nieto, L., Ségui, B., Levade, T., Riond, J., Andrieu-Abadie, N.: Lipid metabolic Reprogramming: Role in Melanoma Progression and Therapeutic Perspectives. Cancers **12**(11) (2020). doi: 10.3390/cancers12113147
176. Pandey, V.V., Varshney, V.K., Pandey, A.: Lovastatin: A Journey from Ascomycetes to Basidiomycetes Fungi. Journal of Biologically Active Products from Nature **9**(3), 162–178 (2019). doi: 10.1080/22311866.2019.1622452
177. Huang, B., Song, B.-L., Xu, C.: Cholesterol metabolism in cancer: mechanisms and therapeutic opportunities. Nature metabolism **2**(2), 132–141 (2020). doi: 10.1038/s42255-020-0174-0
178. Kuzu, O.F., Noory, M.A., Robertson, G.P.: The Role of Cholesterol in Cancer. Cancer research **76**(8), 2063–2070 (2016). doi: 10.1158/0008-5472.CAN-15-2613
179. Tilija Pun, N., Jeong, C.-H.: Statin as a Potential Chemotherapeutic Agent: Current Updates as a Monotherapy, Combination Therapy, and Treatment for Anti-Cancer Drug Resistance. Pharmaceuticals (Basel, Switzerland) **14**(5) (2021). doi: 10.3390/ph14050470
180. Ridone, P., Pandzic, E., Vassalli, M., Cox, C.D., Macmillan, A., Gottlieb, P.A., Martinac, B.: Disruption of membrane cholesterol organization impairs the activity of PIEZO1 channel clusters. The Journal of general physiology **152**(8) (2020). doi: 10.1085/jgp.201912515
181. Buyan, A., Cox, C.D., Barnoud, J., Li, J., Chan, H.S.M., Martinac, B., Marrink, S.J., Corry, B.: Piezo1 Forms Specific, Functionally Important Interactions with Phosphoinositides and Cholesterol. Biophysical journal **119**(8), 1683–1697 (2020). doi: 10.1016/j.bpj.2020.07.043
182. Echarri, A., Del Pozo, M.A.: Caveolae - mechanosensitive membrane invaginations linked to actin filaments. Journal of cell science **128**(15), 2747–2758 (2015). doi: 10.1242/jcs.153940

183. Pascalis, C. de, Etienne-Manneville, S.: Single and collective cell migration: the mechanics of adhesions. Molecular biology of the cell **28**(14), 1833–1846 (2017). doi: 10.1091/mbc.E17-03-0134
184. Abduljauwad, S.N., Ahmed, H.-U.-R.: Enhancing cancer cell adhesion with clay nanoparticles for countering metastasis. Scientific reports **9**(1), 5935 (2019). doi: 10.1038/s41598-019-42498-y
185. Gkretsi, V., Stylianopoulos, T.: Cell Adhesion and Matrix Stiffness: Coordinating Cancer Cell Invasion and Metastasis. Frontiers in oncology **8**, 145 (2018). doi: 10.3389/fonc.2018.00145
186. Menter, D.G., DuBois, R.N.: Prostaglandins in cancer cell adhesion, migration, and invasion. International journal of cell biology **2012**, 723419 (2012). doi: 10.1155/2012/723419
187. Bendas, G., Borsig, L.: Cancer cell adhesion and metastasis: selectins, integrins, and the inhibitory potential of heparins. International journal of cell biology **2012**, 676731 (2012). doi: 10.1155/2012/676731
188. Witz, I.P.: The cross talk between cancer cells and their microenvironments. Biochemical and biophysical research communications **633**, 59–60 (2022). doi: 10.1016/j.bbrc.2022.09.066
189. Baghban, R., Roshangar, L., Jahanban-Esfahlan, R., Seidi, K., Ebrahimi-Kalan, A., Jaymand, M., Kolahian, S., Javaheri, T., Zare, P.: Tumor microenvironment complexity and therapeutic implications at a glance. Cell communication and signaling : CCS **18**(1), 59 (2020). doi: 10.1186/s12964-020-0530-4
190. Skrzypiec-Spring, M., Sapa-Wojciechowska, A., Haczkiewicz-Leśniak, K., Piasecki, T., Kwiatkowska, J., Podhorska-Okołów, M., Szeląg, A.: HMG-CoA Reductase Inhibitor, Simvastatin Is Effective in Decreasing Degree of Myocarditis by Inhibiting Metalloproteinases Activation. Biomolecules **11**(10) (2021). doi: 10.3390/biom11101415
191. Xie, L., Zhu, G., Shang, J., Chen, X., Zhang, C., Ji, X., Zhang, Q., Wei, Y.: An overview on the biological activity and anti-cancer mechanism of lovastatin. Cellular signalling **87**, 110122 (2021). doi: 10.1016/j.cellsig.2021.110122
192. Glynn, S.A., O'Sullivan, D., Eustace, A.J., Clynes, M., O'Donovan, N.: The 3-hydroxy-3-methylglutaryl-coenzyme A reductase inhibitors, simvastatin, lovastatin and mevastatin inhibit proliferation and invasion of melanoma cells. BMC cancer **8**, 9 (2008). doi: 10.1186/1471-2407-8-9
193. Depasquale, I., Wheatley, D.N.: Action of Lovastatin (Mevinolin) on an in vitro model of angiogenesis and its co-culture with malignant melanoma cell lines. Cancer cell international **6**, 9 (2006). doi: 10.1186/1475-2867-6-9

194. Feleszko, W., Młynarczuk, I., Olszewska, D., Jalili, A., Grzela, T., Lasek, W., Hoser, G., Korczak-Kowalska, G., Jakóbisiak, M.: Lovastatin potentiates antitumor activity of doxorubicin in murine melanoma via an apoptosis-dependent mechanism. International journal of cancer **100**(1), 111–118 (2002). doi: 10.1002/ijc.10440
195. Syeda, R., Xu, J., Dubin, A.E., Coste, B., Mathur, J., Huynh, T., Matzen, J., Lao, J., Tully, D.C., Engels, I.H., Petrassi, H.M., Schumacher, A.M., Montal, M., Bandell, M., Patapoutian, A.: Chemical activation of the mechanotransduction channel Piezo1, vol. 4 (2015)
196. Kuriyama, M., Hirose, H., Masuda, T., Shudou, M., Arafiles, J.V.V., Imanishi, M., Maekawa, M., Hara, Y., Futaki, S.: Piezo1 activation using Yoda1 inhibits macropinocytosis in A431 human epidermoid carcinoma cells. Scientific reports **12**(1), 6322 (2022). doi: 10.1038/s41598-022-10153-8
197. Davies, J.E., Lopresto, D., Apta, B.H.R., Lin, Z., Ma, W., Harper, M.T.: Using Yoda-1 to mimic laminar flow in vitro: A tool to simplify drug testing. Biochemical pharmacology **168**, 473–480 (2019). doi: 10.1016/j.bcp.2019.08.013
198. Steinecker-Frohnwieser, B., Kullich, W., Kratschmann, C., Cezanne, M., Toegel, S., Weigl, L.: Activation of the mechanosensitive ion channel PIEZO1/2 by YODA1 modulates cellular functions of human oa chondrocytes. Osteoarthritis and Cartilage **28**, S101 (2020). doi: 10.1016/j.joca.2020.02.158
199. Hanahan, D., Weinberg, R.A.: Hallmarks of cancer: the next generation. Cell **144**(5), 646–674 (2011). doi: 10.1016/j.cell.2011.02.013
200. Greten, F.R., Grivennikov, S.I.: Inflammation and Cancer: Triggers, Mechanisms, and Consequences. Immunity **51**(1), 27–41 (2019). doi: 10.1016/j.immuni.2019.06.025
201. Wen, B., Wei, Y.-T., Mu, L.-L., Wen, G.-R., Zhao, K.: The molecular mechanisms of celecoxib in tumor development. Medicine **99**(40), e22544 (2020). doi: 10.1097/MD.0000000000022544
202. Greenhough, A., Smartt, H.J.M., Moore, A.E., Roberts, H.R., Williams, A.C., Paraskeva, C., Kaidi, A.: The COX-2/PGE2 pathway: key roles in the hallmarks of cancer and adaptation to the tumour microenvironment. Carcinogenesis **30**(3), 377–386 (2009). doi: 10.1093/carcin/bgp014
203. Shim, J.Y., An, H.J., Lee, Y.H., Kim, S.K., Lee, K.P., Lee, K.S.: Overexpression of cyclooxygenase-2 is associated with breast carcinoma and its poor prognostic factors. Modern pathology : an official journal of the United States and Canadian Academy of Pathology, Inc **16**(12), 1199–1204 (2003). doi: 10.1097/01.MP.0000097372.73582.CB

204. Zhang, S., Guo, N., Wan, G., Zhang, T., Li, C., Wang, Y., Wang, Y., Liu, Y.: pH and redox dual-responsive nanoparticles based on disulfide-containing poly(β-amino ester) for combining chemotherapy and COX-2 inhibitor to overcome drug resistance in breast cancer. Journal of nanobiotechnology **17**(1), 109 (2019). doi: 10.1186/s12951-019-0540-9
205. Zhang, X., Yan, K., Deng, L., Liang, J., Liang, H., Feng, D., Ling, B.: Cyclooxygenase 2 Promotes Proliferation and Invasion in Ovarian Cancer Cells via the PGE2/NF-κB Pathway. Cell transplantation **28**(1_suppl), 1S-13S (2019). doi: 10.1177/0963689719890597
206. Tai, Y., Zhang, L.-H., Gao, J.-H., Zhao, C., Tong, H., Ye, C., Huang, Z.-Y., Liu, R., Tang, C.-W.: Suppressing growth and invasion of human hepatocellular carcinoma cells by celecoxib through inhibition of cyclooxygenase-2. Cancer management and research **11**, 2831–2848 (2019). doi: 10.2147/CMAR.S183376
207. Wang, S.-J., Khullar, K., Kim, S., Yegya-Raman, N., Malhotra, J., Groisberg, R., Crayton, S.H., Silk, A.W., Nosher, J.L., Gentile, M.A., Mehnert, J.M., Jabbour, S.K.: Effect of cyclo-oxygenase inhibitor use during checkpoint blockade immunotherapy in patients with metastatic melanoma and non-small cell lung cancer. Journal for immunotherapy of cancer **8**(2) (2020). doi: 10.1136/jitc-2020-000889
208. Finetti, F., Travelli, C., Ercoli, J., Colombo, G., Buoso, E., Trabalzini, L.: Prostaglandin E2 and Cancer: Insight into Tumor Progression and Immunity. Biology **9**(12) (2020). doi: 10.3390/biology9120434
209. Chaiamnuay, S., Allison, J.J., Curtis, J.R.: Risks versus benefits of cyclooxygenase-2-selective nonsteroidal antiinflammatory drugs. American journal of health-system pharmacy : AJHP : official journal of the American Society of Health-System Pharmacists **63**(19), 1837–1851 (2006). doi: 10.2146/ajhp050519
210. Clemett, D., Goa, K.L.: Celecoxib: a review of its use in osteoarthritis, rheumatoid arthritis and acute pain. Drugs **59**(4), 957–980 (2000). doi: 10.2165/00003495-200059040-00017
211. Baselyous, Y., Cocinis, M. de, Ibrahim, M., Kalra, A., Yacoub, R., Ahmed, R.: Potentially inappropriate concomitant medicine use with the selective COX-2 inhibitor celecoxib: Analysis and comparison of spontaneous adverse event reports from Australia, Canada and the USA. Expert opinion on drug safety **18**(3), 153–161 (2019). doi: 10.1080/14740338.2019.1589447
212. Liu, R., Tan, Q., Luo, Q.: Decreased expression level and DNA-binding activity of specificity protein 1 via cyclooxygenase-2 inhibition antagonizes radiation resistance, cell migration and invasion in radiation-resistant lung cancer cells. Oncology letters **16**(3), 3029–3037 (2018). doi: 10.3892/ol.2018.9035

213. Li, J., Hao, Q., Cao, W., Vadgama, J.V., Wu, Y.: Celecoxib in breast cancer prevention and therapy. Cancer management and research **10**, 4653–4667 (2018). doi: 10.2147/CMAR.S178567
214. Bundscherer, A., Hafner, C., Maisch, T., Becker, B., Landthaler, M., Vogt, T.: Antiproliferative and proapoptotic effects of rapamycin and celecoxib in malignant melanoma cell lines. Oncology reports **19**(2), 547–553 (2008)
215. Tudor, D.V., Bâldea, I., Olteanu, D.E., Fischer-Fodor, E., Piroska, V., Lupu, M., Călinici, T., Decea, R.M., Filip, G.A.: Celecoxib as a Valuable Adjuvant in Cutaneous Melanoma Treated with Trametinib. International journal of molecular sciences **22**(9) (2021). doi: 10.3390/ijms22094387
216. Gowda, R., Sharma, A., Robertson, G.P.: Synergistic inhibitory effects of Celecoxib and Plumbagin on melanoma tumor growth. Cancer letters **385**, 243–250 (2017). doi: 10.1016/j.canlet.2016.10.016
217. Arico, S., Pattingre, S., Bauvy, C., Gane, P., Barbat, A., Codogno, P., Ogier-Denis, E.: Celecoxib induces apoptosis by inhibiting 3-phosphoinositide-dependent protein kinase-1 activity in the human colon cancer HT-29 cell line. The Journal of biological chemistry **277**(31), 27613–27621 (2002). doi: 10.1074/jbc.M201119200
218. Neuditschko, B., Janker, L., Niederstaetter, L., Brunmair, J., Krivanek, K., Izraely, S., Sagi-Assif, O., Meshel, T., Keppler, B.K., Del Favero, G., Witz, I.P., Gerner, C.: The Challenge of Classifying Metastatic Cell Properties by Molecular Profiling Exemplified with Cutaneous Melanoma Cells and Their Cerebral Metastasis from Patient Derived Mouse Xenografts. Molecular & cellular proteomics : MCP **19**(3), 478–489 (2020). doi: 10.1074/mcp.RA119.001886
219. Sen, S., Kumar, S.: Cell-Matrix De-Adhesion Dynamics Reflect Contractile Mechanics. Cellular and molecular bioengineering **2**(2), 218–230 (2009). doi: 10.1007/s12195-009-0057-7
220. Gong, J.-S., Li, W., Zhang, D.-D., Xie, M.-F., Yang, B., Zhang, R.-X., Li, H., Lu, Z.-M., Xu, Z.-H., Shi, J.-S.: Biochemical Characterization of An Arginine-Specific Alkaline Trypsin from Bacillus licheniformis. International journal of molecular sciences **16**(12), 30061–30074 (2015). doi: 10.3390/ijms161226200
221. Hajizadeh, K., Mehdian, H., Hajisharifi, K., Robert, E.: A van der Waals force-based adhesion study of stem cells exposed to cold atmospheric plasma jets. Scientific reports **12**(1), 12069 (2022). doi: 10.1038/s41598-022-16277-1
222. Baviskar, S.N.: A Quick & Automated Method for Measuring Cell Area Using ImageJ. The American Biology Teacher **73**(9), 554–556 (2011). doi: 10.1525/abt.2011.73.9.9

223. Lobo, J., See, E.Y.-S., Biggs, M., Pandit, A.: An insight into morphometric descriptors of cell shape that pertain to regenerative medicine. Journal of tissue engineering and regenerative medicine **10**(7), 539–553 (2016). doi: 10.1002/term.1994
224. Cavo, M., Fato, M., Peñuela, L., Beltrame, F., Raiteri, R., Scaglione, S.: Microenvironment complexity and matrix stiffness regulate breast cancer cell activity in a 3D in vitro model. Scientific reports **6**, 35367 (2016). doi: 10.1038/srep35367
225. Zdilla, M.J., Hatfield, S.A., McLean, K.A., Cyrus, L.M., Laslo, J.M., Lambert, H.W.: Circularity, Solidity, Axes of a Best Fit Ellipse, Aspect Ratio, and Roundness of the Foramen Ovale: A Morphometric Analysis With Neurosurgical Considerations. The Journal of craniofacial surgery **27**(1), 222–228 (2016). doi: 10.1097/SCS.0000000000002285
226. Evelyn Png, S.P., Tong, L.: Quantitative Image Analysis of Cellular Morphology Using AmnisÃ, Â® ImageStreamX Mark II Imaging Flow Cytometer: A Comparison against Conventional Methods. Single Cell Biol **s1** (2015). doi: 10.4172/2168-9431.S1-001
227. Liu, X., Zhang, X., Lee, I.: A quantitative study on morphological responses of osteoblastic cells to fluid shear stress. Acta biochimica et biophysica Sinica **42**(3), 195–201 (2010). doi: 10.1093/abbs/gmq004
228. Schöchlin, M., Weissinger, S.E., Brandes, A.R., Herrmann, M., Möller, P., Lennerz, J.K.: A nuclear circularity-based classifier for diagnostic distinction of desmoplastic from spindle cell melanoma in digitized histological images. Journal of pathology informatics **5**(1), 40 (2014). doi: 10.4103/2153-3539.143335
229. Takashimizu, Y., Iiyoshi, M.: New parameter of roundness R: circularity corrected by aspect ratio. Prog. in Earth and Planet. Sci. **3**(1) (2016). doi: 10.1186/s40645-015-0078-x
230. Walters, B., Uynuk-Ool, T., Rothdiener, M., Palm, J., Hart, M.L., Stegemann, J.P., Rolauffs, B.: Engineering the geometrical shape of mesenchymal stromal cells through defined cyclic stretch regimens. Scientific reports **7**(1), 6640 (2017). doi: 10.1038/s41598-017-06794-9
231. Kovarik, J.J., Bileck, A., Hagn, G., Meier-Menches, S.M., Frey, T., Kaempf, A., Hollenstein, M., Shoumariyeh, T., Skos, L., Reiter, B., Gerner, M.C., Spannbauer, A., Hasimbegovic, E., Schmidl, D., Garhöfer, G., Gyöngyösi, M., Schmetterer, K.G., Gerner, C.: A multi-omics based anti-inflammatory immune signature characterizes long COVID-19 syndrome. iScience **26**(1), 105717 (2023). doi: 10.1016/j.isci.2022.105717

232. Smith, P.K., Krohn, R.I., Hermanson, G.T., Mallia, A.K., Gartner, F.H., Provenzano, M.D., Fujimoto, E.K., Goeke, N.M., Olson, B.J., Klenk, D.C.: Measurement of protein using bicinchoninic acid. Analytical Biochemistry **150**(1), 76–85 (1985). doi: 10.1016/0003-2697(85)90442-7
233. Cortés-Ríos, J., Zárate, A.M., Figueroa, J.D., Medina, J., Fuentes-Lemus, E., Rodríguez-Fernández, M., Aliaga, M., López-Alarcón, C.: Protein quantification by bicinchoninic acid (BCA) assay follows complex kinetics and can be performed at short incubation times. Analytical Biochemistry **608**, 113904 (2020). doi: 10.1016/j.ab.2020.113904
234. Li, X.-Y., Pi, Y.-N., Chen, Y., Zhu, Q., Xia, B.-R.: Nicotinamide N-Methyltransferase: A Promising Biomarker and Target for Human Cancer Therapy. Frontiers in oncology **12**, 894744 (2022). doi: 10.3389/fonc.2022.894744
235. Ganzetti, G., Sartini, D., Campanati, A., Rubini, C., Molinelli, E., Brisigotti, V., Cecati, M., Pozzi, V., Campagna, R., Offidani, A., Emanuelli, M.: Nicotinamide N-methyltransferase: potential involvement in cutaneous malignant melanoma. Melanoma research **28**(2), 82–88 (2018). doi: 10.1097/cmr.0000000000000430
236. Peng, H., Zhu, E., Wang, J., Du, X., Wang, C., Yang, M., Zhang, Y.: RAB6B is a potential prognostic marker and correlated with the remolding of tumor immune microenvironment in hepatocellular carcinoma. Frontiers in pharmacology **13**, 989655 (2022). doi: 10.3389/fphar.2022.989655
237. Hakobyan, S., Loeffler-Wirth, H., Arakelyan, A., Binder, H., Kunz, M.: A Transcriptome-Wide Isoform Landscape of Melanocytic Nevi and Primary Melanomas Identifies Gene Isoforms Associated with Malignancy. International journal of molecular sciences **22**(13) (2021). doi: 10.3390/ijms22137165
238. Sharma, A., Mendonca, J., Ying, J., Kim, H.-S., Verdone, J.E., Zarif, J.C., Carducci, M., Hammers, H., Pienta, K.J., Kachhap, S.: The prostate metastasis suppressor gene NDRG1 differentially regulates cell motility and invasion. Molecular oncology **11**(6), 655–669 (2017). doi: 10.1002/1878-0261.12059
239. Wang, J.-F., Chen, Y.-Y., Zhang, S.-W., Zhao, K., Qiu, Y., Wang, Y., Wang, J.-C., Yu, Z., Li, B.-P., Wang, Z., Chen, J.-Q.: ITGA5 Promotes Tumor Progression through the Activation of the FAK/AKT Signaling Pathway in Human Gastric Cancer. Oxidative medicine and cellular longevity **2022**, 8611306 (2022). doi: 10.1155/2022/8611306
240. Nikolovska, K., Spillmann, D., Haier, J., Ladányi, A., Stock, C., Seidler, D.G.: Melanoma Cell Adhesion and Migration Is Modulated by the Uronyl 2-O Sulfotransferase. PloS one **12**(1), e0170054 (2017). doi: 10.1371/journal.pone.0170054

241. Kuo, J.-C.: Mechanotransduction at focal adhesions: integrating cytoskeletal mechanics in migrating cells. Journal of cellular and molecular medicine **17**(6), 704–712 (2013). doi: 10.1111/jcmm.12054
242. Zheng, H., Gao, L., Feng, Y., Yuan, L., Zhao, H., Cornelius, L.A.: Down-regulation of Rap1GAP via promoter hypermethylation promotes melanoma cell proliferation, survival, and migration. Cancer research **69**(2), 449–457 (2009). doi: 10.1158/0008-5472.CAN-08-2399
243. Nakajima, H., Koizumi, K.: Family with sequence similarity 107: A family of stress responsive small proteins with diverse functions in cancer and the nervous system (Review). Biomedical reports **2**(3), 321–325 (2014). doi: 10.3892/br.2014.243
244. Ryan, S.D., Ferrier, A., Kothary, R.: A novel role for the cytoskeletal linker protein dystonin in the maintenance of microtubule stability and the regulation of ER-Golgi transport. Bioarchitecture **2**(1), 2–5 (2012). doi: 10.4161/bioa.20302
245. Berndt, C., Casaroli-Marano, R.P., Vilaró, S., Reina, M.: Cloning and characterization of human syndecan-3. Journal of cellular biochemistry **82**(2), 246–259 (2001). doi: 10.1002/jcb.1119
246. Ridley, A.J.: The GTP-binding protein Rho. The international journal of biochemistry & cell biology **29**(11), 1225–1229 (1997). doi: 10.1016/s1357-2725(97)00052-6
247. Huveneers, S., Danen, E.H.J.: Adhesion signaling - crosstalk between integrins, Src and Rho. Journal of cell science **122**(Pt 8), 1059–1069 (2009). doi: 10.1242/jcs.039446
248. Kim, D.J., Kim, S.H., Lim, C.S., Choi, K.Y., Park, C.S., Sung, B.H., Yeo, M.G., Chang, S., Kim, J.-K., Song, W.K.: Interaction of SPIN90 with the Arp2/3 complex mediates lamellipodia and actin comet tail formation. The Journal of biological chemistry **281**(1), 617–625 (2006). doi: 10.1074/jbc.M504450200
249. Mykkänen, O.M., Grönholm, M., Rönty, M., Lalowski, M., Salmikangas, P., Suila, H., Carpén, O.: Characterization of human palladin, a microfilament-associated protein. Molecular biology of the cell **12**(10), 3060–3073 (2001). doi: 10.1091/mbc.12.10.3060
250. Chen, Y.-S., Huang, T.-H., Liu, C.-L., Chen, H.-S., Lee, M.-H., Chen, H.-W., Shen, C.-R.: Locally Targeting the IL-17/IL-17RA Axis Reduced Tumor Growth in a Murine B16F10 Melanoma Model. Human gene therapy **30**(3), 273–285 (2019). doi: 10.1089/hum.2018.104
251. Zhao, Y., Yang, X.: WWTR1 (WW domain containing transcription regulator 1). Atlas of genetics and cytogenetics in oncology and haematology **18**(11), 849–852 (2014). doi: 10.4267/2042/54169

252. Islinger, M., Costello, J.L., Kors, S., Soupene, E., Levine, T.P., Kuypers, F.A., Schrader, M.: The diversity of ACBD proteins - From lipid binding to protein modulators and organelle tethers. Biochimica et biophysica acta. Molecular cell research **1867**(5), 118675 (2020). doi: 10.1016/j.bbamcr.2020.118675
253. Anderson, C.M., Stahl, A.: SLC27 fatty acid transport proteins. Molecular aspects of medicine **34**(2-3), 516–528 (2013). doi: 10.1016/j.mam.2012.07.010
254. Ibrahim, A., Yucel, N., Kim, B., Arany, Z.: Local Mitochondrial ATP Production Regulates Endothelial Fatty Acid Uptake and Transport. Cell metabolism **32**(2), 309-319.e7 (2020). doi: 10.1016/j.cmet.2020.05.018
255. Venkatesan, P., Das, S., Krishnan, M.M.R., Chakraborty, C., Chaudhury, K., Mandal, M.: Effect of AEE788 and/or Celecoxib on colon cancer cell morphology using advanced microscopic techniques. Micron (Oxford, England : 1993) **41**(3), 247–256 (2010). doi: 10.1016/j.micron.2009.10.008
256. Shellman, Y.G., Ribble, D., Miller, L., Gendall, J., Vanbuskirk, K., Kelly, D., Norris, D.A., Dellavalle, R.P.: Lovastatin-induced apoptosis in human melanoma cell lines. Melanoma research **15**(2), 83–89 (2005). doi: 10.1097/00008390-200504000-00001
257. Song, J., Deng, P.-F., Stinnett, S.S., Epstein, D.L., Rao, P.V.: Effects of cholesterol-lowering statins on the aqueous humor outflow pathway. Investigative ophthalmology & visual science **46**(7), 2424–2432 (2005). doi: 10.1167/iovs.04-0776
258. Sarkar, A., Barui, A., Sengupta, S., Chatterjee, J., Ghorai, S., Mukherjee, A.: Epithelial mesenchymal transition in lung cancer cells: A quantitative analysis. Annual International Conference of the IEEE Engineering in Medicine and Biology Society. IEEE Engineering in Medicine and Biology Society. Annual International Conference **2015**, 5372–5375 (2015). doi: 10.1109/EMBC.2015.7319605
259. Greenlee, J.D., Liu, K., Lopez-Cavestany, M., King, M.R.: Piezo1 Mechano-Activation Is Augmented by Resveratrol and Differs between Colorectal Cancer Cells of Primary and Metastatic Origin. Molecules (Basel, Switzerland) **27**(17) (2022). doi: 10.3390/molecules27175430
260. Menter, D.G., Ramsauer, V.P., Harirforoosh, S., Chakraborty, K., Yang, P., Hsi, L., Newman, R.A., Krishnan, K.: Differential effects of pravastatin and simvastatin on the growth of tumor cells from different organ sites. PloS one **6**(12), e28813 (2011). doi: 10.1371/journal.pone.0028813
261. Xv, L., Qian, X., Wang, Y., Yu, C., Qin, D., Zhang, Y., Jin, P., Du, Q.: Structural Modification of Nanomicelles through Phosphatidylcholine: The Enhanced Drug-Loading Capacity and Anticancer Activity of Celecoxib-Casein Nanoparticles for the

Intravenous Delivery of Celecoxib. Nanomaterials (Basel, Switzerland) **10**(3) (2020). doi: 10.3390/nano10030451

262. Marconi, A., Quadri, M., Farnetani, F., Ciardo, S., Palazzo, E., Lotti, R., Cesinaro, A.M., Fabbiani, L., Vaschieri, C., Puviani, M., Magnoni, C., Kaleci, S., Pincelli, C., Pellacani, G.: In Vivo Melanoma Cell Morphology Reflects Molecular Signature and Tumor Aggressiveness. The Journal of investigative dermatology **142**(8), 2205-2216.e6 (2022). doi: 10.1016/j.jid.2021.12.024
263. Saud, A., Sagineedu, S.R., Ng, H.-S., Stanslas, J., Lim, J.C.W.: Melanoma metastasis: What role does melanin play? (Review). Oncology reports **48**(6) (2022). doi: 10.3892/or.2022.8432
264. In, G.K., Poorman, K., Saul, M., O'Day, S., Farma, J.M., Olszanski, A.J., Gordon, M.S., Thomas, J.S., Eisenberg, B., Flaherty, L., Weise, A., Daveluy, S., Gibney, G., Atkins, M.B., Vanderwalde, A.: Molecular profiling of melanoma brain metastases compared to primary cutaneous melanoma and to extracranial metastases. Oncotarget **11**(33), 3118–3128 (2020). doi: 10.18632/oncotarget.27686
265. Matsuoka, T., Yashiro, M., Nishioka, N., Hirakawa, K., Olden, K., Roberts, J.D.: PI3K/Akt signalling is required for the attachment and spreading, and growth in vivo of metastatic scirrhous gastric carcinoma. British journal of cancer **106**(9), 1535–1542 (2012). doi: 10.1038/bjc.2012.107
266. Yu, W.Y., Hill, S.T., Chan, E.R., Pink, J.J., Cooper, K., Leachman, S., Lund, A.W., Kulkarni, R., Bordeaux, J.S.: Computational Drug Repositioning Identifies Statins as Modifiers of Prognostic Genetic Expression Signatures and Metastatic Behavior in Melanoma. The Journal of investigative dermatology **141**(7), 1802–1809 (2021). doi: 10.1016/j.jid.2020.12.015
267. Yang, S.-H., Lin, H.-Y., Changou, C.A., Chen, C.-H., Liu, Y.-R., Wang, J., Jiang, X., Luh, F., Yen, Y.: Integrin β3 and LKB1 are independently involved in the inhibition of proliferation by lovastatin in human intrahepatic cholangiocarcinoma. Oncotarget **7**(1), 362–373 (2016). doi: 10.18632/oncotarget.6238
268. Stine, J.E., Guo, H., Sheng, X., Han, X., Schointuch, M.N., Gilliam, T.P., Gehrig, P.A., Zhou, C., Bae-Jump, V.L.: The HMG-CoA reductase inhibitor, simvastatin, exhibits anti-metastatic and anti-tumorigenic effects in ovarian cancer. Oncotarget **7**(1), 946–960 (2016). doi: 10.18632/oncotarget.5834
269. Chen, Y., Xu, Y., Wang, J., Prisinzano, P., Yuan, Y., Lu, F., Zheng, M., Mao, W., Wan, Y.: Statins Lower Lipid Synthesis But Promote Secretion of Cholesterol-Enriched Extracellular Vesicles and Particles. Frontiers in oncology **12**, 853063 (2022). doi: 10.3389/fonc.2022.853063

270. Suri, A., Sheng, X., Schuler, K.M., Zhong, Y., Han, X., Jones, H.M., Gehrig, P.A., Zhou, C., Bae-Jump, V.L.: The effect of celecoxib on tumor growth in ovarian cancer cells and a genetically engineered mouse model of serous ovarian cancer. Oncotarget **7**(26), 39582–39594 (2016). doi: 10.18632/oncotarget.8659
271. Kakiuchi, Y., Tsuji, S., Tsujii, M., Murata, H., Kawai, N., Yasumaru, M., Kimura, A., Komori, M., Irie, T., Miyoshi, E., Sasaki, Y., Hayashi, N., Kawano, S., Hori, M.: Cyclooxygenase-2 activity altered the cell-surface carbohydrate antigens on colon cancer cells and enhanced liver metastasis. Cancer research **62**(5), 1567–1572 (2002)
272. Das, S., Srinivasan, S., Srivastava, A., Kumar, S., Das, G., Das, S., Dwivedi, A., Karulkar, A., Makkad, K., Bilala, R., Gupta, A., Sawant, A., Nayak, C., Tayalia, P., Purwar, R.: Differential Influence of IL-9 and IL-17 on Actin Cytoskeleton Regulates the Migration Potential of Human Keratinocytes. Journal of immunology (Baltimore, Md. : 1950) **202**(7), 1949–1961 (2019). doi: 10.4049/jimmunol.1800823
273. Srinivasan, S., Ashok, V., Mohanty, S., Das, A., Das, S., Kumar, S., Sen, S., Purwar, R.: Blockade of Rho-associated protein kinase (ROCK) inhibits the contractility and invasion potential of cancer stem like cells. Oncotarget **8**(13), 21418–21428 (2017). doi: 10.18632/oncotarget.15248
274. Vranic, S., Gatalica, Z., Wang, Z.-Y.: Update on the molecular profile of the MDA-MB-453 cell line as a model for apocrine breast carcinoma studies. Oncology letters **2**(6), 1131–1137 (2011). doi: 10.3892/ol.2011.375
275. Meng, J., Yuan, Y., Li, Y., Yuan, B.: Effects of hirsuteine on MDA-MB-453 breast cancer cell proliferation. Oncology letters **25**(1), 4 (2023). doi: 10.3892/ol.2022.13590
276. Ahram, M., Abdullah, M.S., Mustafa, S.A., Alsafadi, D.B., Battah, A.H.: Androgen downregulates desmocollin-2 in association with induction of mesenchymal transition of breast MDA-MB-453 cancer cells. Cytoskeleton (Hoboken, N.J.) **78**(8), 391–399 (2021). doi: 10.1002/cm.21691
277. Kanno, Y., Saito, N., Saito, R., Kosuge, T., Shizu, R., Yatsu, T., Hosaka, T., Nemoto, K., Kato, K., Yoshinari, K.: Differential DNA-binding and cofactor recruitment are possible determinants of the synthetic steroid YK11-dependent gene expression by androgen receptor in breast cancer MDA-MB 453 cells. Experimental cell research **419**(2), 113333 (2022). doi: 10.1016/j.yexcr.2022.113333
278. Salerno, E.P., Bedognetti, D., Mauldin, I.S., Deacon, D.H., Shea, S.M., Pinczewski, J., Obeid, J.M., Coukos, G., Wang, E., Gajewski, T.F., Marincola, F.M., Slingluff, C.L.: Human melanomas and ovarian cancers overexpressing mechanical barrier

molecule genes lack immune signatures and have increased patient mortality risk. Oncoimmunology **5**(12), e1240857 (2016). doi: 10.1080/2162402X.2016.1240857

279. Leikeim, A., Wußmann, M., Schmidt, F.F., Neto, N.G.B., Benz, F., Tiltmann, K., Junger, C., Monaghan, M.G., Schilling, B., Groeber-Becker, F.K.: A preclinical model of cutaneous melanoma based on reconstructed human epidermis. Scientific reports **12**(1), 16269 (2022). doi: 10.1038/s41598-022-19307-0